Newcastle University

School of Computing

Longitudinal changes following acute brain injuries

Nádia Moreira da Silva

Submitted for the degree of Doctor of Philosophy in the School of Computing, Newcastle University

February 2021

© 2021, Nádia Moreira da Silva

To my mother and grandparents.

Abstract

Although it is known the human brain can recover after a brain lesion, the response mechanisms of recovery are not yet fully understood. Using longitudinal data, our aim was first to characterise the ways in which brain networks change after an acute brain lesion either as a result of trauma/insult or following brain surgery. Secondly, we investigated if those changes are associated with recovery or disease progression.

In this thesis, we analyse longitudinal structural changes in mild TBI, and epilepsy patients following temporal lobe resection using graph theory and connectometry. Alterations in brain structure were later related with cognitive recovery or seizure freedom using regression models. In addition, we analysed longitudinal, functional changes following moderate to severe TBI using clustering algorithms. We investigated the network flexibility over functional connectivity patterns/states by calculating the entropy of time spent in these states. Shifts in entropy were compared with longitudinal white matter integrity and blood biomarkers using linear models.

In patients who underwent temporal lobe resection, we found alterations in structural connectivity and in the density of anisotropic diffusing water over time. Some of the observed changes were related with seizure freedom. Similarly, we found that a set of alterations in structural connectivity following mild TBI were related with changes in cognitive trajectory. When investigating longitudinal functional changes in moderate to severe TBI patients, we found a set of cognitive functional connectivity patterns. Changes in entropy after TBI were related to alterations in the concentration of plasma tau.

Our studies suggest that early alterations in brain structure and function occur following acute brain lesions such as TBI or those as result of temporal lobe resection. While some of these alterations are the result of the injury itself in the network, other alterations may

be a result of brain reorganisation and promote patient recovery.

Declaration

I declare that this thesis is my own work unless otherwise stated. No part of this thesis has previously been submitted for a degree or any other qualification at Newcastle University or any other institution.

Nádia Moreira da Silva

February 2021

Contributions

This work is based on collaborative efforts with several people. I here state their specific roles.

- Chapters 1 and 5 were written entirely by NMS and updated with suggestions from PNT and RF.
- Chapter 2 was written by NMS and updated with suggestions from PNT, RF, YW, JD, SBV and GW. PNT also gave major contributions to the introduction and discussion sections. All figures were produced by NMS and updated with suggestions from PNT and YW. All code was written by NMS with two exceptions. Part of the code for matching tracts found by connectometry in a white matter atlas was developed by both NMS and PNT. The code to fit BrainNet Viewer to our own parcellation atlas was produced by both NS and NMS.
- Chapter 3 was written by NMS and updated with suggestions from PNT, RF and AB. All figures were produced by NMS and updated with suggestions from PNT and YW. All code was written by NMS.
- Chapter 4 was written by NMS and updated with suggestions from PNT and RF. All figures were produced by NMS with suggestions from DS and GS. DS also contributed with conceptualisation and design of the study. Code was written by NMS with the exception of the fMRI preprocessing pipeline which was adapted from code developed by EM. DWI images were preprocessed for a separate study by KZ and included in this study without further preprocessing steps.

NMS = Nadia Moreira da Silva; PNT = Peter Neal Taylor; RF = Rob Forshyt; YW = Yujiang Wang; JD = John Duncan; SBV = Sjoerd B. Vos; GW = Gavin Winston; NS

= Nishant Sinha; AB = Andrew Blamire; DS = David Sharp; GS = Gabrielle Schroeder; EM = Emma Mallas; KZ = Karl Zimmerman.

Publications

Portions of the work within this thesis have been documented in the publications below. Peter N. Taylor owns the copyright of these publications and he has given me the right to use them in this thesis.

Moreira da Silva N, Forsyth R, McEvoy A, Miserocchi A, de Tisi J, Vos SB, Winston GP, Duncan J, Wang Y, Taylor PN. Network reorganisation following anterior temporal lobe resection and relation with post-surgery seizure relapse: a longitudinal study. *NeuroImage: Clinical*. 2020 Jun 26:102320.

Moreira da Silva N, Cowie CJ, Blamire AM, Forsyth R, Taylor PN. Investigating brain network changes and their association with cognitive recovery after traumatic brain injury: a longitudinal analysis. *Frontiers in neurology*. 2020 Jun 9;11:369.

Acknowledgements

This work could not have been done without the support of my supervisors Peter N. Taylor and Rob Forsyth. Their support, either through scientific discussions or letting me challenge myself, were crucial for this work. I thank them for their trust and motivation. I would also like to thank Yujiang Wang, Gabrielle Schroeder, Nishant Sinha and CNNP lab for accompanying me through these past years, especially on improving my data visualisation skills. I also thank David Sharp for the opportunity to learn from him and his group, especially Greg Scott and Emma Mallas. I also thank them for receiving me so well in their group during the last year.

For their support through this last year, with the impact of Covid-19 and lockdowns on work and health, I would like to thank my friends Sofia, Raquel, Margarida and Francisca for helping me keep my sanity with our weekly video calls.

Next, I would like to thank to my mother Margarida Moreira and both my grandparents Joaquim Moreira and Maria Moreira. Their example of responsibility, their hard-working nature, humility and respect for others are guidelines for wisdom. Moreover, I would like to thank my siblings Marcos and Priscila. I could not do this thesis without their presence in my life.

Finally, I would like to thank my partner, Michael Mackay, who makes me happy every day and motivates me to do what I like the most. I could not finish this PhD without our scientific discussions, clinical opinion and his general support. I also thank him for reading everything I write.

Contents

1 Introduction **1**

1.1 Injury Related Alterations 4

1.1.1 Resective surgery in epilepsy 4

1.1.2 Traumatic brain injury 7

1.1.3 Blood biomarkers 10

1.2 Networks in Neuroscience 12

1.2.1 Brain networks 12

1.2.2 Graph theory 13

1.2.3 Machine learning applied to brain networks 15

1.3 Aims and Thesis Structure 17

1.3.1 Research questions 17

2 Network Reorganisation Following ATLR and its Relation with Seizure Relapse **19**

2.1 Introduction 20

2.2 Methods 22

2.2.1 Subjects 22

2.2.2 MRI acquisition and imaging processing 22

2.2.3 Analysis of surgery-induced diffusion changes 24

2.2.4 Statistical analysis 29

2.3 Results 30

2.3.1 Surgery-induced changes within white matter fasciculi 30

2.3.2 Surgery-induced changes in network topology 34

2.4 Discussion 40

2.4.1 Surgery-related effect on white matter 40

2.4.2 White matter alterations associated with post-surgery seizure relapse 43

2.4.3 Limitations 44

3 Changes in Network Structure Following Mild TBI and its Association with Cognitive Recovery 49

3.1 Introduction . . . 50

3.2 Methods . . . 52

3.2.1 Data acquisition and subjects . . . 52

3.2.2 DWI data processing . . . 52

3.2.3 Lesions probability map . . . 54

3.2.4 Components of cognitive function . . . 56

3.2.5 Network metrics selection and association with cognitive function . 57

3.2.6 Experimental design and statistical analysis . . . 58

3.3 Results . . . 60

3.3.1 Network-based metrics of mTBI . . . 60

3.3.2 Cognitive function assessment . . . 60

3.3.3 Longitudinal relationships between network-based metrics of mTBI and cognitive functions . . . 61

3.4 Discussion . . . 66

3.4.1 Areas associated with cognitive function . . . 66

3.4.2 Network topology changes over time after mTBI . . . 68

3.4.3 Limitations . . . 69

4 High Concentration of T-Tau Following TBI Related to Network Functional Inflexibility: a Longitudinal Study 71

4.1 Introduction . . . 72

4.2 Methods . . . 75

4.2.1 Subjects and clinical characteristics . . . 75

4.2.2 MRI acquisition and imaging protocol . . . 76

4.2.3 Image processing . . . 76

4.2.4 Blood biomarkers . . . 78

4.2.5 Analysis of white matter organisation . . . 78

4.2.6 Analysis of dynamical functional connectivity . . . 79

4.2.7 Statistical analysis . . . 82

4.3 Results . . . 83

4.3.1 Demographics and clinical characteristics . . . 83

4.3.2 Dynamic functional connectivity and temporal characteristics . . . 83

4.3.3 Blood biomarkers of injury associated with entropy 85
4.3.4 Relationship with structural organisation 87
4.3.5 Longitudinal characteristics 87
4.3.6 Sedation 90
4.4 Discussion 92
4.4.1 Distinct cognitive-related functional states following moderate-severe TBI 92
4.4.2 Fluid blood biomarkers associated with functional flexibility 94
4.4.3 Limitations 96

5 Conclusion and Future Directions **99**
5.1 Summary of Work 99
5.2 General Considerations 100
5.3 Clinical Implications 102
5.4 Future Directions 103

A Supplementary Material - Alterations following ATLR **105**
A.1 Additional Tables 106
A.2 Additional Figures 115
A.3 Imaging Protocols 129
A.4 Atlas-based Approach: Diffusion Changes in Whole White Matter Bundles 129
A.5 Group Subsections from Connectometry 130
A.6 Association with Postoperative Outcome for Right temporal lobe epilepsy (TLE) Patients 131
A.7 Consistency of Resection Masks 131

B Supplementary Material - Alterations following mTBI **133**
B.1 Additional Tables 134
B.2 Additional Figures 138

C Supplementary Material - dFNC analysis **139**
C.1 Additional Tables 140
C.2 Additional Figures 145

Bibliography **149**

List of Figures

2.1 Processing pipeline 31

2.2 Significant quantitative anisotropy (QA) changes between controls and TLE patients, before and after surgery, in parts of tracts revealed by connectometry 32

2.2 Significant QA changes between controls and TLE patients, before and after surgery, in parts of tracts revealed by connectometry 33

2.3 Tract sections with QA changes over 3 months associated with postoperative seizure freedom in patients with left TLE 35

2.4 Changes over 3 months in node eigenvector and node betweenness centrality between patients and controls 36

2.4 Changes over 3 months in node eigenvector and node betweenness centrality between patients and controls 37

2.5 Connectogram comprising the surgery induced changes detected by graph-theory and connectometry in left TLE patients 46

2.6 Connectogram comprising the surgery induced changes detected by graph-theory and connectometry in right TLE patients 47

3.1 Processing pipeline 55

3.2 Networks metrics that showed strongest power in discriminating distinct TBI phases 60

3.3 Cognitive function component for all subjects 61

3.4 Alterations of network metrics associated with cognitive improvement . . . 63

3.5 Regression model of changed network metrics explains changes in cognitive function 64

3.6 Lesions Probability Map 65

3.7 Effect on local disassortativity by changes in regions' strength 67

4.1 Processing pipeline 80

4.2 Dynamic functional connectivity states 84

4.3 Temporal characteristics of states 86

4.4 Association of blood biomarkers and entropy of stationary distribution of Markov chain . . . 88
4.5 White matter organisation . . . 89
4.6 Association of entropy and blood biomarkers . . . 91

A.1 Diagram of available longitudinal data . . . 115
A.2 Raw QA image for left and right TLE patients . . . 116
A.3 Lesion masks for left and right TLE patients . . . 117
A.4 QA changes over 3 months between controls and left TLE patients . . . 118
A.5 QA changes over 3 months between controls and right TLE patient . . . 119
A.6 Subsections of the bundles with greater changes over 3 months in TLE patients . . . 120
A.7 Significant fractional anisotropy (FA) changes between controls and TLE patients, before and after surgery, in parts of tracts revealed by connectometry . . . 121
A.8 QA changes over 3 months between left TLE patients seizure-free over 5 years and left TLE patients with relapse . . . 122
A.9 Tract sections with QA changes over 3 months that are associated with postoperative seizure freedom in patients with right TLE . . . 123
A.10 QA changes over 3 months between right TLE patients seizure-free over 5 years and right TLE patients with relapse . . . 124
A.11 Tract sections with FA changes over 3 months that are associated with postoperative seizure freedom in patients with left and right TLE . . . 125
A.12 Changes over 3 months in node clustering and node strength patients and controls . . . 126
A.13 Tract sections with QA changes over 3 months that are associated with postoperative seizure freedom in patients with left and right TLE after regressing out the resection volume . . . 127
A.14 Reduced QA after surgery over 3 months . . . 128

B.1 Diagram of available longitudinal data . . . 138

C.1 Diagram of available longitudinal data . . . 145
C.2 Dwell time and stationary distribution of Markov chain . . . 145
C.3 Association between entropy and clinical characteristics . . . 146
C.4 Association between entropy and hospital duration . . . 146
C.5 States of dFNC at 6-months and 12-months . . . 147
C.6 Temporal characteristics in non-sedated patients . . . 147
C.7 Association of blood biomarkers with entropy in non-sedated patients . . . 148

List of Tables

1.1 Main features applied in this thesis and their interpretation when values rise. 18

2.1 Demographic and clinical data of patients and controls with imaging available 3 months after surgery. 23

3.1 Clinical data of controls and patients with mild or moderate TBI 53

A.1 Demographic and clinical data of patients and controls with imaging available 12 months after surgery. 106

A.2 Complete preoperative clinical information of all patients with postoperative ILAE seizure outcomes and relapse data 107

A.3 List of network metrics used to quantify network segregation, integration and centrality. 108

A.4 White matter changes significantly different between left TLE patients and controls 3 months after surgery. The subsections were grouped in the set of bundles of the connectome atlas. Cohen's d between groups, number of altered streamlines (No streamlines) and mean length for each bundle is presented below. The Cohen's d between groups taking into account all the subsections found by connectometry without any grouping is also presented with the label "all bundles". 110

A.5 White matter changes significantly different between right TLE patients and controls 3 months after surgery. The subsections were grouped in the set of bundles of the connectome atlas. Cohen's d between groups, number of altered streamlines (No streamlines) and mean length for each bundle is presented below. The Cohen's d between groups taking into account all the subsections found by connectometry without any grouping is also presented with the label "all bundles". 111

A.6 White matter changes significantly different between left TLE patients with different surgical outcomes over 5 years. The subsections were grouped in the set of bundles of the connectome atlas. Cohen's d between groups, number of altered streamlines (No streamlines) and mean length for each bundle is presented below. The Cohen's d between groups taking into account all the subsections found by connectometry without any grouping is also presented with the label "all bundles". 112

A.7 Automated Anatomical Labelling (AAL) regions and their abbreviation included in the study. . . . 113

A.8 Tracts from the connectome atlas and their abbreviations. . . . 114

A.9 Similarity of the resection masks across patients . . . 132

A.10 Comparison of resection volumes between patients with ILAE equals to 1 and ILAE higher than 1. . . . 132

B.1 Results of neuropsychological tests and first component of PCA of controls and patients in the early (subacute) or late post-injury (chronic) phase . . 134

B.2 Clinical data of each patient assessed in this study. RTA - Road Traffic Accident . . . 135

B.3 Clinical data of each control assessed in this study. . . . 136

B.4 List presenting the network metrics used in this study to quantify network segregation, integration, resilience and centrality. . . . 137

B.5 Standardized coefficients and p-values of eleven network metrics between 9 different regions, which change was predictive of cognitive performance following mTBI . . . 138

C.1 Sample size and clinical characteristics of participants. . . . 140

C.2 Description of demographics, premorbid employment, ethnicity, education, injury details and clinical characteristics. . . . 141

C.3 Description of main findings on the neuroimaging reports, outcomes, sedation and management and clinical course. . . . 142

C.4 Maximum framewise displacement (FD), percentage of volumes with FD above 3 and percentage of agreement between automated and manual labelling of ICA-AROMA components . . . 143

C.5 Montreal Neurological Institute (MNI) coordinates (in mm) of spheres used in dynamic functional network connectivity (dFNC) analysis. . . . 143

C.6 Patients' outcome is not associated with total tau (T-Tau) or entropy. . . . 144

Acronyms

AAD acute axon degeneration

AAL Automated Anatomical Labelling

AC anterior commissure

ACC anterior cingulate cortex

AD axial diffusivity

ATLR anterior temporal lobe resection

AUC area under the ROC curve

BOLD blood-oxygen-level-dependent

CAL calcarine

CFC cognitive function component

CS corticostriatal pathway

CSF cerebrospinal fluid

CST corticospinal tract

CT corticothalamic pathway

CWIT D-KEFS Color-Word-Interference Test

DAI diffuse axonal injury

dFNC dynamic functional network connectivity

DMN default mode network

dMRI diffusion-weighted MRI

DWI diffusion-weigted imaging

EEG electroencephalogram

EMC extreme capsule

EPI echoplanar imaging sequence

FA fractional anisotropy

FAST FMRIB's Automated Segmentation Tool

FAT frontal aslant tract

FD framewise displacement

FDR false discovery rate

FEAT fMRI Expert Analysis Tool

FLIRT FMRIB's linear image registration tool

fMRI functional MRI

FNIRT FMRIB's nonlinear image registration tool

FOV field of view

FPN frontoparietal network

FPT frontopontine tract

FSL FMRIB software library

GARF genetic algorithm based random forest method

GCS Glasgow Coma Scale

GFAP glial fibrillary acidic protein

GIFT group ICA of fMRI toolbox

GOSE Glasgow Outcome Scale Extended

HIP hippocampus

ICA independent component analysis

ICH intracerebral haemorrhage

ICN intrinsic connectivity network

IFOF inferior fronto-occipital fasciculus

ILF inferior longitudinal fasciculus

INS insula

IO inferior occipital cortex

LIN lingual

LOC loss of consciousnes

MD mean diffusivity

MNI Montreal Neurological Institute

MOCA Montreal cognitive assessment

MRI magnetic resonance imaging

mTBI mild TBI

MTC middle temporal cortex

NART National Adult Reading Test

NFL neurofilament light chain

NHNN National Hospital of Neurology and Neurosurgery

nRMSE normalized root mean square error

OLF olfactory

ORB orbitofrontal

PAL pallidun

PASAT Paced-Auditory-Serial-Addition Test

PCA principal components analysis

PCC posterior cingulate cortex

PCL paracentral lobule

PCUN precuneus

PoC postcentral

PTA post-traumatic amnesia

PUT putamen

P-Tau phosphorylated tau

QA quantitative anisotropy

RD radial diffusivity

REC gyrus rectus

ROI region of interest

ROL rolandic operculum

rs-fMRI resting-state fMRI

S100B serum S100 calcium binding protein B

SAH subarachnoid haemorrhage

SDH subdural haematomas

SFMed superior frontal cortex, medial part

SMA supplementary motor area

sMRI structural MRI

SN salience network

SOIP Speed of Information Processing

TBI traumatic brain injury

TBSS tract-based spatial statistics

TLE temporal lobe epilepsy

T-Tau total tau

UCHL-1 ubiquitin C-terminal hydrolase-L1

UF uncinate fasciculus

VIF variance inflation factor

WM white matter

Chapter 1. Introduction

Contents

1.1 Injury Related Alterations 4

1.1.1 Resective surgery in epilepsy 4

1.1.2 Traumatic brain injury 7

1.1.3 Blood biomarkers 10

1.2 Networks in Neuroscience 12

1.2.1 Brain networks 12

1.2.2 Graph theory 13

1.2.3 Machine learning applied to brain networks 15

1.3 Aims and Thesis Structure 17

1.3.1 Research questions 17

An injury to the brain, can cause a wide range of disabilities. It is known that behaviour and cognitive deficits as result of an injury can be restored with time, however some patients still experience long-term deficits or never recover (Stein (2000)). The impact of a head injury in the brain and its response mechanisms of recovery or neurodegeneration are not yet fully understood.

Most studies analysing brain injuries are cross-sectional in design, which is a limiting approach to understanding both recovery and neurodegenerative mechanisms in the human brain. In cross-sectional studies, properties of brain lesions and patient outcomes are simultaneously assessed, making it hard to infer temporal associations between the injury and its outcome (Sedgwick (2014)). Therefore only associations, and not causal relationships, can be inferred with cross-sectional studies. In contrast, longitudinal studies allow one to establish a true cause and effect relationship (Solem (2015)). As the brain's mechanisms of recovery or neurodegeneration are dynamic, longitudinal studies are especially relevant to comparing patients' brain "state" to themselves rather than comparing to an arbitrarily chosen control group, which may not be representative. Thus, longitudinal studies also allow us to capture more subtle differences *within* a patient over time.

Brain alterations assessed by longitudinal studies following head injury, either due to the impact itself or due to brain response in terms of recovery or neurodegeneration, might be useful as potential biomarkers for prognostication and therapy stratification. Some imaging biomarkers have been identified and are commonly used in a clinical setting, such as presence of intracranial haemorrhage in T2-weighted images following TBI. With the advance of imaging techniques, other potential imaging biomarkers might be suitable to capture more subtle differences over time in patients' mechanism for recovery and/or neurodegeneration following a head injury. With increased availability of ultrasensitive immunoassays, blood fluid biomarkers associated with head injury and neurodegeneration are promising to assess injury in a less-invasive and cost-effective way (Obrocki et al. (2020)). Similarly to imaging biomarkers, blood biomarkers able us to assess the severity of the injury and inform on a potential brain recovery or neurodegeneration. An injury to the brain can have various causes with different and complex pathophysiology and show different patterns of plasticity over time. As explained by Desmurget et al. (2007), slow-

growing and acute lesions may lead to different patterns of reorganisation. To simplify the work on this thesis, we focused on acute brain injuries as they might share similarities in terms of brain reorganisation, especially in time scale. Injuries as a result of a Traumatic Brain Injury (TBI) or resective epilepsy surgery are two examples of acute brain injuries that might benefit from a longitudinal analysis. TBI is a heterogeneous and dynamic disorder with some patients experiencing persistent behaviour and cognitive deficits. Similarly, following resective epilepsy surgery, some patients experience seizure relapse even years after the surgery. By capturing more accurately brain changes *within* a patient over time, we may gain a better understanding of brain mechanisms of recovery and neurodegeneration following an injury and identify possible prognostic biomarkers.

Patients with refractory epilepsy undergo resective surgery to remove the epileptogenic area and limit the spread of seizure activity. Incomplete removal of epileptogenic tissue is being recognised as one major reason for post-surgery seizure relapse (Sinha et al. (2020), Alsaadi et al. (2001)). Another possible reason for surgical failure is the surgical resection itself (Arnold et al. (2020)). Surgery induces widespread remote changes in white and grey matter remote from the local tissues that are removed (Li et al. (2019c); Lam et al. (2020)). The mechanisms behind these alterations are not yet well understood. It is also believed that an injury of residual tissue around the resection site is a hypothetical mechanism of recurrent seizures (Alsaadi et al. (2001)). It is important to characterise the longitudinal effects of surgery on the post-surgical brain to better understand differences on patients' surgical outcome and thus, guide future therapies.

In TBI, axonal white matter injury is thought to be a major determinant of adverse outcomes (Shahim et al. (2016)). During impact, localised cortical dysfunction close and far from the injury site occur as result of diffuse axonal injury (DAI). DAI might also occur later as a result of a secondary injury following mitochondrial dysfunction (Smith et al. (2003); Irimia et al. (2012); Maas et al. (2008)). Due to the widespread nature of DAI within the brain and the lack of homogeneity across patients, outcomes are hard to predict. Advances in imaging allow identification of structural and functional damage following TBI and its evolution over time (Mac Donald et al. (2007); Kinnunen et al. (2010)). Additionally, advances in serum sampling techniques allow the quantification of

cytoskeletal proteins released by injured axons (Shahim et al. (2016, 2017); Ljungqvist et al. (2017)). By analysing alterations in white matter (WM) over time through imaging data and concentration of cytoskeletal proteins, one can better characterise the longitudinal effects of TBI on brain structure and function and try to understand why some patients experience long-term deficits. A better understanding of brain responses which result in recovery or neurodegeneration are especially important to improve clinical prognostication.

1.1 Injury Related Alterations

1.1.1 Resective surgery in epilepsy

Although resective surgery is seen as a localised trauma in the brain tissue, studies reported that transection of axonal tracts results in widespread changes of WM (Li et al. (2019c)). Nevertheless, responses of human brain tissue to this trauma have not been extensively investigated. It is known that following transection of axonal tracts, an acute axon degeneration (AAD) occurs early on, with subsequent Wallerian degeneration in the distal part of transected axons. After 5-30min of the nerve transection, AAD occurs on both stumps with influx of Ca^{2+} (Wang et al. (2012)). Subsequently, Ca^{2+} activates protease calpain, which cleaves axonal neurofilament and microtubule-associated components, namely tubulin and spectrin. This process results in slow axonal retraction and formation of axonal bulbs at both stumps with accumulation of axoplasmic organelles from ongoing anterograde and retrograde transport (Wang et al. (2012)). After AAD distal axons show a period of latency of 24-48h. Although no longer connected to the soma, the distal axons are capable of maintaining their physiological functions and are electrically excitable (Wang et al. (2012)). After 72h from the surgery, distal axons start to fragment with cytoskeletal breakdown. An increase in glial influx is seen at the site to clear axonal remains. The process of distal degeneration of axons and their myelin sheaths is known as Wallerian degeneration. In contrast, the proximal part of the transected axon, which is still connected to the soma, begins to generate axoplasmatic sprouts only a few hours after acute axonal degeneration (Kerschensteiner et al. (2005)). Prior studies suggest that calpain-mediated proteolysis of neurofilaments assist in the cytoskeletal restructuring and

formation of growth cones in regenerating axons (Spira et al. (2003)). The extracellular space created between both stumps by the AAD also contributes to glial proliferation and thus, a more permissive environment for regeneration of the proximal axon (Wang et al. (2012)). The reorganisation seen in proximal axons might be an adaptive mechanism for recovery of function after axotomy, or a maladaptive response. Abnormal axonal sprouting could result in the generation of epileptiform events or seizure reoccurrence following resective surgery via synaptic plasticity (Salin et al. (1995)). Thus, resective procedures in epilepsy might also negatively affect patient outcome and lead to cognitive side-effects and seizure reoccurrence (Arnold et al. (2020)).

Diffusion-weighted imaging (DWI) allows assessment of the microstructural properties of white matter on the basis of diffusion of water molecules, which is highly directional in the vicinity of white matter tracts. This technique has been used in epilepsy to characterise and identify structural abnormalities preoperatively and to a lesser extent, postoperatively. Multiple diffusion parameters can be obtained from DWI images, with the most common being fractional anisotropy (FA). FA values vary between 0, when water molecules move in all directions equally, and 1, when they move in a single direction. Other measures such as axial (AD) and radial diffusivity (RD) refer to the magnitude of the diffusion parallel and perpendicular to white matter tracts, respectively. In addition, mean diffusivity (MD) refers to the averaged magnitude of diffusion (Winklewski et al. (2018)). While FA is sensitive to white matter pathology, it is not specific to axonal damage or demyelination (Budde et al. (2008)). Animal studies have suggested an increase of RD in the presence of demyelination, whereas a decrease in AD is suggestive of axonal damage (Aung et al. (2013); Lindsey et al. (2019)), such as axonal swelling (Song et al. (2005); Kim et al. (2010)), Wallerian degeneration (Song et al. (2003); Liu et al. (2013); Xie et al. (2011)) and DAI (Arfanakis et al. (2002); Li et al. (2011); Bennett et al. (2012)). Alterations in MD suggests changes in fibre density, axonal diameter, myelination, and neuronal or glial loss (Lindsey et al. (2019)).

Around one in two patients with refractory temporal lobe epilepsy (TLE) experience seizure reoccurrence in the years following surgery and the reasons remain unknown. By providing insight into structural organisation, prior studies using DWI showed structural

bilateral abnormalities extending beyond the temporal lobe in patients with TLE before surgery (Gross (2011); Winston et al. (2014)). Since a decrease of FA and an increase of radial diffusivity (RD) was observed in these white matter tracts, these abnormalities are likely due to demyelination. Following anterior temporal lobe resection (ATLR), patients show Wallerian degeneration in transected axons (cingulum, uncinate fasciculus, inferior longitudinal fasciculus and fornix) and some nearby axons (inferior-fronto-occipital fasciculus and corpus callosum) as reflected by a decrease in FA and an increase in MD (Winston et al. (2014); McDonald et al. (2010); Yogarajah et al. (2010); Concha et al. (2007)). While a decrease in FA combined with an initial decrease in AD is suggestive of the first stage of Wallerian degeneration, AAD, a later increase in RD with decrease in FA suggests degeneration of myelin sheaths, the second stage of Wallerian degeneration (Winston et al. (2014)). Prior longitudinal studies also reported an increase in FA and axial diffusivity (AD) with reduction in RD in corona radiata and internal and external capsules (Yogarajah et al. (2010); Winston et al. (2014); Li et al. (2019c)). Axonal recovery preceded by remyelination is suggested by increased AD with decreased RD. This process is often associated with a gradual increase in FA (Moore et al. (2017)). An increase in FA can also be due to other mechanisms such as changes in axon diameter, fibre density or axonal membrane structure (Moore et al. (2017)).

The long-term impact of surgery on white and grey matter tissue remains not yet fully understood. More studies using postoperative data are needed to examine structural alterations and its possible association with seizure-reoccurrence. Keller et al. (2017) co-registered preoperative fibre maps with surgical lacuna maps and reported that the extent of resected uncinate fasciculus (UF) was related with seizure reoccurrence. However, to our knowledge no one studied how the long-term impact of surgery on white matter tissue is related with seizure-freedom. Recently, Alizadeh et al. (2019) showed that preoperative tract-density in five white matter segments is associated with seizures after surgery. It would be interesting to examine if alterations in tract density after surgery can lead to seizure freedom.

1.1.2 Traumatic brain injury

Understanding pathophysiological mechanisms following TBI is essential to identify the type and extension of injuries for prognostication and future therapies. Studies in cell lines, animals and humans have improved our knowledge on this topic, but failure of clinical trials for neuroprotective therapies suggest that the pathogenesis of TBI might be more complex and heterogeneous (Andriessen et al. (2010)).

TBI is a dynamic process with an initial primary injury due to direct impact of mechanical forces in the brain, followed by a secondary injury, which involves cellular and molecular pathophysiological responses triggered by the primary injury (Maas et al. (2008)). Brain structures are heterogeneous in terms of degree of mechanical fixation and tissue consistency, resulting in parts of the brain moving slower than others during the impact. This difference causes shear, tensile and compressive forces within brain tissue at the time of the impact (Andriessen et al. (2010)). Fronto-temporal regions are especially vulnerable to these forces and commonly affected in TBI. On the macroscopic level, the impact of a mechanical injury shears blood vessels and axons, resulting in intracerebral bleeding and widespread DAI (Mustafa and Alshboul (2013)). The viscoelastic properties of axons and their highly organised structure within white matter tracts makes them susceptible to mechanical injury (Smith et al. (2003)), with grey and white matter interfaces, corpus callosum and brain stem being vulnerable sites for axonal injury (Andriessen et al. (2010)). Moreover, intracerebral bleeding leads to focal contusions, haematomas (intracerebral and extracerebral), diffuse swelling and increase of intracranial pressure (Maas et al. (2008)).

Different secondary pathophysiological mechanisms are initiated by the primary injury. Mechanical shock results in depolarization of nerve cells with subsequent excitotoxicity, especially by glutamate. High extracellular concentrations of this neurotransmitter result in massive influx of Ca^{2+} and Na^{+} into neurons and glial cells. Ca^{2+} and Na^{+} influx cause water to follow by osmosis producing neuronal swelling. Ca^{2+} influx is exacerbated by further intracellular processes causing neuronal dysfunction, cell membrane lysis, DNA fragmentation, mitochondrial dysfunction and activation of calpain enzymes. Calpain enzymes are implicated in further axonal damage by cleavage of structural proteins and

neuronal cell loss as briefly mentioned on the previous section (Andriessen et al. (2010); Mustafa and Alshboul (2013)). Mitochondrial dysfunction results in oxidative stress, decreased cellular energy production, and subsequent apoptosis and axonal disruption (Maas et al. (2008); Hiebert et al. (2015)). There are two main processes for axonal injury. Release of cytochrome-c from impaired mitochondria results in activation of cysteine proteases which breakdown axonal cytoskeleton products, including microtubules, impeding normal axonal transport (Andriessen et al. (2010)). In this process of axonal injury no termination of axonal transport or axonal swelling is present. In the second process, there is an activation of calcineurin which causes termination of axonal transport with accumulation of organelles and swelling (Andriessen et al. (2010)). Both axonal injury processes result in Wallerian degeneration, which consists of breakdown of the myelin sheath and axonal cylinder as discussed previously. To compensate for its loss, the target neuron of the disrupted axon might undergo synaptic reorganisation, for instance by axonal sprouting of neighbouring intact fibres (Andriessen et al. (2010)). This reorganisation can either be adaptive or maladaptive.

While structural damage such as mass lesions, midline shifts and compression of basal cisterns can be observed in conventional imaging techniques such as CT and magnetic resonance imaging (MRI) imaging (Maas et al. (2008)), microscopic lesions such as DAI can be extremely difficult to detect. As mentioned previously, DWI allows assessment of white matter architecture on the basis of diffusion of water molecules. This technique has been used in the identification and characterisation of axonal injury in TBI. There is a lack of agreement on the direction of changes in DWI measures following TBI. Prior studies have reported reductions in FA and higher MD in WM following TBI (Dennis et al. (2015); Narayana (2017); Dinkel et al. (2014); Farbota et al. (2012); Xu et al. (2007)), which can persist through post-injury phases (Croall et al. (2014); Dinkel et al. (2014); Narayana (2017)). A lower FA value as a consequence of an injury is believed to represent compromised WM (Narayana (2017)). However, some studies also reported an increase in FA and lower MD in the acute phase, which might reflect oedema or even astrogliosis (Croall et al. (2014); Dennis et al. (2015)). The lack of agreement between studies is likely due to variability of injury, the time of injury assessment and techniques used to assess

white matter organisation (eg. voxel-wise vs. tract-specific). While there is a considerable amount of heterogeneity in TBI, the corpus callosum is commonly disrupted due to high strain forces (Ghajari et al. (2017)) and associated with cognitive impairment (Arenth et al. (2014)). Other tracts such as corona radiata, corticospinal tracts, cingulum and inferior longitudinal fasciculi are also commonly affected following TBI and associated with motor, cognitive and functional deficits (Caeyenberghs et al. (2011); Edlow et al. (2016); Wu et al. (2010)). Evidence of white matter plasticity by a normalisation over time of diffusion metrics was also reported after TBI (Dall'Acqua et al. (2017)). Verhelst et al. (2019) reported exploratory findings suggesting possible white matter plasticity in TBI patients following a cognitive intervention.

Traumatic axonal injury can also result in disconnection of key regions within and between functional intrinsic connectivity networks (ICNs) (Sharp et al. (2014)). Functional MRI (fMRI) is widely used to study the functional organization of the human brain and its ICNs, measuring neural activity by detecting changes associated with blood flow. Previous studies showed that abnormal white matter organisation might underpin functional networks associated with cognition (Sharp et al. (2011); Mallas et al. (2020); Bonnelle et al. (2011)). Evidence of disruption in functional connectivity within default mode network (DMN) were previously associated with cognitive impairments in attention (Sharp et al. (2011); Bonnelle et al. (2011)). Similarly, abnormal activation of key nodes in dorsal attention network were associated with memory encoding deficits (Mallas et al. (2020)). Although TBI induces abnormalities within ICNs, longitudinal studies using fMRI showed functional recovery associated with better clinical outcomes (Nakamura et al. (2009); Hillary et al. (2011); Mallas et al. (2020)). Efficient cognitive functioning depends on the coordination between networks, namely DMN and salience network (SN) (Sharp et al. (2014)). Thus, a disruption between hubs (highly-connected regions) connecting different networks, namely DMN and SN, will impair cognitive functions that require the integration of information processing, such as attention and memory. Efficient regulation of DMN activity by SN and their coordination was found to be impaired following TBI, which was associated with deficits in inhibitory control (Bonnelle et al. (2012)). Further studies are needed to study in more detail the coordination between these ICNs

and investigate its possible association with better clinical outcomes.

1.1.3 Blood biomarkers

TBI can result in deficits of brain function, often persisting long after injury, in part due to progressive neurodegeneration and dementia (Graham and Sharp (2019); Gardner et al. (2014)). As explained in the previous section 1.1.2, axonal injury can trigger multiple biochemical events such as excitotoxicity by glutamate, abnormal influx of Ca^{2+} to neurons and glial cells, neuronal swelling, mitochondrial dysfunction and activation of calpain proteases, ultimately leading to apoptosis and Wallerian degeneration. These events can lead to progressive neurodegeneration and cognitive impairment. Recent studies have shown that patients with TBI history tend to develop neurodegenerative diseases such as Alzheimer's disease, Parkinson's disease and chronic traumatic encephalopathy (Graham and Sharp (2019); Zetterberg and Blennow (2016)). Indeed, 5% to 15% of dementia cases are due to TBI (Shively et al. (2012)), and the risk of developing dementia after trauma increases 1.6 fold (Li et al. (2017)). Moderate to severe TBI patients have the risk of developing dementia increased 1.8 fold compared to patients with a mild TBI (mTBI) (Raj et al. (2017)). Moreover, the risk for dementia development persists for long periods (14-30 years) after injury (Nordström and Nordström (2018); Fann et al. (2018)).

Evidence of chronic neurodegeneration in TBI are related with neuropathologies of abnormal tau, amyloid beta and TDP-43 early after head injury which can persist for months or years after the insult (Graham and Sharp (2019)). During the insult, shearing forces cause cytoskeletal disruption and tau dissociation from microtubules (Graham and Sharp (2019)). The subsequent release of calpains causes destruction of neurofilaments and microtubules leading to cytoskeletal failure as well as triggering tau phosphorylation, misfolding and aggregation (Gupta and Sen (2016)). Excitotoxins inhibit phosphatases, resulting in hyperphosphorylated tau, producing a pathogenic tau proteoform P-Tau, and ultimately neurofibrillary tangle deposition (Gupta and Sen (2016)). Evidence also suggests that TBI might induce a prion-like spread of abnormal tau (Edwards III et al. (2020); Poudel et al. (2020)), leading to progression of neurodegenerative disease. Amyloid beta, a product resulting from the accumulation of amyloid precursor proteins and

cleaving enzymes in axonal bulbs after axonal injury, can also spread after trauma and form extracellular plaques, leading to chronic neurodegeneration (Johnson et al. (2013)).

Although MRI imaging has been used in the diagnosis and prognosis of neurodegeneration, the advance of ultrasensitive immunoassays has shown the potential of fluid biomarkers to complement imaging data. Fluid biomarkers resulting from axonal, neuronal and astroglial injuries have been used to measure TBI severity and predict patients' outcome (Zetterberg and Blennow (2016); Shahim et al. (2020); Ost et al. (2006)). Tau, highly expressed in thin unmyelinated axons, is a established CSF biomarker that can be also detected in serum and plasma with the advance of ultrasensitive immunoassays (Zetterberg and Blennow (2016)). Following axonal injury, neurofilament light chain (NFL), a cytoskeletal protein, is released into the extracellular space and subsequently into cerebrospinal fluid (CSF) and blood (Khalil et al. (2018)). NFL, which is highly expressed in large-calibre myelinated axons in contrast to tau, is also a potential biomarker for axonal injury. Elevated concentrations of tau and NFL in CSF have been reported following TBI (Neselius et al. (2012)) and relate to clinical and functional outcome (Magnoni et al. (2012); Shahim et al. (2016, 2020)). Recently, mouse models have also shown a possible role of pathological tau in suppressing neuronal activity and promoting silencing of neurons (Busche et al. (2019); Marinković et al. (2019)), leading to behavioural and cognitive deficits (Rubenstein et al. (2019)). However, when pathological tau is supressed by a kinase-targeted therapeutic intervention, those impairments were restored. Zetterberg and Blennow (2016) mention additional potential biomarkers for TBI including ubiquitin C-terminal hydrolase-L1 (UCHL-1), glial fibrillary acidic protein (GFAP) and serum S100 calcium binding protein B (S100B). While UCHL-1 is a potential biomarker for neuronal injury, GFAP and S100B are potential candidates for astroglial injury. UCHL-1, localised in the cytoplasm of neurons and GFAP, a filament protein expressed in astrocytes, are highly sensitive to mild and moderate TBI injuries and might be used to test for presence of intracranial injuries, limiting the need for CT scans (Bazarian et al. (2018)). In addition, when combined with clinical data GFAP might improve prediction models of patient's outcome (Czeiter et al. (2012)). Elevated concentrations of S100B, a protein mainly expressed by mature astrocytes, in the first 24h after injury has also been related

to patient outcome (Thelin et al. (2013)). Although, fluid biomarkers of axonal, neuronal and astroglial injuries have been shown some potential to complement clinical and imaging data in the diagnosis and prognosis of TBI, it remains unknown how their pathophysiological or injury mechanisms might explain outcome and brain dysfunction. A better understanding of these mechanisms would improve long-term prognosis and clinical trials.

1.2 Networks in Neuroscience

Through their connections to each other, neurons form an exceptionally complex structural network. Furthermore this network supports the emergence of synchronised oscillatory activity across brain regions, forming a functional network. This section is divided into three subsections with the definition of brain networks in terms of structure and function, graph theory metrics commonly extracted from brain networks and more advanced methods using machine learning.

1.2.1 Brain networks

Human brain organisation can be analysed at many spatial scales, from synaptic connections between neurons, to organisation of neuronal populations within distinct regions and to architecture of brain regions and their interconnections (Sporns (2010)). Electron microscopy allowed the complete mapping of cellular connections in *Caenorhabditis elegans* (White et al. (1986)). However, a full mapping of structural organisation of human brain at cellular level is currently impossible. Nevertheless, imaging techniques have allowed the analysis of neuronal populations within distinct regions and the organisation of pathways between individual anatomical regions. At the macroscopic scale there are several techniques for deriving individual regions. Structural imaging can be used for defining regions based on sulci and gyri, histological sections can also reveal anatomical differences, functional imaging can reveal regions involved in certain tasks and diffusion imaging and tractography can define regions based on their connectivity patterns (Bullmore and Sporns (2009)). The Automated Anatomical Labelling (AAL) atlas, proposed by Tzourio-Mazoyer et al. (2002), defines regions based on anatomical landmarks such as sulci and gyri and it is one of the most commonly used atlases in neuroscience.

Brain connectivity can be defined in three main types, structural, functional and effective. Structural connectivity refers to physical connections (edges) linking either neurons or brain regions (nodes). Edges can be binary, weighted and be either directed or undirected. AAL is frequently used in combination with DWI to construct structural networks in which nodes represent AAL regions and edges represent a measure of association between regions, such as number of tracts or fibre density, probability of connection, or mean of diffusion metrics across the tracts between those regions. Structural networks are relatively static at shorter time scales but, at longer time scales, can be dynamic, for instance due to plasticity mechanisms (Sporns (2010)). Functional connectivity refers to the behaviour of neurons or regions deviating from statistical independence, suggesting a dynamic coupling which changes on a scale of hundreds of milliseconds in a resting-state or in a response to a task (Sporns (2010)). The most common techniques to study this dynamic coupling are electroencephalogram (EEG), MEG, fMRI and cellular recordings (Bullmore and Sporns (2009)). A common functional network comprises functional brain regions as nodes and the statistical relationship between regions as edges, either through correlation or covariance, coherence or phase locking between pairs of time series. As opposed to structural and functional connectivity, effective connectivity allows detection of causal interactions between nodes through statistical modelling and time series analysis (Friston et al. (2003)).

1.2.2 Graph theory

Graph theory has become increasingly useful to study large-scale complex networks and its structural and functional organization. Brain networks are organized in an efficient topology supporting both segregated and integrated processing (Olde Dubbelink et al. (2013)) This organisation is known as small-world (Bassett and Bullmore (2006)). Small-world networks were first described by Watts D.J. and Strogatz S.H. in 1998. When randomising a set of connections in a regular network (eg. each node connects to all of its nearest neighbours) to create long-range connections, they observed that a small number of long-range connections would result in a large reduction in average path length (eg. average number of minimum steps between each pair of nodes), as seen in random networks,

and the high clustering (eg. fraction of triangles around a node) of a regular graph would be still preserved (Bassett and Bullmore (2006)). This combination of high clustering and short path length in small-world networks enables segregated and integrated processing. Hence, small-world architecture is suitable to model segregation and integration processes in brain networks (Sporns and Zwi (2004)). Overview figures on how to generate brain networks and estimate graph theory metrics are available in Bullmore and Sporns (2009) and Rubinov and Sporns (2010).

Large-scale brain networks in conscious healthy human subjects identified by magnetoencephalography, EEG and fMRI also exhibit scale-free architecture (Liu et al. (2014)). In scale-free networks, the fraction of nodes with degree k follows a power law $k^{-\gamma}$, a property with implications for network dynamics and structure (Broido and Clauset (2019)). This organisation exhibits a few highly connected nodes known as hubs which allow for a fast dissemination of global information and neural integration, both highly crucial in cognitive tasks. Although scale-free architecture is robust to random failure, it is vulnerable to attacks to its hubs (Wu et al. (2017)), resulting in disconnection and dysfunction in brain disorders. Scale-free network properties are highly dependent on the degree exponent γ. When γ is greater than 2 and less than 3, average path length increases as $ln(ln(N))$. The networks are called ultra-small world as the hubs in this regime significantly shrink the distance between nodes. While for $\gamma > 3$, average path length follows the small-world property (Barabási (2016)).

Small-world and scale-free models allow a better understanding of human brain topology and thus help identify complex patterns (Bassett and Bullmore (2006)). Additional topological properties are also often used to assess brain network such as modularity, centrality, distribution of network hubs and resilience to insults. Alterations to the topology of brain networks have been found in neurodegenerative disorders and neurological diseases such as epilepsy, traumatic brain injury (TBI), attention-deficit hyperactivity disorder, schizophrenia and Parkinson's disease (Ahmadlou et al. (2012); Alexander-Bloch et al. (2012); Olde Dubbelink et al. (2013)).

Evidence from histopathology, electrophysiology and neuroimaging suggest that the pathological substrate of TLE is not limited to the mesiotemporal lobe but associated with a

more widespread pattern of alterations in brain structure and functional networks (Bernhardt et al. (2015)). This evidence supports the idea that graph theoretical analysis is a useful tool to provide insight into brain alterations in epilepsy. Alterations of topology in TLE patients have been associated with disease duration, clinical data, and to unfavourable postoperative seizure outcomes, suggesting an adverse effect on epileptogenesis of network architecture (Bernhardt et al. (2011); Bonilha et al. (2013); Bernhardt et al. (2015); Wang et al. (2014)). Although small-world properties are preserved in epilepsy, a shift towards a more regular network has been observed by an increase in the clustering coefficient and path length in DWI, fMRI and T1w-MRI imaging (Bonilha et al. (2012); Wang et al. (2014); Bartolomei et al. (2013)). Besides its usefulness in identifying topological alterations associated with seizure genesis and development, graph theoretical analysis was also used to infer the impact of resective surgery on the brain connectome of TLE patients (Taylor et al. (2018)).

Axonal injuries disconnect large-scale brain networks, making graph theoretical analyses a practical tool for understanding the impact of brain dysfunction following TBI and predicting clinical outcomes. Traumatic brain injuries to network hubs results in impairments of behavioural and cognitive brain functioning (Van den Heuvel and Sporns (2013); Fagerholm et al. (2015)). Lesioning hubs connecting functional modules/communities results in widespread disruption of the modular organization of the functional brain network, essential for brain communication. Posterior and anterior cingulate cortex are two major hubs commonly affected by TBI (Pandit et al. (2013); Merkley et al. (2013)). A shift from small-world organisation was also observed following TBI in cognitive-related networks, which may result in cognitive deficits (Pandit et al. (2013)).

1.2.3 Machine learning applied to brain networks

With the advance of technology and modern experimental methods, the volume of data created each year has been growing exponentially. As a consequence, machine learning techniques are becoming ever more crucial to identify and establish complex multivariate relationships, allowing us to make accurate predictions in large datasets (Hinton (2011)). In neuroscience, several studies showed that machine learning algorithms are well suited

to identifying structural and functional connectivity patterns from imaging and electrophysiological data and assist in the identification of biomarkers for diagnosis and prognosis of neurological diseases as well as provide novel insights into the biological mechanisms underlying brain recovery and human cognition (Farahani et al. (2019); Khazaee et al. (2015); Pläschke et al. (2020)). Graph theory in conjunction with machine learning has been applied in both TBI and epilepsy. Mazrooyisebdani et al. (2020) trained a prediction model to discriminate TLE patients and healthy controls and found that TLE patients have a reduction in network segregation with a shift of network hubs to the contralateral side. The authors also predicted neurocognitive performance from topological metrics. The combination of graph theory and machine learning allows a better understanding of how epilepsy affects brain networks over time by finding topological patterns. As mentioned previously, traumatic axonal injury affects brain connectivity by disrupting large-scale networks that support cognition. By combining graph theory with machine learning, Fagerholm et al. (2015) studied how the disruption of these networks affects the overall network structure and function of the human brain. They found a set of graph metrics, or topological pattern, predictive of axonal injury and associated with cognitive impairment.

In addition to prediction models, unsupervised machine learning techniques have been recently applied to identify dynamic functional connectivity patterns/states. As mentioned before, functional MRI can capture connectivity changes on a scale of hundreds of milliseconds in response to stimulus or internal state. By clustering functional connectivity matrices within a sliding-window framework, a set of connectivity patterns/states that reoccurred in time were identified in healthy controls (Allen et al. (2014)). Some preliminary studies have suggested that in neurological conditions the dynamic functional connectivity patterns are altered as well as their temporal characteristics (Bonkhoff et al. (2020)). These findings suggest that dynamic neural mechanisms may give better insight into disease severity and recovery. In TBI, some preliminary studies suggest a reduction in network functional dynamics as a potential biomarker of poor prognosis (Hou et al. (2019); Gilbert et al. (2018)).

1.3 Aims and Thesis Structure

The present work explores the use of imaging, graph theory and machine learning to better characterise the impact of insults to the brain over time, either as a result of a TBI or resective surgery in patients with refractory epilepsy. The main imaging, graph theory and biological features used in this thesis are summarised in Figure 1.1 as well as their interpretation when their values rise.

This work comprises three independent studies which are described in detail in Chapters 2, 3 and 4. All studies use longitudinal data to investigate recovery or neurodegeneration in the brain over time. In Chapter 2, we assess the effects of resective surgery for epilepsy on brain network topology and white matter tracts in TLE patients. Longitudinal alterations promoted by surgery were investigated for a possible association with seizure relapse. Similarly, in Chapter 3, we assessed the effects of mTBI on brain network topology and its possible association with cognitive performance. Chapters 2 and 3 are focused on the characterisation of longitudinal effects of an insult to the brain in terms of recovery and neurodegeneration trajectories and the possible association with persistence of symptoms. In contrast, Chapter 4 investigates the association between proteinopathy and longitudinal alterations in brain function after moderate-severe TBI, namely the impairment of functional coordination between DMN and SN. We finish in Chapter 5 with a summary of the findings and some future directions.

1.3.1 Research questions

To our knowledge no one investigated the impact of resective surgery on brain structure and function and its possible association with seizure relapse. Therefore, in the Chapter 2 we intended to answer the following questions: *What is the impact of surgery within white matter fasciculi? Do these changes to white matter fasciculi and/or network topology relate to post-operative seizure freedom ?*

Alterations in brain topology following TBI have been widely reported in moderate-severe TBI and its effect on cognitive performance. Several studies also identified alterations on brain topology following milder injuries, with a strong focus on global network metrics

Features	Interpretation of increase
QA	Higher density of anisotropic diffusing water
FA	Higher fraction of water diffusing anisotropically
Eigenvector/Page Ranks centrality	Region connected to more relevant nodes
Betweenness centrality	Region behaves more like a bottleneck for information transfer
Closeness centrality	Regions closer to all other nodes by shortest paths
Strengh	Stronger connection to its connected regions
Local Assortativity	Higher integration of information
Clustering Coefficient	Neighboring regions are more connected
Local Efficiency	Region exchanges information more efficiently
Shannon's Entropy of stationary distribution of Markov chain	Unpredictability behaviour of the next state
GFAP	Higher astroglial injury
UCHL1	Higher neuronal injury
S100B	Higher astroglial injury
T-Tau	Higher axonal injury
NFL	Higher axonal injury
Mahalanobis distance	Higher distance from controls' group variance

Table 1.1: Main features applied in this thesis and their interpretation when values rise.

such as small-worldness (Imms et al. (2019), Kuceyeski et al. (2019), Dall'Acqua et al. (2017)). In Chapter 3, we opted to build on this and focused as well on understanding how alterations of network metrics at node/region level can be used as biomarkers and its potential association with recovery. As opposed to assessing the alterations at the connectome level, a combination of local changes at specific nodes may be more predictive of patient outcome. Therefore, in chapter 3, we intended to answer the following questions: *Does mTBI induce longitudinal alterations in network topology? Do these changes relate to cognitive performance?*

Since tau proteinopathy can induce silencing of neurons in mice models, we intended to investigate in Chapter 4 a possible association of tau with the functional coordination between ICNs following trauma and thus answering the questions: *Do moderate to severe injuries induce alterations in the functional coordination between cognitive-related functional networks and their regions? Are those alterations over time associated with tau concentration? Are those alterations in functional coordination related to white matter organisation?*

Chapter 2. Network Reorganisation Following ATLR and its Relation with Seizure Relapse

Contents

2.1 Introduction 20

2.2 Methods 22

2.2.1 Subjects 22

2.2.2 MRI acquisition and imaging processing 22

2.2.3 Analysis of surgery-induced diffusion changes 24

2.2.4 Statistical analysis 29

2.3 Results 30

2.3.1 Surgery-induced changes within white matter fasciculi 30

2.3.2 Surgery-induced changes in network topology 34

2.4 Discussion 40

2.4.1 Surgery-related effect on white matter 40

2.4.2 White matter alterations associated with post-surgery seizure relapse 43

2.4.3 Limitations 44

2.1 Introduction

Temporal lobe epilepsy (TLE) is the most common form of drug-refractory focal epilepsy. For patients with intractable temporal lobe epilepsy (TLE), surgery can be a viable treatment option. In individuals with TLE, an anterior temporal lobe resection (ATLR) leads to seizure freedom in 50–80% after at least 1 year of follow-up (Spencer and Huh (2008); De Tisi et al. (2011)). An ATLR involves the removal of most of the amygdala, hippocampus as far posterior as the widest part of the brainstem, entorhinal, and other temporal neocortical areas. White matter pathways including the uncinate fasciculus, inferior longitudinal fasciculus and optic radiation may be transected.

Microstructural properties of subcortical white matter pathways can be measured in vivo using diffusion magnetic resonance imaging (MRI). Many previous studies have investigated white matter properties in TLE patients and found microstructural differences in temporal and extratemporal structures compatible with altered myelination relative to controls (Winston et al. (2014); Li et al. (2019c); Keller et al. (2017); Schoene-Bake et al. (2009); Elliott et al. (2018); Gross et al. (2006); Riley et al. (2010); Taylor et al. (2015)). As referred in Chapter 1, some studies have additionally related pre-surgical white matter properties to post-surgical seizure-freedom. Alizadeh et al. (2019) showed an association between seizure-recurrence and tract density. Furthermore, Keller et al. (2017) and Taylor et al. (2018) demonstrated that preoperative white matter alterations that were later resected were associated with post-operative outcomes. Both studies investigated associations with postoperative seizure freedom, but did not use postoperative diffusion MRI. Therefore, these studies are limited by not accounting for network changes induced by the surgery itself.

As mentioned in Chapter 1, some studies have investigated postoperative white matter properties using diffusion MRI. Concha et al. (2007) showed reduced postoperative fractional anisotropy (FA) in a cohort of eight seizure-free patients in the fornix, cingulum, and other areas. McDonald et al. (2010) demonstrated, in seven seizure-free patients, reduced postoperative FA in the uncinate fasciculus, inferior longitudinal fasciculus, and fornix. Other studies also found ipsilateral reductions in FA, likely due to Wallerian de-

generation (Yogarajah et al. (2010); Nguyen et al. (2011); Faber et al. (2013); Liu et al. (2013); Pustina et al. (2014); Winston et al. (2014)). Although several of those studies have related surgery-induced changes to neuropsychological consequences, such as visual field deficits (McDonald et al. (2010)) and verbal fluency (Pustina et al. (2014); Yogarajah et al. (2010)), none have investigated associations with postoperative seizure-freedom.

In this study we characterised surgery induced white matter changes in a longitudinal cohort of 48 patients who underwent ATLR using both preoperative and postoperative data and addressed the following questions: What is the impact of surgery within white matter fasciculi? Do these changes to white matter fasciculi and/or network topology relate to seizure-freedom?

2.2 Methods

2.2.1 Subjects

We studied 48 patients who underwent ATLR at the National Hospital of Neurology and Neurosurgery (NHNN), London, United Kingdom and 17 healthy controls, with no significant medical history of neurological or psychiatric problems. Twenty-two of the 48 patients had right ATLR and 26 on the left. All patients had resection of the majority of the amygdala and hippocampus as far posteriorly as the widest part of the brainstem, using a modified Spencer ATLR (Spencer et al. (1984)), without complication. All surgeries went according to plan, as verified by post-operative MRI at 3–4 months following surgery. Patients were followed up for 2–5 years and at every 12 months surgical outcome was recorded according to the ILAE scale (Wieser et al. (2003)). Two-year ILAE outcomes were available for all patients, with three-, four- and five-year outcomes available for 46, 40 and 34 patients respectively. Eleven patients with left TLE and 5 with right TLE had remained entirely seizure free (ILAE 1) throughout a 5-year follow-up period. Eleven patients with left TLE and 12 with right TLE had postoperative seizures (seizure-recurrence) at least once during their follow-up period of 2 to 5 years.

A χ^2 test and two-tailed non-parametric Wilcoxon ranksum test confirmed differences in sex but not in age between controls and patients. Differences were regressed out in further analysis. Tables 2.1, A.1 and A.2 summarise patient details.

The study was approved by the NHNN and the Institute of Neurology Joint Research Ethics Committee, and written informed consent was obtained from all subjects.

2.2.2 MRI acquisition and imaging processing

For each patient in this study, T1-weighted structural MRI (sMRI) and diffusion-weighted MRI (dMRI) data were acquired pre-operatively and 3–4 months post-operatively. A subset of these patients (N = 13) were scanned again 12-months following surgery. Controls also underwent sMRI and dMRI at three time points: baseline (N = 17) followed by 3 months (N = 17) and 12 months (N = 16) later. Control data were used as a normative measure for the longitudinal changes obtained from patients over 3–4 months after

	Left TLE	Right TLE	Controls	Significance
Subjects (n)	26	22	17	-
Sex (Male/Female)	13/13	2/20	9/8	Chi2 (Left TLE; Controls) = 0.035 p = 0.850 Chi2 (Right TLE; Controls) = 9.106 p = 0.003
Age at baseline scan	35.86±9.57	39.83±12.26	40.06±11.06	t (Left TLE; Controls) = -1.318 p = 0.195 t (Right TLE; Controls) = -0.060 p = 0.953
Onset	16.19±10.93	14.93±10.75	-	-
Age at surgery	36.52±9.62	41.00±12.42	-	-
Epilepsy Duration	20.33±13.67	26.07±13.35	-	-
Status Epilepticus (n)	3	1	-	-
Secondary generalised seizures (n)	20	14	-	-
Hippocampal Sclerosis (n)	18	11	-	-
Seizure-Free for 5 years (n)	11	5	-	-
Seizure recurrence (n)	11	12	-	-

Table 2.1: Demographic and clinical data of patients and controls with imaging available 3 months after surgery.

surgery and 12 months after surgery. Detailed imaging protocols are described in section A.3 in Appendix as well as a diagram with available data per group (Figure A.1). Post-operative sMRI, linearly registered to preoperative sMRI using FMRIB's linear image registration tool (FLIRT) from FMRIB software library (FSL), was used to accurately delineate the resected tissue in patients. More details on how the resection mask was drawn in T1w-images for these subjects are available in Taylor et al. (2018).

Diffusion data were reconstructed using generalized q-sampling imaging (GQI) with a diffusion sampling length ratio of 1.2 and cerebrospinal fluid (CSF) calibration, as in our previous study using DSI Studio (`http://dsi-studio.labsolver.org`) (Taylor et al. (2018)). The deterministic fibre tracking algorithm was used, allowing for crossing fibres within voxels, and to reduce false positive connections, which can critically alter graph metrics in comparison with false negative connections (Zalesky et al. (2016)). As part of the diffusion reconstruction, GQI performs a non-linear transformation of each image to Montreal Neurological Institute (MNI) ICBM2009c template space. GQI reconstruction is a model-free reconstruction method that estimates the density of diffusing water at different orientations Yeh et al. (2010), solving the problem of crossing fibres. It outputs per voxel and orientation an estimation of the density of spin density at that direction, called quantitative anisotropy (QA). Additionally, FA images were also obtained using

dtifit and all subjects' preoperative FA data was aligned to the FMRIB58_FA standard space template using a nonlinear registration tool FMRIB's nonlinear image registration tool (FNIRT). Each subjects' postoperative FA image was co-registered to its preoperative FA image using the linear registration tool FLIRT. Since there are slight anatomical differences between MNI ICBM2009c and the 6th generation of 152-MNI space available in FSL (Mai and Majtanik (2017)), we applied a non-linear registration between MNI templates. The warps derived from both analyses were combined and applied to the original resection masks and FA images as in our previous study (Yogarajah et al. (2010)). Quantitative anisotropy QA is related to fibre volume fraction (Yeh et al. (2013b)) and measures the density of anisotropic diffusing water at each fiber direction. It is highly correlated with other measures such as FA and mean diffusivity (MD). Although it is less commonly used, QA has important advantages. Phantom studies have shown it to be less susceptible to partial volume effects, and artefactual reductions in areas of crossing fibres (Yeh et al. (2013b)). Visual assessment of registration quality was conducted for all images. The resection masks aligned into the MNI ICBM2009c template were binarized and joined into a single mask using FSL. We performed this step for left and right TLE patients, separately. The overlaid resection masks were used to delineate resected tissue in further analyses. To quantify the similarity of resected tissue across TLE patients, we computed Dice overlap (Moreira da Silva et al. (2017); Traynor et al. (2010)) separately for left and right TLE patients. Furthermore, we investigated if resection volume was related to outcomes of seizure freedom.

2.2.3 Analysis of surgery-induced diffusion changes

We performed two complementary analyses to study post-operative changes in diffusion MRI. Connectometry allows characterisation of specific focal and spatial structural changes within subsections of tracts which may drive alterations in brain connectivity or network topology (Yeh et al. (2016, 2018)). Graph theory allows quantification of those alterations in network topology locally; by measuring properties of grey matter regions, and globally; by measuring properties of the network as a whole (Yeh et al. (2016)).

Connectometry: Diffusion changes in subsections of white matter bundles

Connectometry is sensitive to changes in subsections of tracts, which otherwise could be hidden by conventional atlas-based or connectome approaches (Yeh et al. (2013a,b, 2016); Faraji et al. (2015); Sinha et al. (2019)). These conventional approaches compute mean diffusion measures along the entire length of white matter tracts (Appendix: section A.4). Connectometry is robust to crossing fibres and, while identifying diffusion alterations, does not depend on tractography, which has limited reliability near the grey matter targets. These are two main advantages in comparison to other methods for characterisation of focal changes within tracts (Yeh et al. (2016)).Thus, we studied the structural alterations in subsections of tracts using diffusion MRI connectometry to compare patient and control groups and patient association with postoperative outcome.

First, we created two connectometry databases comprising controls and left or right TLE patients (26 left TLE patients and 17 controls; 22 right TLE patients and 17 controls) with QA as the index of interest. The default Human Connectome Project HCP1021 template was used from which the local fibre directions were sampled to create the local connectome matrix.

Secondly, we ran the group connectometry analysis in DSI studio to correlate the local connectome matrix with subject category (patient or control) in a multiple linear regression model, while controlling for age and sex. We constrained the analysis to the non-resected area to estimate only regional differences of the local connectome within non-resected tissue. Thus, overlaid resection masks were used as region of avoidance to discard any voxel that was resected across any patient. We employed this analysis separately for left and right TLE patients. To compare patient and control groups, we applied the same approach to controls using the left and right overlaid resection masks separately.

We ran connectometry analysis with different t-score thresholds to select local connectomes (T-score: 1, 2 and 3) at different significance levels (false discovery rate (FDR): 0.05, 0.075 and 0.1) (Wang et al. (2019)). Higher values of t-score give more specific and confirmatory results, whereas lower values give more sensitive results, which are useful for exploratory studies. Although low FDR values might filter most of the false discoveries,

they might not detect subtle differences (Yeh et al. (2013a)). Thus, a wider range was employed for exploratory purposes.

At each point on this two dimensional grid, local connectomes for every seed voxel under analysis are inspected for positive and negative associations with subject category. The local connectomes were tracked using a deterministic fibre tracking algorithm (Yeh et al. (2013a,b)), track trimming was iterated once, and the seed count was set to 10,000. These are the default settings for fibre tracking in connectometry analysis from the 9 September 2018 version of DSI Studio. Connectometry analysis controls for false discoveries by comparing the positive and negative associations of QA with a null distribution obtained by randomly permuting the group labels. Further details of this procedure are available in the section "Local connectomes and their statistical inference" in Yeh et al. (2016) and also in the methods section of Yeh et al. (2013a) and Yeh et al. (2013b). In our study, we used the default permutation count of 2000.

Thirdly, we quantified the output of the connectometry analysis at each point of the two-dimensional grid. The subsections of tracts found to be significantly different between patients and controls were grouped as in the population-average atlas of the connectome (Yeh et al. (2018)). This atlas identifies 550,000 white-matter tracts verified manually by experienced neuroanatomists, which are grouped in 80 main bundles. Cranial nerves, cerebellum and brainstem bundles were not considered in this study. Thus, subsections located in the same bundle as in the atlas were grouped (Appendix: section A.5). Then, for each group, we computed the mean QA for each subject and timepoint. Effects of age and sex were regressed out using fitlm function in MATLAB.

Investigating which grey matter regions these subsections connect to may improve our understanding of patterns of degeneration and plasticity following ATLR. Thus, tracts in which subsections were found to be significantly different by connectometry were found by identifying the nearest tract in the connectome atlas to each subsection. Only tracts within 1 mm were included. After estimating the entire tracts, we quantified a connectivity matrix using Automated Anatomical Labelling (AAL) parcellation scheme. Voxels of the AAL regions overlapping with the overlaid resection mask were removed. This was conducted separately for left and right TLE patients.

In order to investigate how changes within tracts were related with postoperative outcomes, we split patients into seizure-free or seizure-recurrence groups and repeated the previous steps in this analysis. Therefore, we created a database with patient data and used their postoperative outcome as the variable of study in the multiple linear regression model.

To support the interpretation of QA results, the previous steps were repeated using FA as index of interest.

Graph theory: Changes in network topology

To study how alterations in the tracts drive changes in the network topology, we used graph theory to estimate longitudinal changes in network metrics between patients and controls. We characterised the changes in network topology locally, by studying different grey matter regions (nodes) and globally, by studying the overall differences in the whole brain.

Tracts from the population-average atlas of the connectome (Yeh et al. (2018)) were projected to each individuals' QA image using DSI Studio. The mean QA along the tracts connecting each pair of regions of the AAL atlas (Tzourio-Mazoyer et al. (2002)) was estimated and saved in a connectivity matrix for each individual and timepoint. Voxels of the AAL regions overlapping with the resection mask were removed. This was conducted separately for left and right TLE patients.

To facilitate comparison with earlier work using this data (Taylor et al. (2018)), network metrics such as betweenness and eigenvector centrality were estimated from the connectivity matrices to quantify network properties. Additionally network metrics were also included such as node strength and clustering coefficient (Rubinov and Sporns (2010)). Effects of age and sex were regressed out using fitlm function in MATLAB. A detailed description of all the metrics used is provided in Table A.3 in Appendix.

After calculating network metrics from the connectivity matrix of each participant at each timepoint, we computed the longitudinal change in graph metric (K) for each AAL region (X) over 3–4 months:

$$K_{X_{3-4months-postoperative}} - K_{X_{baseline}}$$

and over the following 8-9 months:

$$K_{X_{12months-postoperative}} - K_{X_{3-4months-postoperative}}$$

For visualisation, we computed the z-score of the longitudinal changes in patient group as the number of standard deviations away from the mean, where the standard deviation and mean were obtained from the control distribution. High |z-score| indicates high deviation of network properties from normality. To observe if there were statistical differences over the same time period between patients and controls, we used inference statistical tests. These differences might be associated with (1) the impact of surgical resection on the network and (2) plasticity of white matter tracts following surgery. We run two further analyses to distinguish both mechanisms. The first analysis is similar to that described in Taylor et al. (2018); we inferred the impact of surgical resection on network topology using preoperative data only. Thus, we computed the expected change on network metrics using the difference between the preoperative network without the resected tracts and the preoperative network with all tracts. For ease of interpretation we will refer to this analysis as the null model. For the second analysis, we computed for all patients the difference between the postoperative network and the preoperative network with all tracts. This difference represents both the impact of surgical resection on the network and plasticity/degeneration following it. For ease of interpretation, we will refer to this analysis as an observed model since the network is generated from the empirically observed postoperative data. By comparing both analyses we are able to distinguish the postoperative changes in network metrics due to the impact of surgical resection from changes due to reorganisation of the connectome.

To study the association of postoperative outcome with network metrics, patients were split into seizure-free and seizure-recurrence groups. The longitudinal changes in network metrics between both groups were compared using inference statistical tests.

2.2.4 Statistical analysis

Inferential statistical tests were used to compare longitudinal changes between patient and control groups and subclasses in patients based on their postoperative outcome. We applied nonparametric Wilcoxon rank-sum test to compare longitudinal changes in network metrics between groups and applied an FDR (Benjamini-Hochberg) correction at q = 0.05.

Connectometry uses permutation tests to obtain a null distribution of the connectometry findings and estimate a FDR value. Further details are available in (Yeh et al. (2013a,b, 2016)).

2.3 Results

We first characterised surgery-induced changes on white matter and network topology in TLE patients relative to longitudinal measurements in controls over the same time period. Secondly, we investigated the association of those surgery-induced changes with postoperative seizure-freedom. Two complementary approaches were used (Figure 2.1).

2.3.1 Surgery-induced changes within white matter fasciculi

Connectometry detected widespread surgery-induced changes over time in subsections of the tracts located in temporal and extratemporal structures (Figure 2.2). Only changes over the first 3–4 months after the surgery were significantly different between patients and controls (FDR<0.05; T-score=3; Reduction in QA: $Cohen - D_{LeftTLE} = -2.30$, $Cohen - D_{RightTLE} = -2.76$; Increase in QA: $Cohen - D_{LeftTLE} = 0.87$). During this period, QA changes in controls were around zero in contrast to TLE patients. Figure 2.2A and C show the subsections of white matter tracts with significant changes in QA (FDR < 0.05; T-score $= 3$) and the three bundles with greater difference in cohen-D between groups. TLE patients showed a greater reduction in QA in the vicinity of the resected tissue, particularly in ipsilateral inferior fronto-occipital fasciculus (IFOF) and uncinate fasciculus (UF). Greater reductions in QA were also observed in ipsilateral corticothalamic pathway (CT) in left TLE patients and anterior commissure (AC) in right TLE patients. The full list of bundles with affected subsections is available in the Tables A.4 and A.5 in Appendix. The results are consistent with different t-score thresholds to select local connectomes and at different significance levels (Figure A.4 and A.5). Figure A.6 shows in more detail the location of the subsections in these bundles.

In addition to the reductions in QA, left TLE patients also showed subsections with significant postoperative QA increases over 3–4 months. Specifically, those increases were found in parts of the ipsilateral corticostriatal pathway (CS) and corona radiata, namely in frontopontine tract (FPT) and corticospinal tract (CST) (Figure 2.2A).

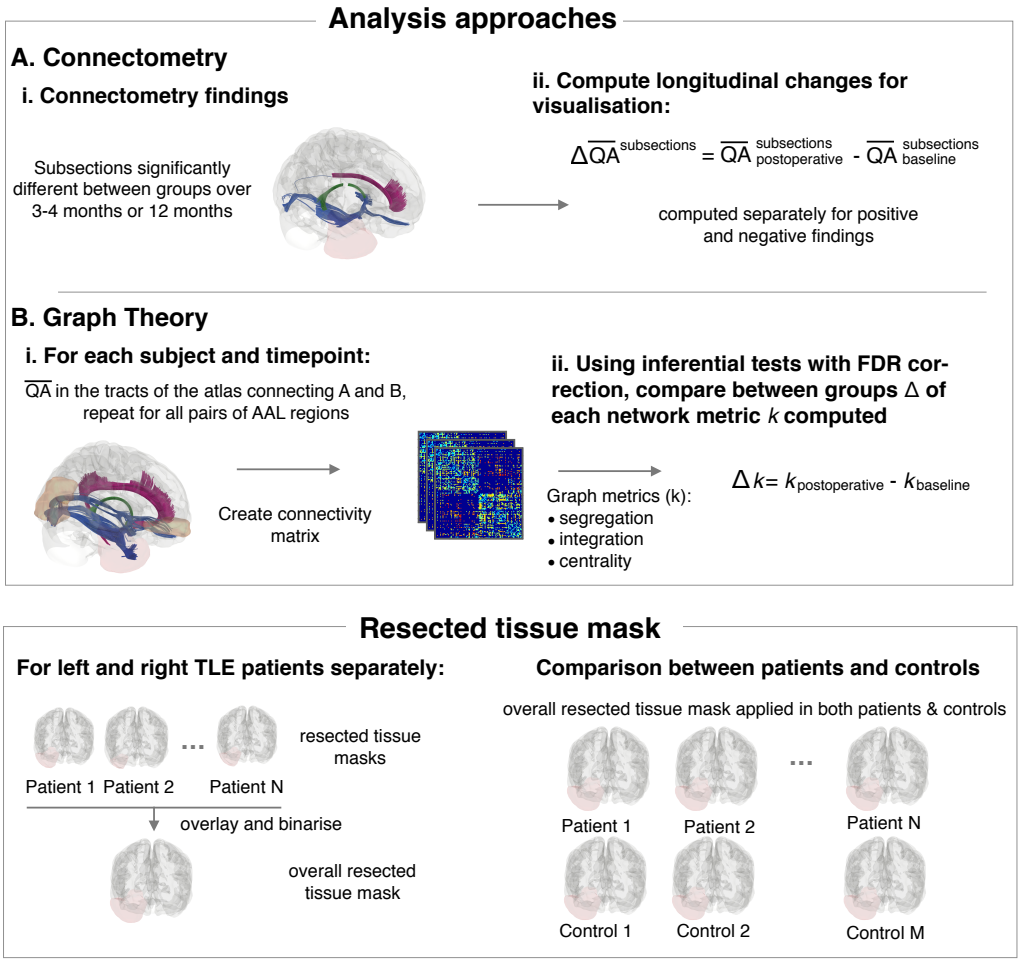


Figure 2.1: Processing pipeline: To compare patient and control groups or patients with different postoperative outcome, two complementary analyses were performed.(A) A connectometry analysis which is sensitive to changes in subsections of bundles was employed to investigate local differences within bundles: Connnectometry identified subsections within bundles in the whole brain where QA changes over time were significantly different between groups.(B) A graph theory approach was applied to integrate connectivity across the wider brain network: To produce connectivity matrices, mean QA along the bundles of the connectome atlas connecting each pair of AAL regions was computed for each subject. Graph theory was used to compare changes in network properties over time. Resected tissue mask: The resected tissue masks of all patients were overlaid in a single mask to be used as region of avoidance in (A) and (B). When comparing patient and control groups, that single mask was applied in both groups to restrict the analyses to the same non-resected brain area.

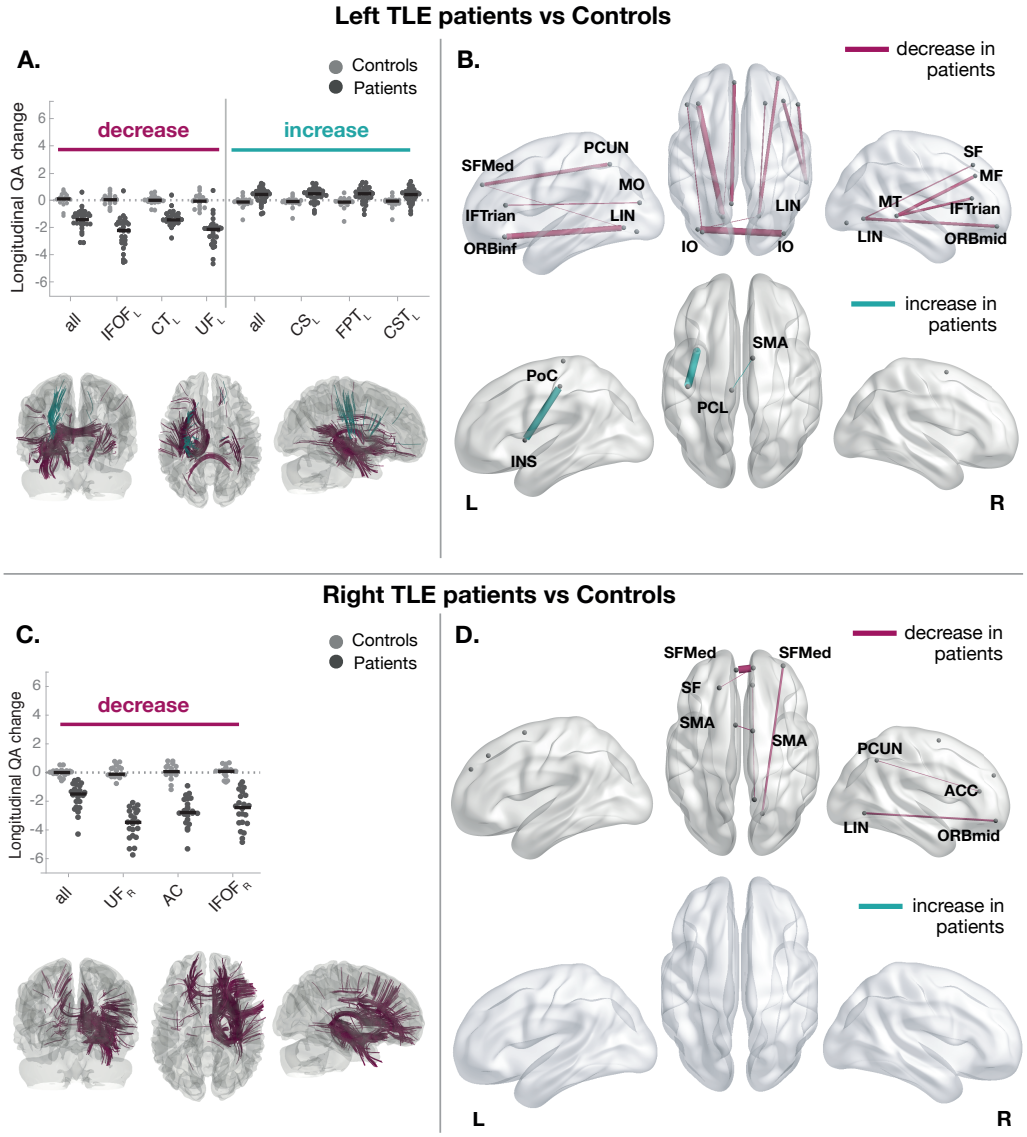

Left TLE patients vs Controls
A.
Controls
Patients
Longitudinal QA change
decrease
increase
all
IFOF L
CT L
UF L
all
CS L
FPT L
CST L
B.
decrease in patients
SFMed
PCUN
MO
IFTrian
LIN
ORBinf
IO
IO
LIN
SF
MF
MT
IFTrian
LIN
ORBmid
increase in patients
PoC
INS
SMA
PCL
L
R
Right TLE patients vs Controls
C.
Controls
Patients
Longitudinal QA change
decrease
all
UF R
AC
IFOF R
D.
decrease in patients
SFMed
SFMed
SF
SMA
SMA
PCUN
ACC
LIN
ORBmid
increase in patients
L
R

Figure 2.2 *(previous page)*: Significant QA changes between controls and TLE patients, before and after surgery, in parts of tracts revealed by connectometry: Significant QA changes in subsections of bundles were found between groups (confirmatory grid point: FDR < 0.05; T-score $= 3$). Subsections of tracts in which patients had a significant QA reduction or increase relative to controls are coloured in purple and green, respectively (A,C). Left and right TLE patients had a greater decrease of QA in ipsilateral IFOF and UF. Greater reductions in QA were also observed in ipsilateral CT in left TLE patients and AC in right TLE patients. Left TLE also showed a greater increase of QA in ipsilateral CS, FPT and CST. The beeswarm plots show the longitudinal changes in QA between groups for all subsections found by connectometry (label all in the plot) and the bundles with greater difference between groups. Each datapoint indicates a single subject. For visualisation purposes, only the three bundles with highest values of cohen-D are presented in the beeswarm plot.(see Tables A.5 and A.6 for complete list). (B,D) The tract bundles where subsections were found to be significantly different by connectometry were determined to estimate the AAL regions those subsections are connecting to. The weight of the connections/edges is proportional to the amount of tracts with altered subsections. For visualisation, only the top 70% of strongest connections are shown. All the connections in which the subsections in Figure 2.2A and C were found are presented in Figures 2.5 and 2.6. ACC - *Anterior cingulum cortex*; CUN - *Cuneus*; ORBinf - *Inferior frontal, orbital*; IFTrian - *Inferior frontal, triangular*; IO - *Inferior occipital*; IT - *Inferior temporal*; INS - *Insula*; LIN - *Lingual*; MF - *Middle frontal*; ORBmid - *Middle frontal, orbital*; MO - *Middle occipital*; MTC - *Middle temporal cortex*; PCL - *Paracentral lobule*; PoC - *Postcentral*; PCUN - *Precuneus*; SF - *Superior frontal, dorsolateral*; SFMed - *Superior frontal, medial*; *SMA - Supplementary Motor Area*

Figure 2.2B and D show the main connections/edges in which the subsections in Figure 2.2A and C were found. The main connections/edges with changes in QA were predominantly ipsilateral in right TLE but more bilateral in left TLE. Left and right TLE patients showed greater reduction between ipsilateral lingual (LIN) and orbitofrontal (ORB) cortices. Left TLE also showed a greater decrease in QA in the interhemispheric connections between occipital lobes as compared to right TLE patients, in which the main altered interhemispheric connections were located in frontal cortex. Furthermore, left TLE patients also showed a greater increase in QA in the connections mainly located between ipsilateral insula (INS) and postcentral (PoC) cortices.

Comparable results were obtained with FA (Figure A.7 in Appendix). Greater FA reductions were also observed in the vicinity of the resected tissue, namely in IFOF and inferior longitudinal fasciculus (ILF) for left TLE and IFOF and UF for right TLE. Similar to QA results, left TLE patients also showed a significantly increased FA in white matter

tracts connecting INS and PoC. Right TLE showed increased FA in CS and temporo-pontine tracts, which was not observed using QA. Greater reductions were observed in interhemispheric and contralateral connections in left TLE patients using QA. However, those alterations were less pronounced using FA.

With respect to changes associated with postoperative seizure-freedom, left TLE patients who were seizure free had a widespread decrease in QA greater than patients with seizure-recurrence ($FDR < 0.05$; $T - score = 3$, $cohen - D = -1.24$) (Figures 2.3 and A.8). As depicted in Figure 2.3A, a greater reduction in QA was observed in IFOF, UF and extreme capsule (EMC)(see Table A.6 in Appendix for complete list). Figure 2.3B depicts the connections where the affected subsections were mainly found, namely between LIN and ORB cortices and inter-hemispheric connections located in the frontal lobe and supplementary motor area (SMA). Figures A.9 and A.10 show the corresponding results for right TLE patients. Figure A.11 shows the corresponding results using FA where greater reductions of FA in seizure-free patients for the tracts connecting contralateral precuneus (PCUN) and anterior cingulate cortex (ACC), which is in agreement with our QA findings.

2.3.2 Surgery-induced changes in network topology

Graph-theory identified surgery-induced changes to graph theory metrics between patients and controls mainly in the ipsilateral side. In the left panels of Figure 2.4A we show those regions with altered metrics in patients relative to controls. Note that voxels within the resection area are excluded for all subjects (including controls) in this analysis to therefore allow visualisation of only the most pronounced changes outside of the resection. Over the first 3–4 months following surgery, only local changes in strength, clustering coefficient, eigenvector and betweenness centrality were significantly different between groups (FDR p-value < 0.005).

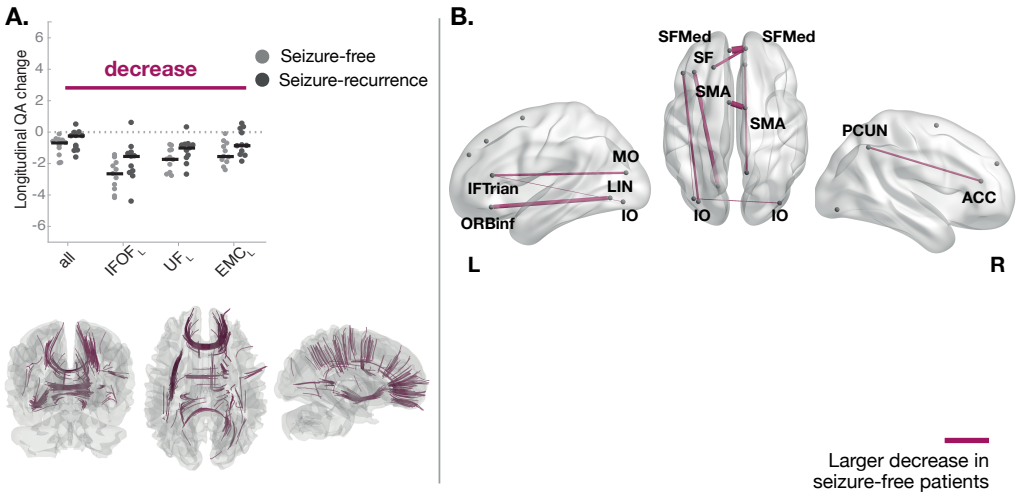


Figure 2.3: Tract sections with QA changes over 3 months associated with postoperative seizure freedom in patients with left TLE: Significant QA changes in subsections of bundles were found between outcome groups (FDR < 0.05; T-score $= 3$). (A) Seizure-free patients had a significantly larger QA reduction over 3–4 months relate to patients with seizure-recurrence in IFOF, UF and EMC. The beeswarm plot shows the longitudinal changes in QA between groups for all subsections found by connectometry (label all in the plot) and the bundles with greater reductions. For visualisation purposes, only the three bundles with the highest cohen's D are displayed. (Table A.6 contains complete list). (B) The tract bundles where subsection were found to be sign different by connectometry were determined to estimate the AAL regions those subsections are connecting to. The weight of the connections/edges is proportional to the amount of tracts with altered subsections. For visualisation purposes, a threshold was applied to hide the edges with a weight less than 30% of the strongest connection. ACC - *Anterior cingulum cortex*; ORBinf - *Inferior frontal, orbital*; IFTrian - *Inferior frontal, triangular*; IO - *Inferior occipital*; *LIN – Lingual*; MO - *Middle occipital*; PCUN – *Precuneus*; SF - *Superior frontal, dorsolateral*; SFMed - *Superior frontal, medial*; SMA - *Supplementary Motor Area.*

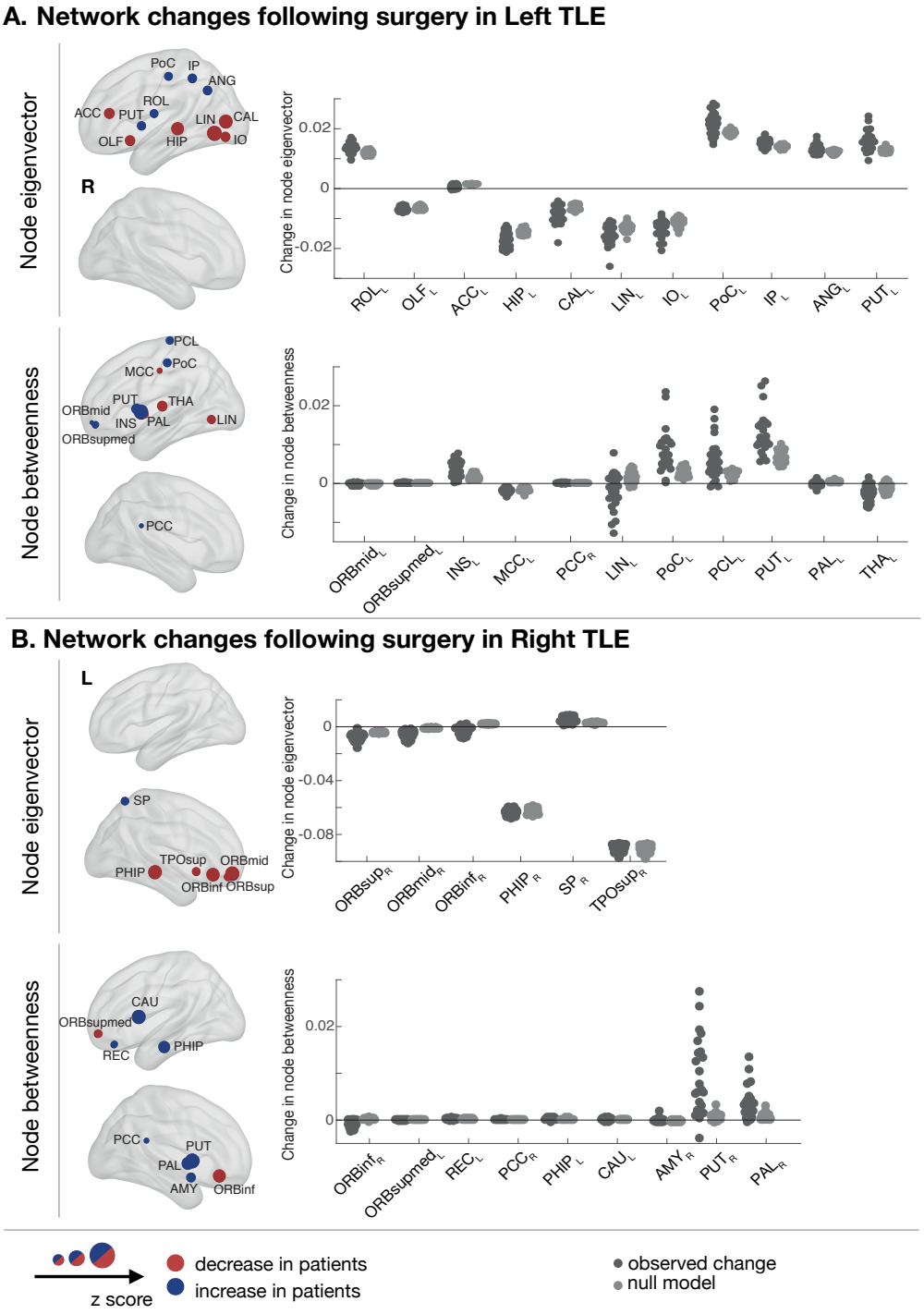

A. Network changes following surgery in Left TLE
Node eigenvector
PoC
IP
ANG
ROL
ACC
PUT
LIN
CAL
OLF
HIP
IO
R
Change in node eigenvector
0.02
0
-0.02
ROL_L
OLF_L
ACC_L
HIP_L
CAL_L
LIN_L
IO_L
PoC_L
IP_L
ANG_L
PUT_L
Node betweenness
PCL
PoC
MCC
PUT
THA
ORBmid
INS
PAL
LIN
ORBsupmed
PCC
Change in node betweenness
0.02
0
ORBmid_L
ORBsupmed_L
INS_L
MCC_L
PCC_R
LIN_L
PoC_L
PCL_L
PUT_L
PAL_L
THA_L
B. Network changes following surgery in Right TLE
Node eigenvector
L
SP
TPOsup
ORBmid
PHIP
ORBinf
ORBsup
Change in node eigenvector
0
-0.04
-0.08
ORBsup_R
ORBmid_R
ORBinf_R
PHIP_R
SP_R
TPOsup_R
Node betweenness
CAU
ORBsupmed
PHIP
REC
PCC
PUT
PAL
AMY
ORBinf
Change in node betweenness
0.02
0
ORBinf_R
ORBsupmed_L
REC_L
PCC_R
PHIP_L
CAU_L
AMY_R
PUT_R
PAL_R
z score
decrease in patients
increase in patients
observed change
null model

Figure 2.4 *(previous page)*: Changes over 3 months in node eigenvector and node betweenness centrality between patients and controls: The AAL regions that showed significant differences in node centrality between patients and controls over 3 months are represented by a node/circle and overlaid within a brain volume. Nodes coloured in blue show the AAL regions where patients had an increase in node eigenvector/betweenness centrality in comparison to controls over 3 months. Nodes coloured in red show the AAL regions in which patients had a significant reduction in eigenvector or betweenness centrality in comparison to controls. Scatter plots show the observed and predicted (null model) change in patients after surgery for those AAL regions. Positive values suggest an increase of eigenvector or betweenness centrality following surgery. The scatter plots therefore compare the impact on centrality measures of the surgical resection alone with the overall changes seen post-operatively. A table with the names and abbreviations of all regions can be found in Table A.7. ACC – *Anterior cingulum cortex*; AMY – *Amygdala*; ANG – *Angular*; CAL – *Calcarine*; CAU – *Caudate*; HIP – *Hippocampus*; INS – *Insula*; IO – *Inferior occipital*; IP – *Inferior parietal*; LIN – *Lingual*; MCC - *Middle cingulum*; OLF – *Olfactory*; ORBinf - *Inferior frontal, orbital*; ORBmid - *Middle frontal, orbital*; ORBsup - *Superior frontal, orbital*; ORBsupmed - *Superior frontal, medial*; PAL – *Pallidum*; PCC - *Posterior cingulum*; PCL – *Paracentral lobule*; PHIP – *Parahippocampal*; PoC – *Postcentral*; PUT – *Putamen*; REC – *Rectus*; ROL - *Rolandic operculum*; SP – *Superior parietal*; THAL – *Thalamus*; TPOsup – *Superior Temporal Pole*

To support the interpretation of these results, scatter plots in Figure 2.4 show the observed and predicted changes in patients by the observed and null model, respectively. Although widespread reductions and increases of network metrics were identified by the null and observed model, we only plotted the changes for a set of network metrics, which showed a significant longitudinal difference between patients and controls over 3–4 months following surgery (i.e. corresponding to those regions in the left panels).

Node eigenvector centrality measures the influence a region has on a network. When removing a region in full or partially, nodes connected to that region or with neighbours connected to it might lose influence on the network. Longitudinal changes in node eigenvector centrality were ipsilateral for both left and right TLE. In left TLE, a decrease in node eigenvector centrality in patients in comparison to controls was observed in hippocampus (HIP), olfactory (OLF), ACC and occipital lobe, namely in LIN, calcarine (CAL) and inferior occipital cortex (IO). These changes were expected by the null model and a significant decrease in QA in the white matter tracts connected to LIN, CAL, IO and ACC was also observed using connectometry (Figure 2.5). Therefore, these

regions and/or their neighbours were likely to be connected to the resected tissue or having connections passing through it. An increase of eigenvector centrality was also observed in putamen (PUT), rolandic operculum (ROL), and parietal lobe. Similarly, these changes were expected by the null model. However, PoC and PUT showed a much higher increase postoperatively than the one predicted by the null model, suggesting a possible reorganisation to reinforce these regions to pass shortest topological paths. This is supported by connectometry results, in which PoC and PUT tracts showed a significant QA increase over time (Figure 2.6). In right TLE, a decrease of node eigenvector centrality, node clustering coefficient and strength were observed in ORB cortex and temporal lobe (Figures 2.4 and A.12). Those changes were expected by the null model and some of these regions showed a significant QA reduction in their connections (Figure 2.6). Similarly to left TLE, these regions and/or their neighbours were likely to have connections passing or ending in the resected area.

Node betweenness centrality measures how important a region is by virtue of being on shortest paths between other regions: i.e. in integrating information across the network. When removing a region in full or partially, the shortest path between regions can change by traversing other areas. Thus, the betweenness centrality in this region can either increase or decrease following surgery (Taylor et al. (2018)). As depicted in Figure 2.4, changes in node betweenness centrality were mainly ipsilateral and more widely distributed in left TLE patients, while in right TLE were bilateral and mainly in central structures. A decrease of node betweenness were observed for ipsilateral thalamus, middle cingulum in left TLE and ORB cortex in right TLE. The decrease of betweenness centrality in these regions is expected by the null model (Figure 2.4, right panel). A significant QA reduction of these regions' connections is also shown by connectometry in Figure 2.6. Therefore, these regions were likely to be connected to the resected tissue or having connections passing through it. In addition, LIN also showed decreased node betweenness centrality in left TLE in comparison to controls. Although by the null model it was expected an increase of betweenness centrality, it was observed a reduction by the observed model (Figure 2.4, right panel). Connectometry also showed a significant QA reduction of connections between LIN to/from ORB cortex. This suggests secondary degeneration of LIN connec-

tions not assessed by the null model or brain reorganization. With disconnection of some tracts following surgery, the shortest paths redirect and might also lead to increase of node betweenness centrality. Left TLE patients showed increase of node betweenness in ipsilateral ORB cortex, PoC, INS, paracentral lobule, PUT, pallidun (PAL) and contralateral posterior cingulate cortex (PCC). In contrast, right TLE patients showed increased node betweenness centrality in parahippocampal, gyrus rectus, PCC and several central structures such as PUT, PAL, caudate and amygdala. Most of the regions showing an increase of betweenness centrality in left TLE also showed significantly increased QA in their white matter tracts to other regions, namely ipsilateral PoC, paracentral lobule (PCL), INS and PUT. In the observed change model those regions showed an increase of betweenness centrality greater than expected, suggesting possible reinforcement of those regions to be involved in the shortest paths. In right TLE, the observed model also showed an increase of betweenness centrality much higher than the null model for ipsilateral PAL and PUT. Although a significant increase of QA in their connections was not observed using connectometry, it is likely that other white matter alterations occurred in neighbouring nodes leading to a reinforcement of their role on passing shortest paths.

No longitudinal changes in network topology after the surgery were found to be significantly different between TLE patients with different postoperative outcomes of seizure-freedom.

2.4 Discussion

In this study we performed a comprehensive investigation of longitudinal white matter QA changes after epilepsy surgery and their association with postoperative seizure freedom. In the 3–4 months after surgery, we found surgery-induced changes in white matter and network topology in the temporal lobe and beyond.

First, surgery induced longitudinal white matter changes were primarily ipsilateral in right TLE but more bilateral in left TLE. The largest post-operative reductions in QA, likely related to primary Wallerian degeneration, were in tracts which were transected by surgery (ipsilateral UF and IFOF). Decreased node eigenvector and betweenness centrality was therefore expected and observed in regions partially resected and/or connected to the resected tissue. Secondary processes may also explain further reductions in QA, namely in white matter tracts connecting LIN and orbitofrontal cortices.

Secondly, left TLE patients showed increased QA in cortico-striatal and corona radiata tracts, likely related to improvements in verbal fluency (Yogarajah et al. (2010)). These tracts mainly connect the PoC gyrus and INS, which both showed a higher increase of betweenness centrality after surgery than expected by the null model, suggesting possible strengthening of these connections.

Thirdly, with respect to postoperative seizure outcome, left TLE seizure-free patients showed greater QA reductions compared to seizure-recurrence patients in interhemispheric connections in frontal lobe and tracts transected by surgery (ipsilateral UF and IFOF). Seizure-freedom was not significantly related to alterations in the network topology or resection volume.

2.4.1 Surgery-related effect on white matter

More bilateral and widespread white matter disruptions have been reported in patients with left TLE as opposed to right TLE using preoperative data (Ahmadi et al. (2009); Kemmotsu et al. (2011); Besson et al. (2014)). Following the surgery, left TLE patients also had more bilateral disruptions in white matter than right TLE 3–4 months after surgery (Figures 2.5 and 2.6), suggesting different mechanisms of degeneration.

Our observation of reduced QA in tracts close to the resection area agrees with previous literature. Specifically, postoperative reductions in UF and IFOF have been described by McDonald et al. (2010), Yogarajah et al. (2010) and Winston et al. (2014). As in our study, Yogarajah et al. (2010) also reported a decrease in AC following surgery in right TLE patients, which may be explained by larger right-sided resections compared to smaller left-sided resections. Furthermore, reduced QA might have also been explained by secondary degeneration. An increase of betweenness centrality was expected in the LIN as shortest paths were expected to be rerouted to this node by the null model. However, in postoperative data we observed a decrease of betweenness centrality, supported by a reduction of QA in its connections to orbitofrontal cortex. Atrophy propagation through white matter or reorganisation to reroute shortest paths due to the loss of function of LIN and neighbouring regions following surgery, could explain a secondary degeneration in this region. Atrophy propagation has been analysed in the context of neurodegeneration using models such as the cascading failure model (Jones et al. (2016)) and network-diffusion model (Raj et al. (2012)), which could be used in future studies for a better understanding of neurodegeneration pre- and post-resective surgery. Reduced QA, a measure of fibre volume fraction and highly correlated with FA, can be caused by Wallerian degeneration as surgery disconnects white matter tracts, potentially causing myelin degradation and reduction in axonal packing (Concha et al. (2007)). We build on this by demonstrating that there are substantial changes beyond normative changes over the same time period. The results are also spatially similar to those obtained with FA. A reduction of FA suggested axonal damage or Wallerian degeneration and demyelination 3 months following the surgery.

In addition to previously described QA reductions, we found QA increases in corticopontine tracts, CS and CST. Winston et al. (2014) reported a significant increase in FA following ATLR in the corona radiata, which includes tracts from CST and corticopontine bundles. Following a mean of 4.5 months after ATLR, Yogarajah et al. (2010) also reported a significant increase in FA in CST and corticopontine tracts associated with increased verbal fluency, suggesting it was related to early structural plasticity of language networks. Furthermore, the affected subsections found in these bundles involved INS, a

network hub for perception of speech and receptive and expressive language (Oh et al. (2014)). Insula showed a significant increase in betweenness centrality following surgery as expected by the null model. However, in our postoperative data we saw an even higher increase than expected, suggesting reinforcement of the redistribution of shortest paths through this hub for language recovery (Figure 2.4). As connections to/from the posterior part of the INS might be resected in ATLR (Taylor et al. (2018)), future research should examine if larger resections of insular connections lead to worse language recovery after surgery. In agreement with our findings, McDonald et al. (2010) also reported an increase in CS, although in their study of 9 patients it did not meet significance $p = 0.079$. Corticostriatal pathways are related with the limbic system (Shipp (2017)), thus an increase in QA might be related with structural plasticity. Connectometry results showing an increase in FA were spatially similar to those using QA, namely in CS and corticopontine bundles. An increase of FA might be due to several mechanisms including increased myelination, axon diameter, fiber density or changes in axonal membrane structure (Moore et al. (2017)). However, in this study, a plausible mechanism underlying the observed FA increase and, possibly, QA increase, is remyelination. Using the same dataset as in this study, Yogarajah et al. (2010) reported increased axial diffusivity (AD) and decreased in radial diffusivity (RD) in the same tracts showing an increased FA and QA in our study. Axonal recovery preceded by remyelination is suggested by increased AD with decreased RD. This process is often associated with a gradual increase in FA Moore et al. (2017), as seen in Yogarajah et al. (2010).

Since connectometry isolates only the affected segment of the tract, it achieves greater statistical sensitivity. In contrast, graph-theory may only detect significant changes in a node/region when there is a considerable amount of nearby affected connections (Yeh et al. (2018)). Figures 2.5 and 2.6 integrate the results from graph theory and connectometry in terms of the AAL regions involved in white matter longitudinal changes. AAL regions showing changes in network topology are consistent with the AAL regions connected by tracts with greater affected subsections. However, connectometry also detected affected subsections in tracts connecting other regions. Taylor et al. (2018) inferred the impact of surgical resection on network topology using preoperative data as in the null model in this

study. Similarly to our study, Taylor et al. (2018) reported widely distributed increases in betweenness centrality, suggesting rerouting of shortest paths and strengthening of tracts to avoid cognitive deficits. Comparing null model with the postoperative data, we observed that rerouting of shortest paths occurs similarly to the null model. However, strengthening of some white matter tracts leads to a reinforcement of the rerouting for some regions, namely in putamen in left and right TLE and INS, PoC and paracentral lobule in left TLE. A weakening of the expected white matter tracts to reroute was also observed either due to atrophy propagation or reorganization.

In terms of timescale of the imaging, our analysis is performed during the chronic phase several months after surgery as were most others (McDonald et al. (2010); Li et al. (2019c); Winston et al. (2014)). Our findings of no substantial QA changes between 3 and 12 months is in agreement with previous studies (McDonald et al. (2010)), suggesting the largest changes occur within the first months after surgery. However, the lower sample size of 12 month imaging may also contribute to the lack of significant results during this time.

2.4.2 White matter alterations associated with post-surgery seizure relapse

We observed postoperative QA decreases 3–4 months after surgery associated with postoperative seizure freedom, which has not been shown previously to our knowledge. We found that greater chances of postoperative seizure freedom relate to greater QA reductions in interhemispheric connections and in the vicinity of resection area (Figure 2.3). The greater reductions in seizure free patients may be explained by larger resection volume (Shamim et al. (2009)). However, in our cohort the resection masks were consistent across patients (Appendix: section A.7) and no significant differences were observed in total resection volume between patients with different outcomes. When regressing out the resection volume, connectometry results still show greater reductions in seizure free patients in these bundles (Figure A.13 in Appendix). Nevertheless, small variations in the extent of resection, especially in piriform cortex, might have driven larger reductions in QA. Galovic et al. (2019) recently reported that if surgery included the piriform cortex, there was a greater chance of seizure freedom. In right TLE, we found widespread differ-

ences between outcome groups in subsections of tracts. However, given the small sample size for right TLE outcomes we caution against overinterpretation of this result.

With respect to the network topology, the affected subsections of tracts significantly different between groups did not contribute to changes in the network topology. Preoperatively, seizure-freedom has been associated with hub redistributions and reduced local efficiency, which might reduce the spread of epileptic discharges (Ofer et al. (2019)). Taylor et al. (2018) inferred the impact of surgical resection on network topology and reported a reduction in local efficiency. Similar to the present study, reductions in node local efficiency were not associated with postoperative seizure-freedom. Using machine learning, Taylor et al. (2018) reported that changes in the number of tracts between some regions in frontal and temporal lobes were predictive of seizure freedom. Similarly, we observed a reduction in QA in connections in the temporal and frontal lobes using connectometry. Furthermore, we also report greater reductions in inter-hemispheric connections in frontal and occipital lobe. Inferring the impact of surgical resection in preoperative data, as in Taylor et al. (2018), does not allow to take into account secondary degeneration or plasticity. This might explain why in our longitudinal study we also report greater reductions in inter-hemispheric connections.

2.4.3 Limitations

Our study has some limitations that should be considered. First, we only analysed changes over time which were made possible by the longitudinal aspect of our data. We did not compare our findings to cross sectional pre- or post-operative diffusion MRI data which may, in isolation, explain postoperative seizure-freedom (Keller et al. (2017); Bonilha et al. (2013); Bonilha and Keller (2015); Bonilha et al. (2015)). Future studies could investigate pre- and postoperative networks, in addition to the changes in those networks as described here. Second, we only measured network changes in absolute terms without normalising by the baseline value. Future studies should also include relative measures, especially if the variance of the baseline values between groups is high. Third, our sample size - although fairly large compared to other similar studies of white matter postoperative changes - is small for our analysis of post-surgical patient outcomes (group size: Left TLE

- 11 seizure-free and 11 seizure-recurrence; Right TLE - 5 seizure-free and 12 seizure-recurrence). A way to boost sample size is to perform an ipsi- and contralateral analysis as in some previous studies (Seidenberg et al. (2005)). However, given that right-sided resections are substantially larger than left sided-resections we chose not to do that here - further supported by the different findings ipsilateral to left and right TLE. Fourth, our sample size for 12 month scans is limited to only 13 patients. Finally, when estimating the mean change in QA/FA per bundle between groups, we did not account that bundles with longer and more streamlines may have a higher probability to have more altered subsections and thus, mean values of QA/FA might be smoother in those bundles in comparison to other ones with less and shorter streamlines.

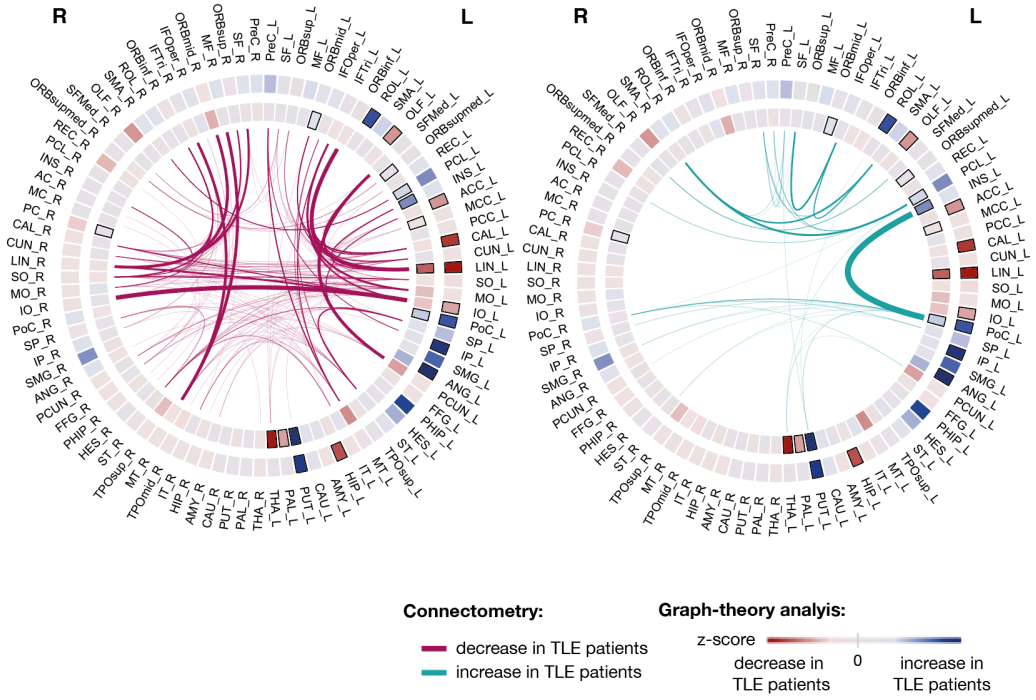


Figure 2.5: Connectogram comprising the surgery induced changes detected by graph-theory and connectometry in left TLE patients: Graph theory: Graph-theory changes between patients and controls are displayed in the circles. The outer and inner circle indicates the z-score between groups for eigenvector and betweenness centrality, respectively. Z-score values are represented by a red-blue gradient, in which red indicates the minimum calculated z-score and blue the maximum value. Z-score for node eigenvector changed between -2.35 and 1.17 and z-score for node betweenness between -1.83 and 3.15. The black rectangles indicate the AAL regions with significant change in node eigenvector or node betweenness centrality after FDR correction. Connectometry: The connections with significant changes in their subsections as identified by connectometry are displayed in the centre. The weight of the connection is proportional to the amount of streamlines in which QA changes were detected. A table of AAL region names and abbreviations can be found in Table S8.

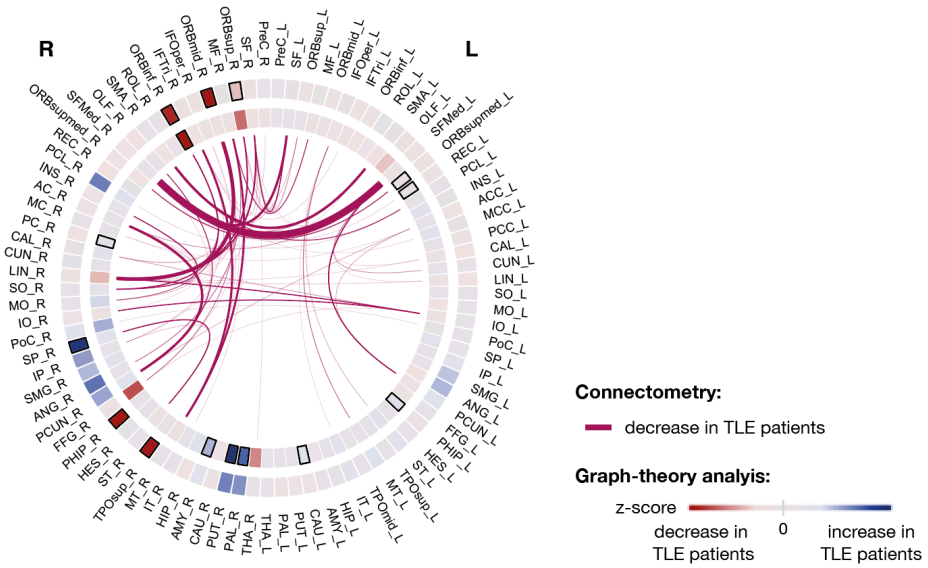


Figure 2.6: Connectogram comprising the surgery induced changes detected by graph-theory and connectometry in right TLE patients: Graph theory: Graph-theory changes between patients and controls are displayed in the circles. The outer and inner circle indicates the z-score between groups for eigenvector and betweenness centrality, respectively. Z-score values are represented by a red-blue gradient, in which red indicates the minimum calculated z-score and blue the maximum value. Z-score for node eigenvector changes between -4.13 and 1.89 and z-score for node betweenness between -2.02 and 2.50. The black rectangles indicate the AAL regions with significant change in node eigenvector or node betweenness centrality after FDR correction. Connectometry: The connections with significant changes in their subsections as identified by connectometry are displayed in the centre. The weight of the connection is proportional to the amount of streamlines in which QA changes were detected. A table of AAL region names and abbreviations can be found in Table S8.

Chapter 2: Network Reorganisation Following ATLR and its Relation with Seizure Relapse

Chapter 3. Changes in Network Structure Following Mild TBI and its Association with Cognitive Recovery

Contents

3.1 Introduction 50

3.2 Methods 52

3.2.1 Data acquisition and subjects 52

3.2.2 DWI data processing 52

3.2.3 Lesions probability map 54

3.2.4 Components of cognitive function 56

3.2.5 Network metrics selection and association with cognitive function . 57

3.2.6 Experimental design and statistical analysis 58

3.3 Results 60

3.3.1 Network-based metrics of mTBI 60

3.3.2 Cognitive function assessment 60

3.3.3 Longitudinal relationships between network-based metrics of mTBI and cognitive functions 61

3.4 Discussion 66

3.4.1 Areas associated with cognitive function 66

3.4.2 Network topology changes over time after mTBI 68

3.4.3 Limitations 69

3.1 Introduction

Traumatic brain injury (TBI), which frequently involves white matter connectivity damage, is the leading cause of morbidity, death among children, and individuals under the age of 45 (Forsyth and Kirkham (2012); Werner and Engelhard (2007)). Every year in England and Wales, around 1.4 million patients attend hospital after sustaining a recent head injury, which represents 10% of all emergency admissions (Lawrence et al. (2016)). Although, mild TBI (mTBI) patients usually make good recoveries, a significant proportion experience persistent cognitive deficits (Carroll et al. (2004)).

Diffuse axonal injury (DAI), one of the most common pathologies in traumatic brain injury (TBI) (Smith et al. (2003); Newcombe et al. (2016)), is triggered by mechanical disruption of axons, resulting in complex, and diverse effects on brain function as explained in detail in Chapter 1 (Sharp et al. (2014)). Diffusion-weighted imaging (DWI) is particularly suited to the study of diffuse axonal injury (DAI) and has been used to investigate white matter brain connectivity changes after TBI (Dall'Acqua et al. (2017); Fagerholm et al. (2015)). To understand how widespread DAI lesions affect brain function, it may be necessary to analyze the global impact of these lesions on the whole-brain network (Fagerholm et al. (2015)).

Interpreting widespread network changes is challenging. Graph theory allows the description and analysis of human brain network properties and have successfully been applied in cognitive neuroscience (Fagerholm et al. (2015); Aerts et al. (2016); Bullmore and Bassett (2011)). As referred in Chapter 1, this technique can use anatomically defined gray matter regions as nodes and a measure of association (e.g., number of tracts, mean diffusion along tracts, etc.) between pairs of nodes based on the white matter tracts or edges connecting them (Bullmore and Sporns (2009)). Those tracts can be estimated from tractography techniques or extracted from white matter atlases. All pairwise associations between regions are compiled in a connectivity matrix. The approach offers alternative analysis of how brain network changes may lead to cognitive variability over time.

Several cross-sectional studies have already identified alterations in the global connectome following milder injuries in comparison to controls (Dall'Acqua et al. (2016); Van

Der Horn et al. (2017); Yuan et al. (2017)). As mentioned in Chapter 1, TBI is a heterogeneous disorder with a dynamic behavior thus, longitudinal studies are vital to capture brain changes over time, and establish longitudinal relationships (Solem (2015); Cole et al. (2018)). Dall'Acqua et al. (2017) found structural hyperconnectivity in a subnetwork including cingulate cortex in which normalisation over time was associated with recovery of working memory, attention and verbal recall in mTBI patients. More recently, Kuceyeski et al. (2019) found an increase in structural connectome integration over time associated with mTBI recovery. Additionally, the authors assessed how alterations in strength at node level can affect patients' recovery. More studies are needed to evaluate how longitudinal alterations in the connectome at both global and node level may work as future biomarkers and its association with long-term recovery. More importantly, it may be relevant to understand the predictive power for recovery of the trajectories of alterations in specific brain regions.

In this study, we identified brain network properties at global and local level that change over the first 12 months after a mild TBI using longitudinally acquired data and investigated if these properties relate to changes in cognitive functioning. Thus, we addressed the following questions: Does mTBI induce longitudinal alterations in network topology? Do these changes relate to cognitive performance?

3.2 Methods

3.2.1 Data acquisition and subjects

Twenty-three TBI patients were scanned twice on a 3T magnetic resonance imaging (MRI) scanner (Phillips Achieva MRI) initially a mean of 6 days after injury (early phase) and again 1 year later (late phase) (Figure B.1 in Appendix). The study protocol consisted of structural T1-weighted sequences [magnetization-prepared rapid-acquisition gradient echo, repetition time (TR) = 8.1 ms, echo time (TE) = 4.6 ms, matrix size 240x216x180, isotropic 1 mm resolution] and diffusion-weighted images (TR/TE = 2,524/71 ms; 24 slices; b = 0; 1000 s mm-2; 16 diffusion directions; 2x2x6 mm3 resolution), and it was consistent across all sessions. Acquisition methods have been described previously, as has the effect of injury on the basic DWI-derived metrics in these same participants (Croall et al. (2014)). Patients were classified as mild or moderate TBI based on Glasgow Coma Scale (GCS). Five patients had moderate TBI [GCS: median = 12, IQR = 10-12] and 18 had a mild TBI (GCS: median = 14, IQR = 14-15) (Table 1). Twenty-eight healthy controls matched for age, gender, level of education, and National Adult Reading Test (NART), a proxy for pre-injury educational status, were scanned once. Detailed description of imaging protocols and subject's clinical data (e.g., age, gender, level of education, NART, injury mechanism, GCS, loss of consciousnes (LOC), and post-traumatic amnesia (PTA)) can be found in Croall et al. (2014) and in Appendix (Tables B.1, B.2, B.3).

3.2.2 DWI data processing

Fiber orientation reconstruction was carried out using FMRIB Diffusion Toolbox to create fractional anisotropy (FA) images. FA images were then normalized to standard space by a combination of linear and non-linear transformations (Figure 3.1) (Jenkinson et al. (2012)). All registrations were visually inspected. In standard space, tracts from the recently published structural connectome atlas space were projected to each individuals' FA image using DSI Studio (`http://dsi-studio.labsolver.org`) (Yeh et al. (2018)). This atlas contains 550,000 white-matter tracts verified manually by experienced neu-

Clinical data	Controls	mild TBI Patients	moderate TBI Patients	all TBI Patients	Controls vs Patients
GCS	-	Med = 14 IQR = 14-15	Med = 12 IQR = 10-12	Med = 14 IQR = 13.5-15	-
LOC (min)	-	Med = 1 IQR = 0-4.5	Med = 3 IQR = 1-10	Med = 1 IQR = 0-5	-
PTA (h)	-	Med = 0 IQR = 0-1.75	Med = 4 IQR = 1-240	Med = 0.5 IQR = 0-3	-
NART	Med = 112.5 IRQ = 106.8-115	Med = 105.5 IQR = 92.5-116	Med = 105 IQR = 105-105	Med = 105 IQR = 93-105	p = 0.053
Age	Med = 37.5 IRQ = 27.25-51	Med = 35.5 IQR = 26.8-48.5	Med = 38 IQR = 24-53	Med = 36 IQR = 25-51	p = 0.933
Level of Education	Med = 10 IRQ = 9-14	Med = 9 IQR = 9-14	Med = 9 IQR = 9-14	Med = 9 IQR = 9-14	p = 0.868
Sex	22 (M) 6 (F)	15 (M) 3 (F)	3 (M) 2 (F)	18 (M) 5 (F)	p = 1

p value at an alpha value of 0.05; LOC - Loss Of Consciousness); PTA - Post-Traumatic Amnesia.

Table 3.1: Clinical data of controls and patients with mild or moderate TBI. The p-values of the statistical tests to compare if both groups (controls vs patients) matched in NART, age, level of education or gender are presented in the last column.

roanatomists. Mean FA along the paths between each of the 90 regions of the Automated Anatomical Labelling (AAL) atlas were computed and saved in a connectivity matrix for each individual. This approach is inspired by a previous TBI study (Squarcina et al. (2012)).

Network metrics were estimated from the connectivity matrices to quantify network integration, segregation, centrality, and resilience to perturbations, properties related to cognitive processes (Rubinov and Sporns (2010); Farahani et al. (2019); Lord et al. (2017)). A detailed description of all network metrics is available in Table B.4 in the Appendix. Network integration and segregation measures describe the ability of a network to integrate information from distributed regions and the ability for local specialized information processing, respectively. Examples of those metrics are strength (the sum of all connection strengths to a given region), local clustering coefficient (measure the connectedness of neighbours of a region), local efficiency (the inverse of the average shortest path length of a node to their nodes), local assortativity (measure the contribution of a region to maintain the integration of information in the network after disruption), eigenvector and page rank centrality (measure the influence of a region has on a network), betweenness centrality (measure how often a region is traversed by the shortest paths in the network), and closeness centrality (measure the average shortest path of a region to all other regions in the network). More detailed descriptions are provided in Rubinov and Sporns (2010).

3.2.3 Lesions probability map

Lesion masks were manually drawn for 19 patients by a neurosurgeon on the baseline scans, as described in Aribisala et al. (2014). Lesion masks are defined as a binary mask where the lesioned voxels are labeled as 1 and the remaining voxels are labeled as 0. The masks include any visible contusion, hematoma, or edema. Visible lesions were not present for the remaining four patients. Lesion masks were then co-registered to the MNI-152 space using the warp fields of T1-MRI registration to standard space, which was conducted with linear and non-linear transformations in FMRIB software library (FSL) (Jenkinson et al. (2012)).

To create a probability map, lesion masks were summed, and normalized to 0–100% range

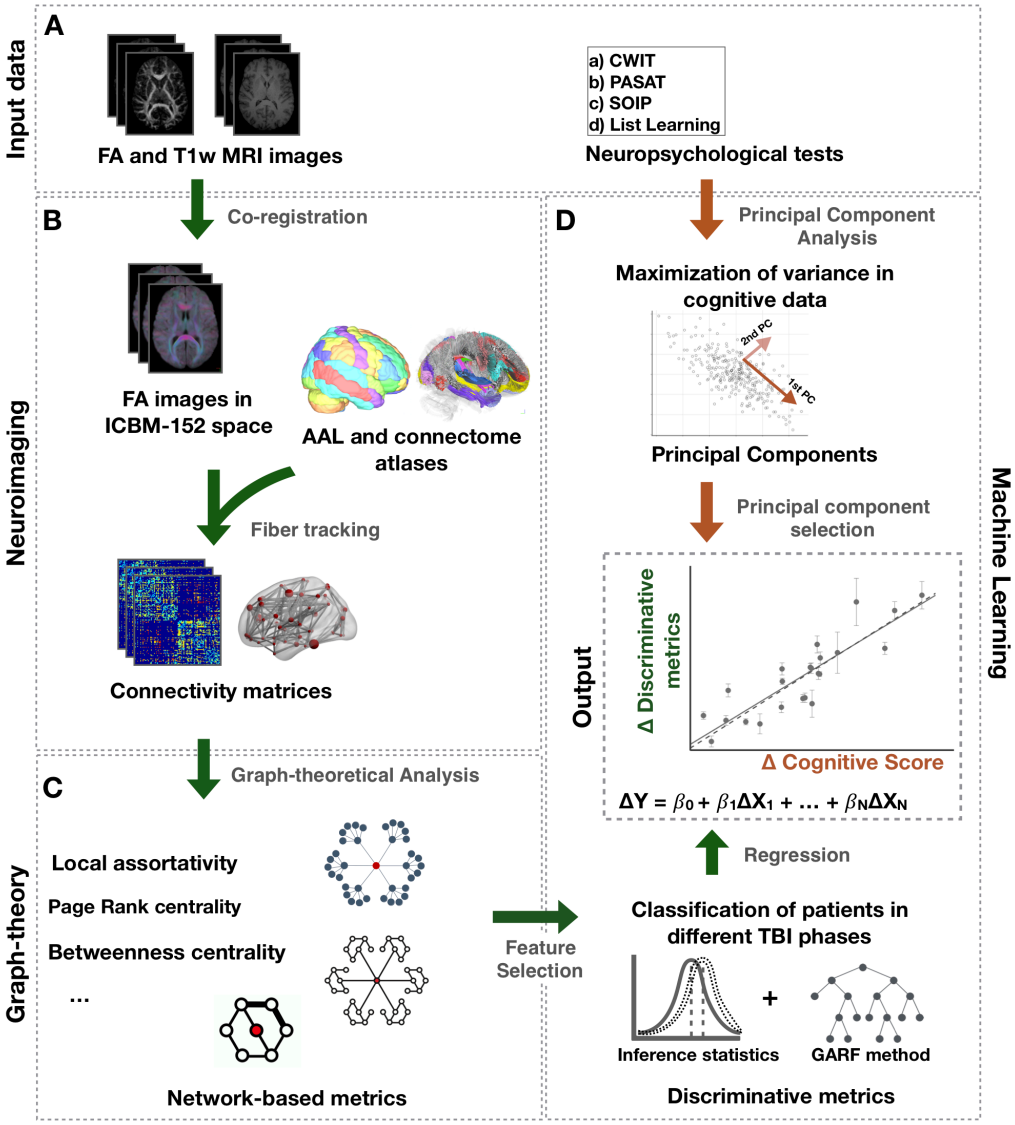


Figure 3.1: Processing pipeline. (A) Input data comprise FA and T1-weighted images and neuropsychological tests. (B) Connectome and AAL atlases were mapped to each individual FA image in ICBM-152 space. Mean FA along the tracts of the connectome atlas between the AAL regions was computed to create a connectivity matrix for each individual. (C) Network metrics were calculated from those matrices. (D) Statistical tests and GARF were used to classify patients in different TBI post-injury phases and, thus, identify the network metrics assessing changes following TBI. The change over time of those metrics, ΔX, were further investigated to explain changes in cognitive function, ΔY, using regression models. The change in cognitive function, ΔY, represents the change of the principal components obtained after applying PCA to the neuropsychological tests.

with 100% (0%) indicating the presence of a lesion in all patients. Due to the heterogeneity of TBI, we applied a threshold to keep the most prevalent lesions and remove more sporadic ones. Therefore, only the lesions observed in at least three patients were considered as in voxel-based lesion-symptom mapping Pisoni et al. (2018).

We additionally calculated the Sørensen–Dice similarity coefficient to measure the overlap/similarity ratio of the Lesions Probability Map as an region of interest (ROI) with each AAL ROIs. This allowed us to inspect the impact of injuries to the observed changes in network metrics at a region level in our cohort.

Dice overlap $= \frac{2*N(X \bigcap Y)}{N(X)+N(Y)}$

with X and Y being the paired images to be overlapped and N the number of voxels. Sørensen–Dice similarity coefficient is a common metric used to assess medical image segmentation (Taha and Hanbury (2015)) and was used previously (Moreira da Silva et al. (2017)).

3.2.4 Components of cognitive function

Patients and controls underwent a full battery of standardized neuropsychological tests sensitive to cognitive impairments in mild TBI at each time of scanning. The tests included assessments of attention, memory, executive functions, and semantic knowledge. Due to missing data for some follow-up assessments, we restricted our analysis to the following tests: Speed of Information Processing (SOIP), Paced-Auditory-Serial-Addition Test (PASAT), D-KEFS Color-Word-Interference Test (CWIT), and List Learning (Delis et al. (2012); Gronwall (1977); Coughhlan, AK et al. (2007)). Early and late post-injury neuropsychological scores were compared with controls by inferential tests with false discovery rate (FDR) correction.

Following Irimia et al. (2012) and Kuceyeski et al. (2011), principal components analysis (PCA) was used to combine multiple cognitive scores in a set of principal components that maximize the variance of the neuropsychological tests and represent main cognitive functions. Since PCA is sensitive to skewness (Hubert et al. (2009)), cognitive scores with z-skewness higher than 1.96 were prior transformed using Box-Cox transformation (Rigon

et al. (2017)).

3.2.5 Network metrics selection and association with cognitive function

We conducted a two-step feature selection to identify the most discriminative network metrics between different TBI phases using R (`http://caret.r-forge.r-project.org/`). This allowed us to identify a set of network metrics that changed over time and we interpreted as being causally related to the injury. Since the two-step feature selection was a cross-sectional analysis, a sample size of 46 was used (i.e., 23 samples for each TBI phase/time point or class).

Finally, using a regression model, we investigate how changes in those network metrics may be predictive of cognitive function over time.

Connectivity metrics of mTBI

Initially, we used inferential tests to rank standardized network metrics that differed significantly between mTBI patients in the early and late post-injury phases. Following Thatcher et al. (2005), Barik et al. (2019) and Haury et al. (2011), correction for multiple comparison was considered not relevant as the goal of this step was to reduce the number of features by separating the most significant metrics from the less significant and not draw inferential conclusion.

In the second step, a cross-sectional and multivariate study was conducted to select combinations of the previously selected metrics that best discriminate between patients in early or late post-injury time phases. To that end, a 5-fold cross-validation with genetic algorithm based random forest method (GARF) approach was used to classify patients in the different TBI phases. Although classification algorithms are often used to generate predictive models, our main intention was to identify the most discriminative network metrics between TBI phases. We opted to use GARF as it boosts the Random Forests performance while reducing considerably the number of metrics needed for classification (Bader-El-Den and Gaber (2012)).

Longitudinal analysis

After identifying network metrics discriminating between different TBI phases, we investigated their association with cognitive score. This was achieved by a linear regression model, as described in the following equation:

$$\Delta Y = \beta_0 + \beta_1 \Delta X_1 + \beta_2 \Delta X_2 + \cdots + \beta_N \Delta X_N$$

where Δ represents the difference between late and early post-injury data for the N standardized network metrics (X) and the new neuropsychological score obtained by PCA (Y). The fitting of the linear regression model was achieved using stats package in R, which uses the least-squares method to minimize the sum of the squares of residuals. Initially, we included all selected network metrics in the linear regression model. However, to overcome multicollinearity and remove unnecessary metrics, we discarded, at each round, the metric with the highest p-value, until the regression model and its coefficients were statistically significant.

3.2.6 Experimental design and statistical analysis

Inferential statistical tests were used to compare neuropsychological scores, PCA components, and network metrics for both groups. Depending on whether parametric assumptions were satisfied, paired t-test or Wilcoxon signed-rank and independent t or Mann–Whitney U were used at a significance level of 5%. For multiple comparisons, FDR correction using Benjamini-Hochberg method was applied at a significance level of 5%.

The regression model was evaluated by normalized root mean square error (nRMSE), adjusted R^2, and residuals inspection. To verify whether some of the underlying assumptions of regression had been violated, variance inflation factor (VIF) was used to identify multicollinearity among regression network metrics, and the inspection of residuals included the analysis of the scatter plot of residuals vs. predicted scores, lag, and normal probability plots of residuals. F test was used to test the null hypothesis that the fitting either using intercept-only model or our proposed regression model is the same. The rejection of the null hypothesis suggests a better fitting by the proposed model and its predictors.

The final regression model was investigated to examine the presence of bias, overfitting, and the significance of the network metrics selected by GARF. The former was achieved by randomly selecting 20 patients for training and three for testing. We ran this analysis 1,000 times and tested different split sizes (20-3, 18-5, 19-4, etc.). The significance of the network metrics selected by GARF was assessed by random selection of metrics followed by fitting of a linear regression model to predict changes in new neuropsychological score. The network metrics were selected from the set obtained in the first step of feature selection. We ran this analysis 1,000 times and, for each run, computed the nRMSE, and adjusted R^2.

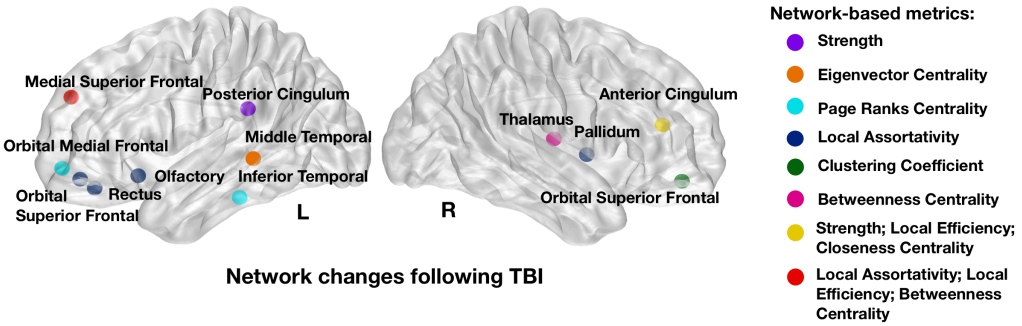


Figure 3.2: Network metrics that showed strongest power in discriminating between early and late post-injury time phases: strength in left posterior and right cingulum, Eigenvector centrality in left middle temporal; Page Ranks centrality in left inferior temporal and left orbital medial frontal; Local Assortativity in right pallidum, left REC, left orbital superior frontal, left olfactory, and left medial superior frontal; Clustering Coefficient in right orbital superior frontal; Betweenness Centrality in right thalamus and left medial superior frontal; Local Efficiency in right ACC and left medial superior frontal and Closeness Centrality in left medial superior frontal. Colors illustrate the network metrics identified in each region. L, Left Side; R, Right Side.

3.3 Results

3.3.1 Network-based metrics of mTBI

The GARF model selected a total of 16 network metrics involving 12 brain regions and showed a 5-fold cross-validation accuracy of 83.3%, confirming robust discrimination between early and late post-injury time phases. Figure 3.2 shows the brain regions and properties that were selected by the model, with a majority located in the fronto-temporal cortex.

3.3.2 Cognitive function assessment

Inferential statistics were used to compare cognitive functioning between patients in early or late post-injury phase along with controls (Figure 3.3). Cognitive functioning was assessed by PCA to reduce Type 1 errors commonly found in multiple statistical comparisons. This approach resulted in one main component, explaining 62.3% of the variance. PASAT and CWIT showed the highest weightings/contributions to the first PCA component, supporting the interpretation that the first PCA component predominantly represents executive functions. For ease of interpretation, we will refer to the first PCA

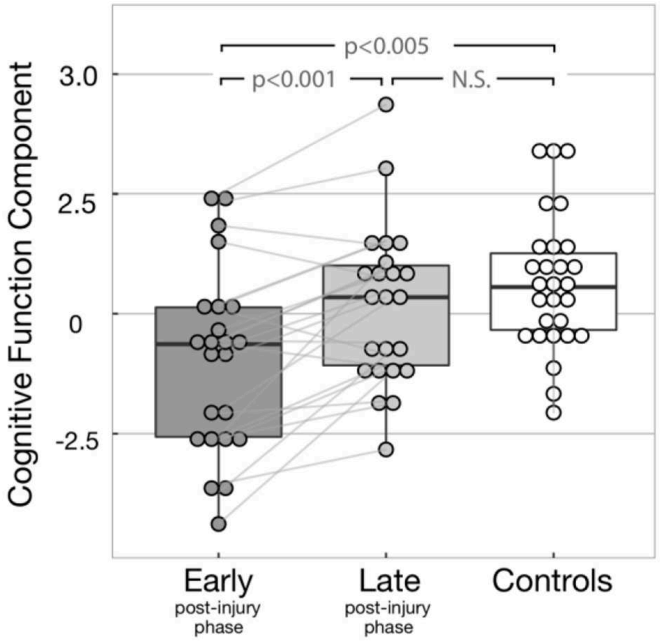


Figure 3.3: Cognitive function component (CFC) for all subjects. The light gray lines display the change of CFC between early and late post-injury phases display for each patient. Significant differences were found between early post-injury CFC and both controls (p-value = 0.001) and late post-injury CFC (p value < 0.001). As expected, no significant difference was observed between controls and late post-injury CFC (p-value = 0.268), due to the recovery of most patients.

component as cognitive function component (CFC). In our recent study, CFC showed to be correlated with a multivariate measure for intrinsic injury severity (Taylor et al. (2020)). An increase over time in CFC suggests an overall improvement of cognitive function. A total of 18 patients showed an increase in cognitive functioning at 12 months, four showed a low decay, while one did not show change in its cognitive functioning over 1 year.

3.3.3 Longitudinal relationships between network-based metrics of mTBI and cognitive functions

After identifying the network metrics associated with mTBI, we performed a longitudinal analysis to investigate associated changes in cognitive performance, namely, in CFC. A significant multiple linear regression equation (F test: $p < 0.0001$) was achieved by a total of 11 significant network metrics between nine brain regions. All metrics had an acceptable (O'brien (2007)) VIF lower than 10. Figure 3.4A shows the 11 network metrics

with the greatest power in explaining changes in cognitive function and their correlation sign with recovery (3.4B). The importance of these 11 features to explain changes in cognitive function is ranked based on the standardized coefficients of the regression model, which are available in Table B.5 in Appendix. From the 11 network metrics identified by the model, 45% measured local assortativity, and the most important network change to explain changes in cognitive function was local assortativity in left medial superior frontal. For most of the network metrics, late post-injury patients in our study showed higher or lower median values than controls. However, an increase on the network metrics was observed early after the injury in ACC and REC, followed by a normalization to controls values in the late post-injury phase. The most common of the network metrics assesses local assortativity. Global assortativity quantifies the tendency of regions to be connected to regions with similar strength. A network with positive assortativity is likely to maintain its ability to integrate information after disruption (i.e., it is more resilient to insults), as it may contain interconnected high-strength regions (Rubinov and Sporns (2010)). Local assortativity measures the contribution of each node to network global assortativity (Thedchanamoorthy et al. (2014)).

The linear regression equation proposed in this study showed an adjusted R^2 of 90% and nRMSE of 0.06. These results indicate that the model explains 90% of the variability found in the CFC over time in patients. Figure 3.5A shows the bootstrap line close to the ideal line, when the observed and expected responses are equal. This result implies consistency of our model performance and no presence of overfitting. Similar results were achieved with different split sizes (Figure 3.5B). Figure 3.5C shows the distribution of nRMSE and adjusted R^2 by taking random selections of different sets of 11 network metrics after the first feature selection step. The vertical lines correspond to the results of the significant regression equation. The low p-values suggest that network metrics in Figure 3.4A are associated with changes following TBI and not random variability.

Figure 3.6A shows the Dice overlap of the AAL regions assessed by the 11 network metrics with the Probability Map of Lesions (Table B.5 in Appendix). Although most of the areas showed overlap, frontal brain areas were particularly affected (Figure 3.6B).

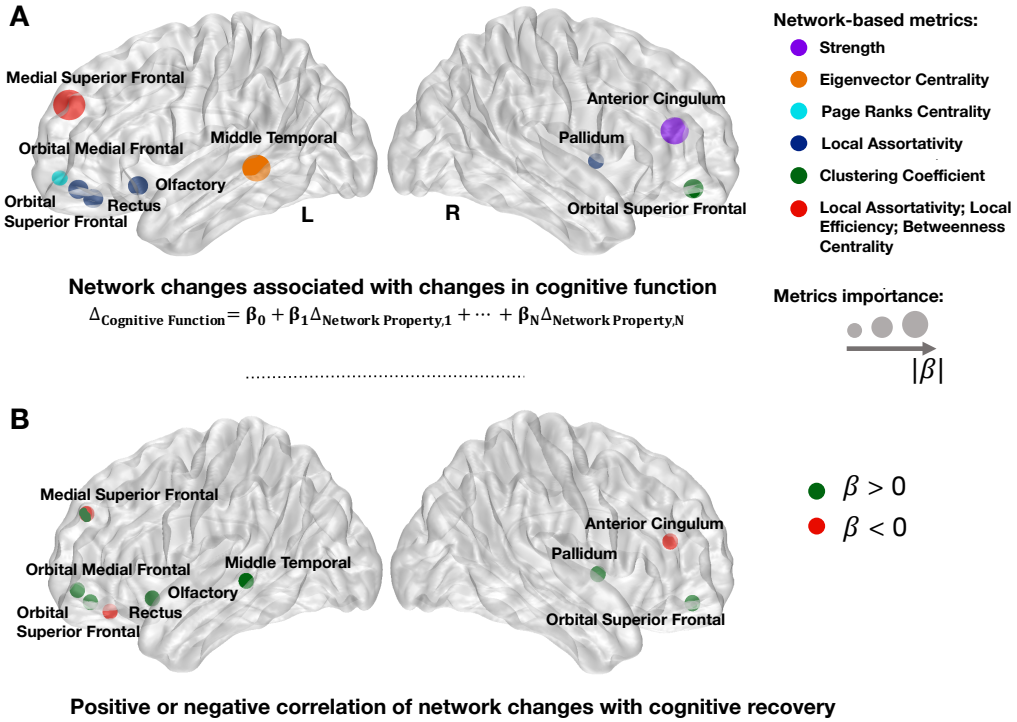


Figure 3.4: Changed network metrics associated with cognitive improvement. Colors in (A) illustrate the network metrics identified in each region and the circles' radius indicates the importance for prediction based on the standardized coefficients of regression model. The list of network changes associated with changes in cognitive function were strength in right cingulum; eigenvector centrality in left middle temporal; page ranks centrality in left orbital medial frontal; local assortativity in right pallidum, left REC, left orbital superior frontal, left olfactory, and left medial superior frontal; clustering coefficient in right orbital superior frontal; betweenness centrality in left medial superior frontal; and local efficiency in left medial superior frontal cortices. Red circles in (B) represent regions in which an increase in their network metrics is negatively correlated with recovery. Possible justifications to these changes are secondary brain injuries, inability to recover after the trauma, or brain maladaptation. Green circles in (B) illustrate the regions in which an increase in their network metrics over 1 year is positively correlated with improvement, therefore suggesting brain adaptation or recovery. L, Left Side; R, Right Side.

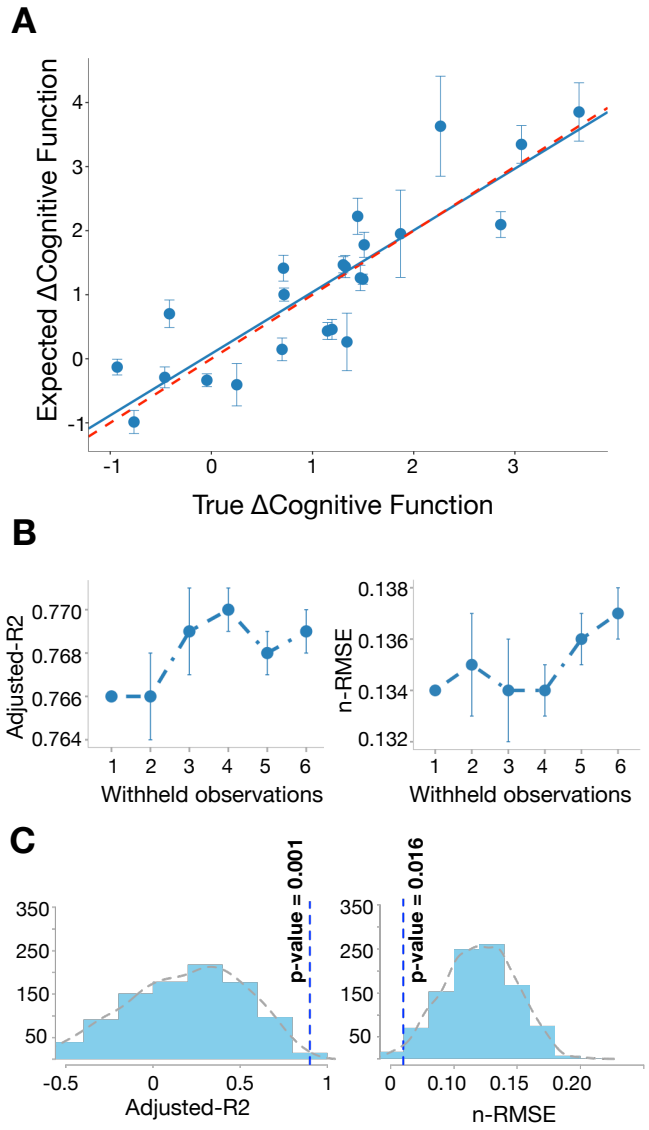


Figure 3.5: Regression model of changed network metrics explains changes in cognitive function. (A) Bootstrap line (blue) closely approximates to the ideal line in red (adjusted R^2 = 76%), when observed and expected responses are equal. The vertical lines indicate the prediction standard deviation for each patient across 1,000 runs. (B) Bootstrap analysis: for each different split size, we saved the mean predictions after 1,000 runs and repeated this process 10 times. The vertical lines indicate the standard deviation of the adjusted R^2 and nRMSE after repeating the bootstrap analysis 10 times. (C) Distribution of adjusted R^2 and nRMSE by taking random selection of different sets of discriminative network metrics between early and late post-injury stages 1,000 times.

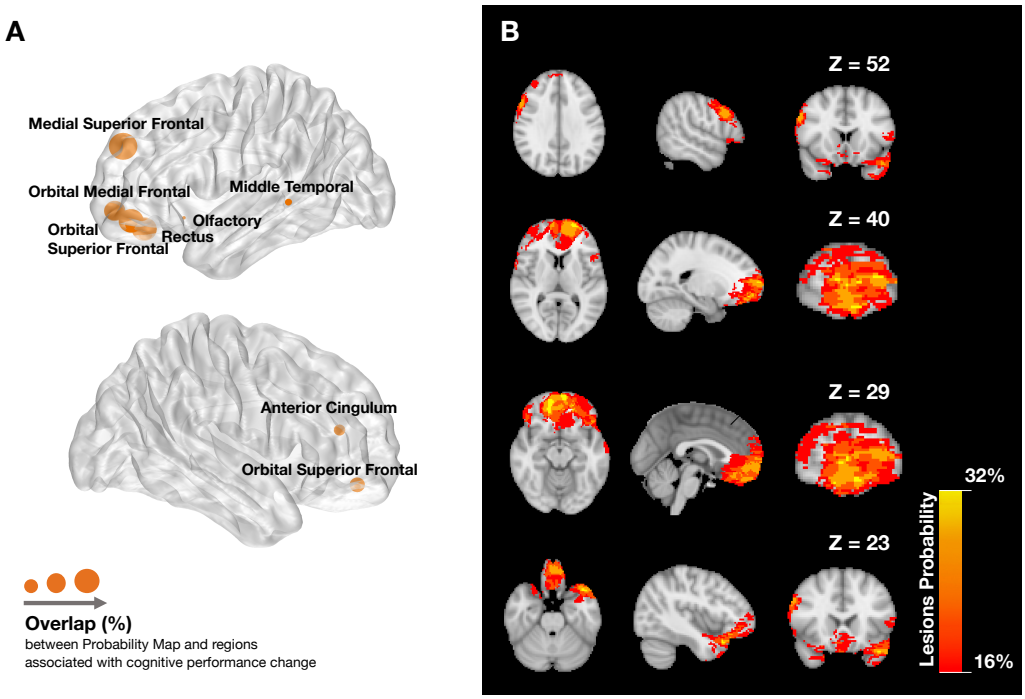


Figure 3.6: Lesions overlap with (A) regions associated with cognitive function component (CFC) change and (B) across patients. (A) Dice overlap between Lesions Probability Map in (B) and AAL regions found to be predictive of changes in cognitive function. Node radius indicates the amount of Dice overlap for the predictive AAL regions, which can be found in Appendix (Table B.5). (B) Lesions Probability Map for different Z voxel coordinates of MNI space, showing the visible overlapping amount across patients. The lesions are found mainly in the frontal lobe, temporal lobe, and slightly in the anterior cingulate cortex. The colormap ranges between an overlap of 16 and 32% patients.

3.4 Discussion

In this preliminary study of 23 patients, we investigated the existence of longitudinal relationships between changes in structural connectivity and changes in cognitive function following TBI. Using graph theory and a regression model, we identified 11 changes in structural connectivity explaining 90% of the observed variability in cognitive function change over 1 year. The observed brain reorganization suggests possible involvement of frontal regions and the anterior cingulate cortex in cognitive function recovery. The regression model also combines information from other brain regions, emphasizing the value of graph-theoretical network-wide perspectives in cognitive neuroscience.

3.4.1 Areas associated with cognitive function

Although behavioural functions can be seen as a consequence of anatomo-functional relationships, there is a degree of function localization in the brain. The regions identified by our regression model are consistent with previous cognitive function localization literature (Barbey et al. (2011); Bubb et al. (2018); Leisman et al. (2014); Mai, Jürgen K. and Paxinos, George (2012); McAllister (2011); Peng et al. (2018)). For instance, Zhou et al. (2013) found white matter (WM) volume loss in the left and right rostral ACC to be correlated with changes in memory and attention. Furthermore, left superior frontal cortex, medial part (SFMed), REC, and middle temporal cortex (MTC) are known to be associated with specific tasks involved in the neuropsychological tests assessed in this study, such as auditory verbal attention, scores on sequencing, semantic retrieval, semantic memory, and semantic control (Elderkin-Thompson et al. (2009); Nakai et al. (2005); Shallice et al. (2008); Xu et al. (2016)). Changes in the left olfactory (OLF) also contributed to the prediction model: to our knowledge, no cognitive functions are directly supported by it. Although two patients lost sense of smell, the OLF has connections to both orbitofrontal cortex and basal ganglia and is implicated in executive function pathways.

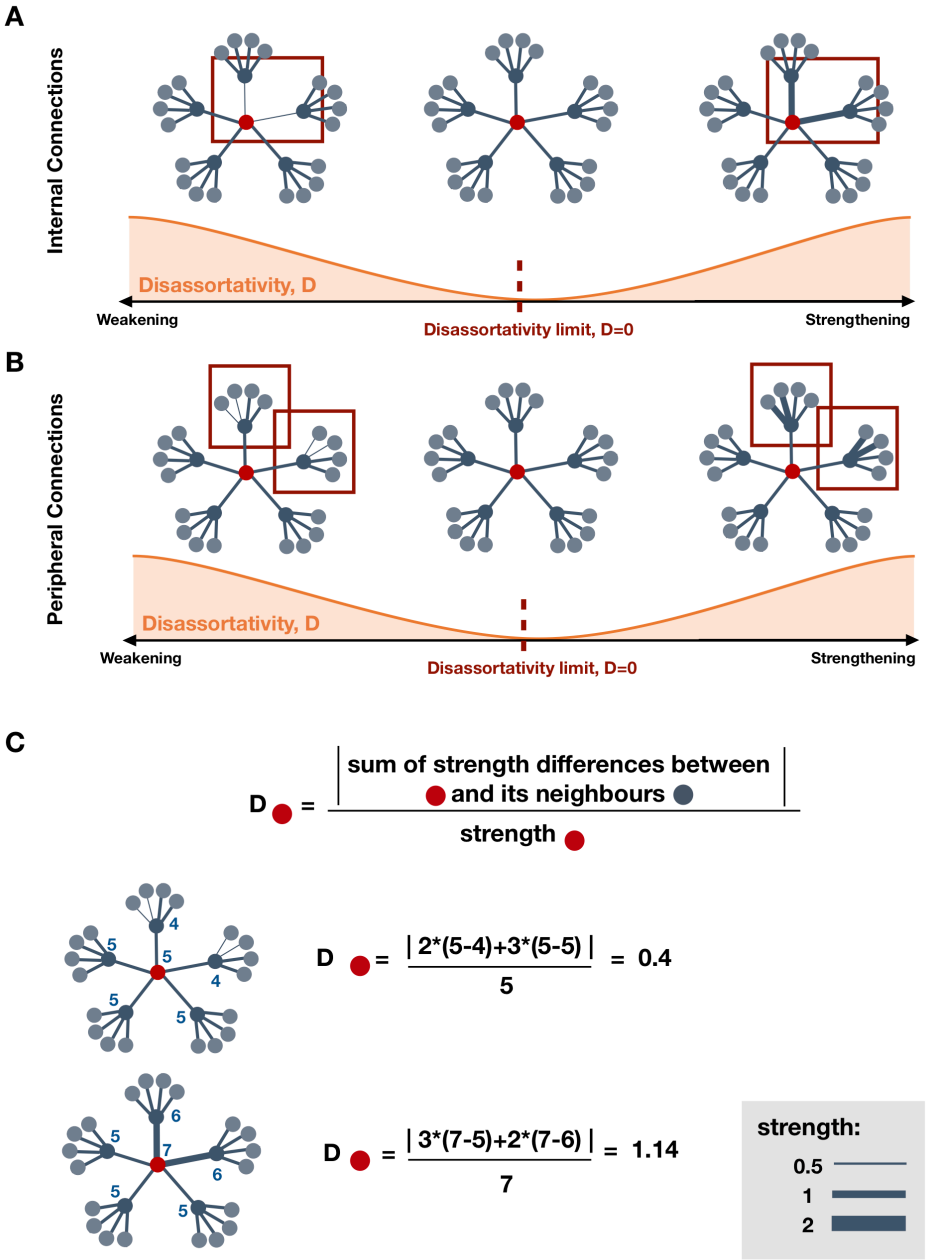


Figure 3.7: Effect on local disassortativity by changes in regions' strength. (A,B) indicate some possible mechanisms of local disassortativity change. (A) Local disassortativity of the red region decreases when the strength differences between red regions and its neighboring regions is reduced. This reduction may occur by strengthening or weakening of internal connections. When disassortativity decreases, the red region is more assortative. (B) Similarly, local disassortativity decreases with peripheral weakening or peripheral strengthening. When the red region is connected to other regions with lower strength, disassortativity may decrease by strengthening of its low-strength neighbors. However, when connected to regions with higher strength, strengthening of those neighbors will increase disassortativity. (C) Examples on how to calculate local disassortativity for regions colored in red.

3.4.2 Network topology changes over time after mTBI

A set of local network metrics were found to change over time after mTBI and a subset was associated with changes in cognitive performance. The network metric changes observed in MTC, pallidum, and OLF showed a positive correlation with ΔCFC (Figure 3.4B). Those changes suggest strengthening to regions that are highly connected, which may be a brain response to improve or establish a "rich-club organization" for information integration (Fagerholm et al. (2015)), either due to local lesions or disruptions in cognitive subnetworks. Since the pallidum is highly connected to other high-connected regions in the brain (Leisman et al. (2014)), the increase in local assortativity suggests that it connects to other similar regions, preferably high-strength regions (Figure 3.7A). Similarly, a positive correlation between an increase of local assortativity in OLF and ΔCFC may indicate a strengthening of its neighbors' connections involved in executive function circuits, such as orbitofrontal and basal ganglia (Figures 3.7B and C) (Mai, Jürgen K. and Paxinos, George (2012)). Some possible explanations for network metric changes, which are negatively correlated with ΔCFC, may be continuous deterioration, incapacity to recover, maladaptive plasticity, or compensatory pathways recruitment, which are no longer required after brain recovery. Increased local assortativity in SFMed was observed to be negatively correlated with ΔCFC (Figure 3.4B). Since the SFMed is highly susceptible to injury (McAllister (2011)), internal disconnections may contribute to the reduction in the average strength differences, which leads to increased local assortativity (Figures 3.7A and C).

We observed an increase in early post-injury phase in ACC strength and REC local assortativity, followed by a decrease in 1 year. This is in agreement with a longitudinal study by Dall'Acqua et al. (2017), who also observed increased structural connectivity in a subnetwork within 7 days post-injury in mTBI patients, including pathways from or to ACC, and REC. As postulated by Dall'Acqua et al. (2017), a plausible explanation to this hyperconnectivity brain reorganization, early after the trauma, is rerouting of damaged regions to the highest-degree hubs to compensate for cognitive impairment. Considering that ACC is one of the regions with higher predictive power in our study (Figure 3.2), the observed reduction of its strength over time for most patients seems to be a crucial sign of

recovery. As hypothesized by Cazalis et al. (2011), the recruitment of ACC may decrease over time with the recovery of other regions. Therefore, an increase in strength in this area over time is negatively correlated with ΔCFC, as it may imply lack of recovery in other brain regions, such as frontal cortex, pallidum and middle temporal cortex. Another possible explanation for the increase in ACC strength and REC local assortativity early after the trauma, could be due to astrogliosis, which may increase FA (Croall et al. (2014)).

Regarding changes in global network metrics, GARF method did not select any when classifying patients as early or late-phase TBI. Since genetic algorithms have a degree of randomness, other sets of features including global network metrics could have been selected. Nevertheless, the majority of network features included in this study were at node level and additional global network metrics such as rich-club coefficient could have been included in this analysis.

3.4.3 Limitations

Limitations of our work include the relatively small size of our dataset, which reflects the challenges of recruiting large longitudinal cohorts with repeated clinical and imaging data. Furthermore, the patient imaging and psychological data were acquired at only two time points, within days of injury and a year later, so we could not establish the starting and stopping point for each different reorganization pattern or its causality. Another limitation in this study is the resolution of diffusion-weigted imaging (DWI) images, which could negatively affect fiber tracking. We overcome it by a two-step co-registration followed by quantification of FA values along a connectome atlas. The pathways comprised in this atlas were manually examined and labeled by experienced neuroanatomists (Yeh et al. (2018)). A similar approach has also been used in previous severe TBI studies (Squarcina et al. (2012)). Finally, our dataset comprises patients with both mild and moderate TBI, which could potentially prejudice our understanding about recovery in mTBI. Using the same dataset, Croall et al. (2014) did not observe any significant differences between patients with mild or moderate TBI in any diffusion metrics. Since only one moderate patient had a GCS lower than 10 and the majority had 12, the moderate group is close to the milder end of injuries. As in Croall et al. (2014), we assume that these patients have

microstructural changes similar to mild injuries.

Chapter 4. High Concentration of T-Tau Following TBI Related to Network Functional Inflexibility: a Longitudinal Study

Contents

4.1 Introduction 72

4.2 Methods 75

4.2.1 Subjects and clinical characteristics 75

4.2.2 MRI acquisition and imaging protocol 76

4.2.3 Image processing 76

4.2.4 Blood biomarkers 78

4.2.5 Analysis of white matter organisation 78

4.2.6 Analysis of dynamical functional connectivity 79

4.2.7 Statistical analysis 82

4.3 Results 83

4.3.1 Demographics and clinical characteristics 83

4.3.2 Dynamic functional connectivity and temporal characteristics . . . 83

4.3.3 Blood biomarkers of injury associated with entropy 85

4.3.4 Relationship with structural organisation 87

4.3.5 Longitudinal characteristics 87

4.3.6 Sedation 90

4.4 Discussion 92

4.4.1 Distinct cognitive-related functional states following moderate-severe TBI 92

4.4.2 Fluid blood biomarkers associated with functional flexibility 94

4.4.3 Limitations 96

4.1 Introduction

Blood biomarkers have showed already to complement imaging findings in the diagnosis and progression of neurodegenerative diseases such as Alzheimer's disease (Olsson et al. (2016); Mattsson et al. (2017); Festoff et al. (2016); Byrne et al. (2017)). As referred in Chapter 1 fluid biomarkers have been associated with injury severity, risk of long-term sequelae and even prediction of functional outcome in traumatic brain injury (TBI) (Zetterberg and Blennow (2016); Shahim et al. (2020); Ost et al. (2006)). However, it remains unknown how the pathological or injury mechanisms of fluid biomarkers might explain severity and brain dysfunction after TBI. A better understanding would help on long-term prognosis and improve clinical trials.

TBI results in impairment of brain function which can persist long after injury, in part due to progressive neurodegeneration and dementia (Graham and Sharp (2019); Gardner et al. (2014)). As mentioned in detail in Chapter 1, diffuse axonal injury triggers neurodegeneration by tau dissociation from microtubules in axons followed by an abnormal hyperphosphorylation. Studies in mice have shown that soluble pathological tau species suppress neuronal activity and promote silencing of neurons (Busche et al. (2019); Marinković et al. (2019)). Using a mouse tauopathy model for repetitive mild TBI (mTBI), Rubenstein et al. (2019) showed a link between high concentrations of tau in plasma with behaviour and cognitive deficits. When supressing pathological tau, through a kinase-targeted therapeutic intervention, the abnormal behaviour and cognitive deficits were restored. This finding suggests that tau might supress the functional flexibility or coordination of neural systems to segregate and integrate information, a requirement of complex cognitive processes (Sharp et al. (2014)). Further studies in humans are needed to examine functional flexibility of neural systems in presence of soluble tau.

The brain must be able to flexibly transition between functional connectivity patterns in order to respond appropriately to external or internal demands (Hou et al. (2019)). The functional flexibility to transition between patterns can be examined through the analysis of dynamic functional network connectivity (dFNC). The vast majority of resting-state fMRI (rs-fMRI) studies on TBI still assumes a spatial and temporal stationary of con-

nectivity over the entire duration of the scan (Allen et al. (2014)). In contrast, dFNC analysis examines functional connectivity between regions over shorter periods of time. It allows the identification of reoccurring patterns or states of functional connectivity in the brain and its ability to flexibly transit between them (Bonkhoff et al. (2020)). Previous studies in mTBI patients using dFNC suggested that global damage to the overall flexibility across the brain in an early stage after brain injury is linked with chronic symptoms and poor outcomes (Hou et al. (2019); Vergara et al. (2018); Horn et al. (2020)). In particular they showed a more rigid and less flexible functional coordination in mTBI patients, which was associated with long-term deficits. They also found that mTBI patients spent less time in efficient brain functional conectivity patterns/states. Further studies are needed to explain the neural mechanisms for lack of functional flexibility following TBI and how we can reverse it to improve patient's long-term outcome. Additionally, studies are also needed to examine functional flexibility in moderate-severe TBI patients and assess dFNC potential as biomarker for recovery and severity. Previous studies examined dynamic functional connectivity over the whole brain. By focusing on resting state networks known for their role on cognitive processes, one could find more subtle differences in the interactions between these networks. Therefore, by focusing on these regions one might better understand the neural mechanisms behind long-term cognitive deficits found in moderate-severe TBI.

The goal of this study was to first investigate the impact of moderate-severe TBI on functional flexibility of resting state networks related to cognition and second, examine if longitudinal changes on the flexibility to transit between functional networks were related to total tau (T-Tau) concetration and white matter organisation. Thus, we addressed the following questions: Do moderate-severe injuries induce alterations in the functional flexibility between cognitive-related functional networks and their regions? Are those alterations over time associated with tau concentration? Are those alterations in functional coordination related to white matter organisation? We hypothesized the existence of distinct dynamical functional connectivity patterns among cognitive-related brain regions of default mode network (DMN), frontoparietal networks (FPNs) and salience network (SN). Abnormalities within DMN and its interactions with cognitive-control networks have been

related with cognitive deficits following TBI (Sharp et al. (2011, 2014); De Simoni et al. (2016b); Bonnelle et al. (2012)). Thus, we expect moderate-severe TBI patients will show impairment on network flexibility over these networks. We also hypothesized that pathogenic blood biomarkers such as tau, will supress neural circuits as seen in mice models and thus, promote a more rigid functional flexibility between cognitive brain areas. Longitudinal scans will allow to assess if a decrease of T-Tau and/or an improvement on white matter organisation are associated with improvement of functional flexibility over time.

4.2 Methods

4.2.1 Subjects and clinical characteristics

One hundred and two patients were recruited for a rs-fMRI and T1-weighted scans across four European major trauma centres 10 days to 6 weeks following moderate-severe TBI. Inclusion criteria include moderate-severe TBI as defined by the Mayo classification and age ranging between 18-80 at time of injury. Exclusion criteria included previous TBI requiring hospitalisation, moribund patients, cardiac arrests, inability or unwillingness to participate in study, prior significant neurological or psychiatric condition and previous significant disability from any cause (Graham et al. (2020b)).

A subset of these patients were scanned again at 6 months (N=55) and 12 months (N=38) after the injury. Thirty seven rs-fMRI scans at the subacute phase were excluded due to movement (59.5%), poor quality of co-registration/brain extraction in the presence of major lesions (32.4%), and inconsistencies of the imaging protocol (8.1%). Additionally, thirteen and eight scans collected at 6 and 12 months respectively, were excluded due to movement (61.5% at 6-months, 75% at 12-months), poor quality of co-registration/brain extraction in the presence of major lesions (23.1%; 12.5%) and inconsistencies of the imaging protocol (15.4%; 12.5%). In total, our dataset comprises 76 patients, 65 with subacute functional MRI (fMRI) scans, 42 with scans at 6 months and 30 with fMRI scans at 12-months. Further details on sample size and clinical demographics can be found in Appendix (Tables C.1,C.2 and C.3). Functional outcome was assessed using the Glasgow Outcome Scale Extended (GOSE) subacutely (N=44), 6 months (N=64) and 12 months (N=56). Montreal cognitive assessment (MOCA) was also assessed to 40 patients 12 months after injury. Diffusion imaging data and blood biomarkers taken at the time of the scans were also acquired for a subgroup of these patients as part of a separate study (Graham et al. (2020a)) (Table C.1 in Appendix).

Fifty-two healthy controls were scanned once and a subgroup (N=44) had blood taken to estimate their blood biomarkers concentration. Four rs-fMRI scans were excluded due to movement. Controls matched patients for age at both timepoints but not for sex. A diagram of the available data per group is shown in Figure C.1 in Appendix.

4.2.2 MRI acquisition and imaging protocol

Image acquisition across all four sites was performed on a 3-T scanner. Resting-state fMRI images were obtained using a T2*-weighted gradient-echo echoplanar imaging sequence (EPI) (repetition time (TR) 2000 ms, echo time (TE) 30 ms, slices thickness 3mm, voxel size 3x3x3mm, flip angle 80°, field of view (FOV) 192x192x105mm, matrix 64x64). Resting-state fMRI scans had a duration of 10 min, equivalent to 300 volumes. During the scan, subjects were instructed to keep their eyes closed. The imaging protocol also included T1-weighted sequences (TR 2300 ms, TE 2.98 ms, matrix size 160x240x256, isotropic 1 mm resolution) and diffusion-weighted images (TR 9500 ms, TE 103 ms, matrix size 128x128x64, b =1000 s mm^{-2}, 4 slices with b=0, 64 diffusion directions, voxel size 2x2x2 mm). Imaging protocol was consistent across all sessions. Further details on the imaging protocol can be found in Graham et al. (2020b).

4.2.3 Image processing

T1-weighted images were skull-stripped using brain extraction tool in FMRIB software library (FSL). Resting-state fMRI images were preprocessed to reduce the influence of structured noise resulting from magnetic resonance imaging (MRI) hardware, motion and physiology. Preprocessing steps included initially realignment of EPI images, slice-timing correction, registration to MNI 2-mm space and spatial smoothing with a Gaussian kernel (FWHM = 6 mm). These steps were performed using fMRI Expert Analysis Tool (FEAT) in FSL (Woolrich et al. (2001)). Preprocessing of the images continued with white matter (WM) and cerebrospinal fluid (CSF) regression. WM and CSF tissues were segmented on skull-stripped T1w images using FMRIB's Automated Segmentation Tool (FAST) (Zhang et al. (2001)). Resulting partial volume images were masked with a threshold of 0.8. WM and CSF masks were co-registered to EPI images space using FMRIB's linear image registration tool (FLIRT) (Jenkinson and Smith (2001); Jenkinson et al. (2002)). Average timeseries in CSF and WM tissues were extracted and regressed out from EPI images. In a final preprocessing step, images were filtered with a temporal high-pass filter with a cut-off of 0.01 using FEAT and registered to Montreal Neurological Institute (MNI) 2-mm space using FLIRT.

Reduction of motion was performed in three steps. First, framewise displacement (FD), a measure of head motion, was estimated for each volume using the FSL motion outliers tool. Images were excluded if they would fill the criterion of movement exceeding 3 mm in at least one volume or 15% of volumes having FD above 0.5 mm (De Simoni et al. (2018)). Secondly, six realignment parameters and their temporal derivatives were regressed out. Finally, before temporal filtering, each scan was subjected to independent component analysis (ICA) decomposition using ICA-AROMA (Pruim et al. (2015)) in Python 2.7. For efficient data denoising, all components were visually inspected using spatial maps, timeseries, power spectra and motion-correction realignment parameters. Following the guidance in Griffanti et al. (2017), each component was labelled as noise or signal and those manually labelled as noise were removed. More details on the agreement between our manual classification and ICA-AROMA's automatic classification are available in Appendix (Table C.4).

Feis et al. (2015) showed ICA-based removal reduces scan site differences in multi-site resting-state fMRI studies by diminishing structured noise. By manually classifying each component from ICA-AROMA, we were ensuring not only an efficient data denoising but also ensuring differences on structured noise across sites were also removed. As indicated by Feis et al. (2015), ICA-based artefact removal cannot account for differences in the magnitude of the blood-oxygen-level-dependent (BOLD) effect across sites. Thus, site-wise confound regressors were used in further analysis.

Diffusion-weighted images were preprocessed using the tract-based spatial statistics (TBSS) pipeline (Smith et al. (2006)) after being corrected for both susceptibility and eddy current induced distortions and fitted with a diffusion-tensor model. A tensor-based registration using DTI-TK (Zhang et al. (2007)) was integrated with TBSS to create a group tensor image in which all subjects were registered to. A mean fractional anisotropy (FA) map was created from the mean tensor image in DTI-TK and thresholded at 0.2 to produce a white matter skeleton. Individuals FA images were estimated and z-scored in a voxelwise manner using the mean and standard deviation values of controls from the same site. Further details on the preprocessing of diffusion weighed images is available in Graham et al. (2020a).

Brain extracted images and all intermediate and final images, resulting from the pre-processing steps for rs-fMRI and diffusion-weigted imaging (DWI) images, were visually inspected.

4.2.4 Blood biomarkers

Blood samples were collected twice in the first ten days after injury and at subsequent visits for scanning sessions. Neurofilament light chain (NFL), T-Tau, glial fibrillary acidic protein (GFAP) and ubiquitin C-terminal hydrolase-L1 (UCHL-1) concentrations in plasma were sampling from peripherally venous blood or by central access line using the Quanterix Neurology 4-plex B assay on the Simoa-HD1 platform. Serum S100 calcium binding protein B (S100B) was measured using a separate Simoa assay. More details on the sampling protocol are available in Graham et al. (2020b).

4.2.5 Analysis of white matter organisation

Next, we examined white matter organisation measured by FA over a set of tracts between patients and controls. Mean z-scored FA values were estimated in non-lesioned voxels. This analysis included tracts from Jolly et al. (2020) and an additional subset from Bonnelle et al. (2012); De Simoni et al. (2018); Yeh et al. (2018). We selected tracts from Jolly et al. (2020) for their clinical relevance to TBI as defined by prior evidence of relationships to motor, cognitive and function outcomes. Tracts were taken from Bonnelle et al. (2012) for their role in the specific disconnection between DMN and SN following TBI, impairing cognitive processes. Additionally tracts were taken from De Simoni et al. (2018) which were shown to impair executive function when these tracts were disrupted following TBI. Finally, the cingulum bundle was taken from Yeh et al. (2018) which was shown to disrupt memory by altering functional connectivity within DMN following TBI (De Simoni et al. (2016a)). Given the heterogeneity of TBI, we computed a Mahalanobis distance measure to combine in a single score the many ways a given injured brain's white matter can vary from that of healthy controls. The Mahalanobis distance is the multivariate generalization of a z-score that incorporates covariance between the variables (Taylor et al. (2020)).

4.2.6 Analysis of dynamical functional connectivity

We performed a dynamic connectivity analysis to identify reoccurring large-scale patterns of connectivity across a set of cognitive-related brain regions. The analysis involved three main steps. First the selection of cognitive-related regions, second, clustering functional connectivity in a set of patterns within a sliding window framework and third, analysis of the temporal characteristics of those patterns (Figure 4.1). Abnormalities within DMN and its interactions with cognitive-control networks, such as SN and FPNs have been associated with cognitive impairments following TBI (Sharp et al. (2011, 2014); De Simoni et al. (2016b); Bonnelle et al. (2012)), thus main regions from these networks were selected as cognitive-related regions of interest.

Selection of regions of interest

Regions of interest (ROIs) in DMN and SN were selected from previous studies (De Simoni et al. (2016b); Li et al. (2019a,b); Leech et al. (2011). Additional regions were selected from the peaks of the frontoparietal networks in Smith et al. (2009). Peaks on ICA spatial maps from Smith et al. (2009) were extracted using cluster tool in FSL after a threshold of 3.1. Peaks in the cerebellum or outside the FOV of the imaging protocol were discarded. Peaks were named as the most likely region for that coordinate in Harvard-Oxford cortical structural atlas. Coordinates of the centre of each region of interest (ROI) in MNI space are available in the Appendix (Table C.5). For each ROI, a 5mm sphere was created around the centre coordinate and multiplied by a mean brain mask to exclude voxels outside the brain. BOLD signal was extracted using dual regression in FSL for all ROIs and subsequently, variance-normalised to limit our analysis on temporal modulation rather than magnitude. Using group ICA of fMRI toolbox (GIFT) built-in functions, timeseries were detrended in MATLAB to remove linear, quadratic and cubic trends related to scanner drift and low-pass filtered with a high-frequency cutoff of 0.15Hz (Allen et al. (2014); Bonkhoff et al. (2020))

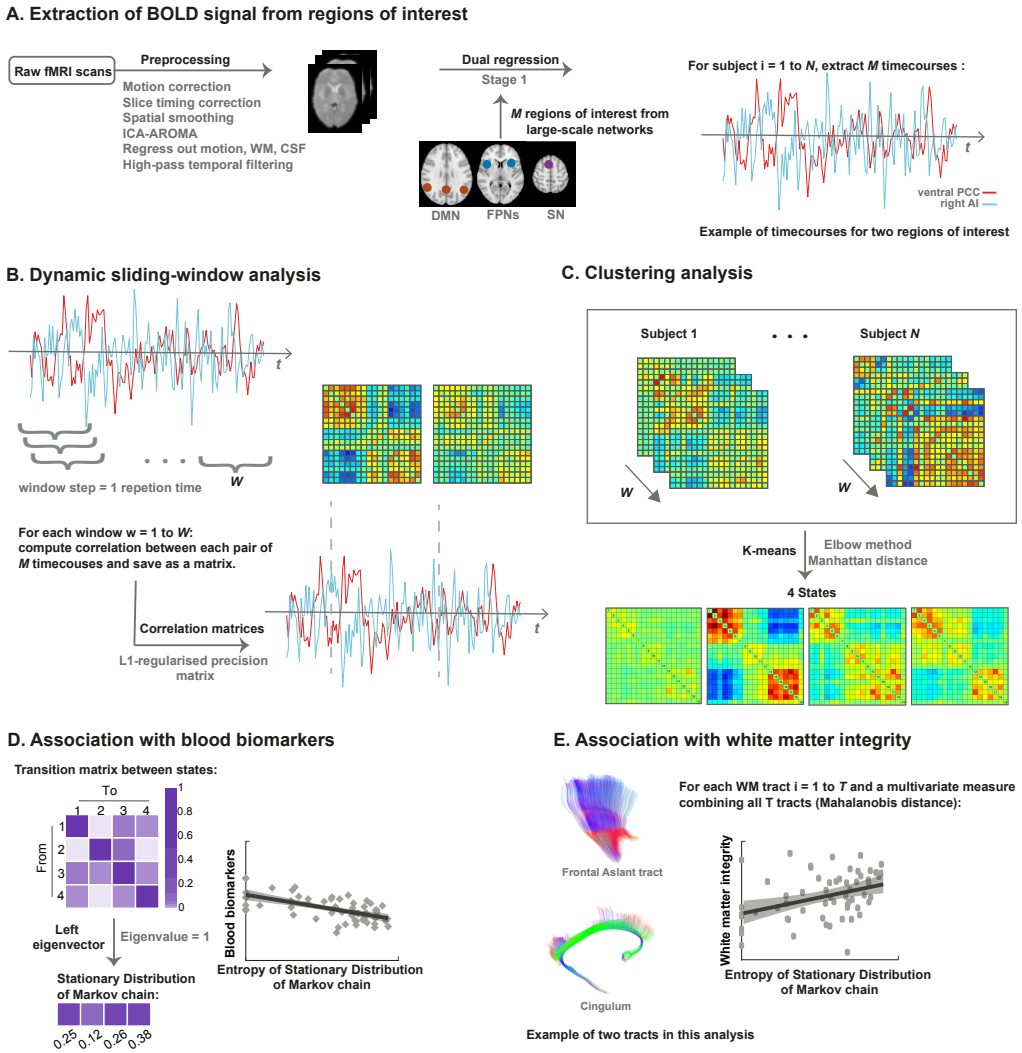


Figure 4.1: Processing pipeline: (A) To compare dynamic functional connectivity between groups and within patients, fMRI scans were initially pre-processed to remove noise and reduce site differences. BOLD signal was extracted for a set of regions in DMN, SN and FPNs by dual regression. An example of the timecourses extracted for ventral PCC and right anterior insula (AI) are shown. (B) A dynamic sliding-window analysis was applied to compute the correlation between timecourses of each pair of regions. Correlation values were saved in a matrix and regularised to promote sparsity. An example of two correlation matrices for two windows are shown. (C) Correlation matrices of all subjects were concatenated and clustered using K-means. A set of four clusters or states were found using elbow method. (D) By determining the number of transitions between states, we calculated the transition matrix per subject. The stationary distribution of Markov chain was estimated from the transition matrices by the left eigenvector. The Shannon's entropy of the stationary distribution was compared with blood biomarkers and (E) white matter organisation. White matter organisation was given by the fractional anisotropy in a set of tracts and the Mahalanobis distance, a multivariate measure taking in account FA values of all tracts.

Identify large-scale functional connectivity patterns

Dynamic functional connectivity was estimated within a sliding-window framework, where covariance matrices were generated by a sliding-window rectangle of 44 sec convolved with a Gaussian (σ=3) and shifted in steps of one repetition time. These parameter settings were used previously (Bonkhoff et al. (2020); Allen et al. (2014); Horn et al. (2020)) and shown to be robust to noise (Preti et al. (2017)). This resulted in 278 windowed functional connectivity matrices per patient for each fMRI scan.

Since short segments of signal might not carry enough information to characterise a full covariance matrix, GIFT toolbox computes a L1-regularized precision matrix from the connectivity matrices to promote sparsity (Allen et al. (2014)). Dynamic functional connectivity matrices were Fisher transformed to stabilise variance for further analysis. Variance associated with sex and site covariates were regressed out from covariance matrices as implemented in GIFT toolbox before the clustering analysis.

K-means clustering algorithm was applied to cluster functional connectivity matrices across all subjects in a set of clusters/states. We used Manhattan distance, as it was shown to be more suitable for high-dimensional data than Euclidean distance (Allen et al. (2014)). Using the elbow method, we identified the optimal number of clusters/states on our data, representing distinct connectivity patterns across cognitive-related regions that reoccurred across all subjects. Each functional connectivity matrix was labelled to one of the states.

Temporal characteristics

To assess the temporal characteristics of the distinct functional connectivity patterns, we estimated for each subject the time spent in each state (eg. fraction time), time spent in a given state before changing it (eg. dwell time), number of times a subject changes to a different state (eg. number of transitions) and transition matrices (eg. likelihood of transition between states) Bonkhoff et al. (2020). We also computed the fraction time over an infinite time as given by the stationary distribution of a Markov chain. Stationary distribution was computed by the left eigenvector of the transition matrices when eigenvalue

equals to 1 Privault (2013). We also quantified the ability to transition between states or functional flexibility by calculating the Shannon's entropy of the stationary distribution Shannon and Weaver (1949). It measures the unpredictability of guessing the next state in time. Low values of entropy reflect a tendency to spend more time in fewer states, while higher entropy reflects a more even distribution of time spent in all states. We compared the above measures in a group-level to assess differences between patients and controls.

4.2.7 Statistical analysis

Inferential statistical tests were used in group-level analyses. Depending on whether parametric assumptions were satisfied, paired t-test or Wilcoxon signed-rank and independent t or Mann-Whitney U were used at a significance level of 5%. Spearman's correlation was used to assess the relationship between subacute entropy with clinical data, subacute white matter organisation and subacute blood biomarkers concentration. We also computed Spearman's correlation between changes in entropy and changes in blood biomarkers over a period of 6 months after injury. In order to examine if the correlation between changes in entropy and changes in blood biomarkers was not just a consequence of the initial concentration of biomarkers, we used a linear-mixed effects model with random slopes. Initial concentration of blood biomarkers was added as independent variable. For multiple comparisons, false discovery rate (FDR) correction using Benjamini-Hochberg method was applied at a significance level of 5%. Area under the ROC curve (AUC) was applied to compare the ability to discriminate between patients and controls on the basis of the selected white matter tracts and Mahalanobis distance measure.

We also inspected if there was a relationship between GOSE and MOCA with entropy and T-Tau concentration. GOSE was binarized into favourable and unfavourable outcomes, where a score of 7 or above was considered favourable, resulting in a balanced sample size between groups. Four separate logistic regression models were used to predict GOSE groups using entropy, changes in entropy over 6 months, initial T-Tau concentration and changes in T-Tau over 6 months as independent variables.

4.3 Results

4.3.1 Demographics and clinical characteristics

The majority of injuries in this study cohort resulted from an accident (88.2%), the largest group following a road traffic collision (46.1%). Half of injuries were classified as high energy (48.7%). Initial Glasgow Coma Scale (GCS) was assessed in 54 patients and 32 patients scored between 14-15. Loss of consciousness (LOC), retrograde amnesia and post-traumatic amnesia (PTA) were present or suspected in 76.4%, 67.1% and 78.9% of patients respectively. The most frequent subacute focal pathologies on CT included subdural haematomas (SDH, 63.2%), subarachnoid haemorrhage (SAH, 61.4%) and parenchymal contusions (46.1%). Clinical MRI reports from the subacute scan showed parenchymal contusions in 65.8%, acute subarachnoid haemorrhage (SAH) in 38.2%, extradural haematoma in 30.3% and axonal injury in 28.9% of patients. Functional outcome assessments showed that six patients (13.6%) had an initial good outcome on GOSE followed by a good recovery in 27 patients at 6 months (42.2%) and in 28 patients at one year (50%).

4.3.2 Dynamic functional connectivity and temporal characteristics

To assess temporal properties of functional connectivity during the subacute scan, we first extracted BOLD signal from cognitive-related ROIs. Functional connectivity matrices between those ROIs were estimated using a sliding-window approach resulting in 278 matrices per subject. A K-means clustering algorithm was applied to group connectivity matrices across all subjects in a set of clusters/states. Using the elbow method, we identified four states representing connectivity patterns across cognitive-related regions that reoccurred across all subjects during the subacute scan. States are arranged in order of emergence given by K-means algorithm (Figure 4.2).

The first state, accounting for 45% of the functional connectivity matrices/windows, represents an undifferentiated state, which may be the result of an average of a set of states that given their low frequency of occurrence were not able to be separated Allen et al. (2014). Since the focus of this study is on cognitive-related regions, it is expected that

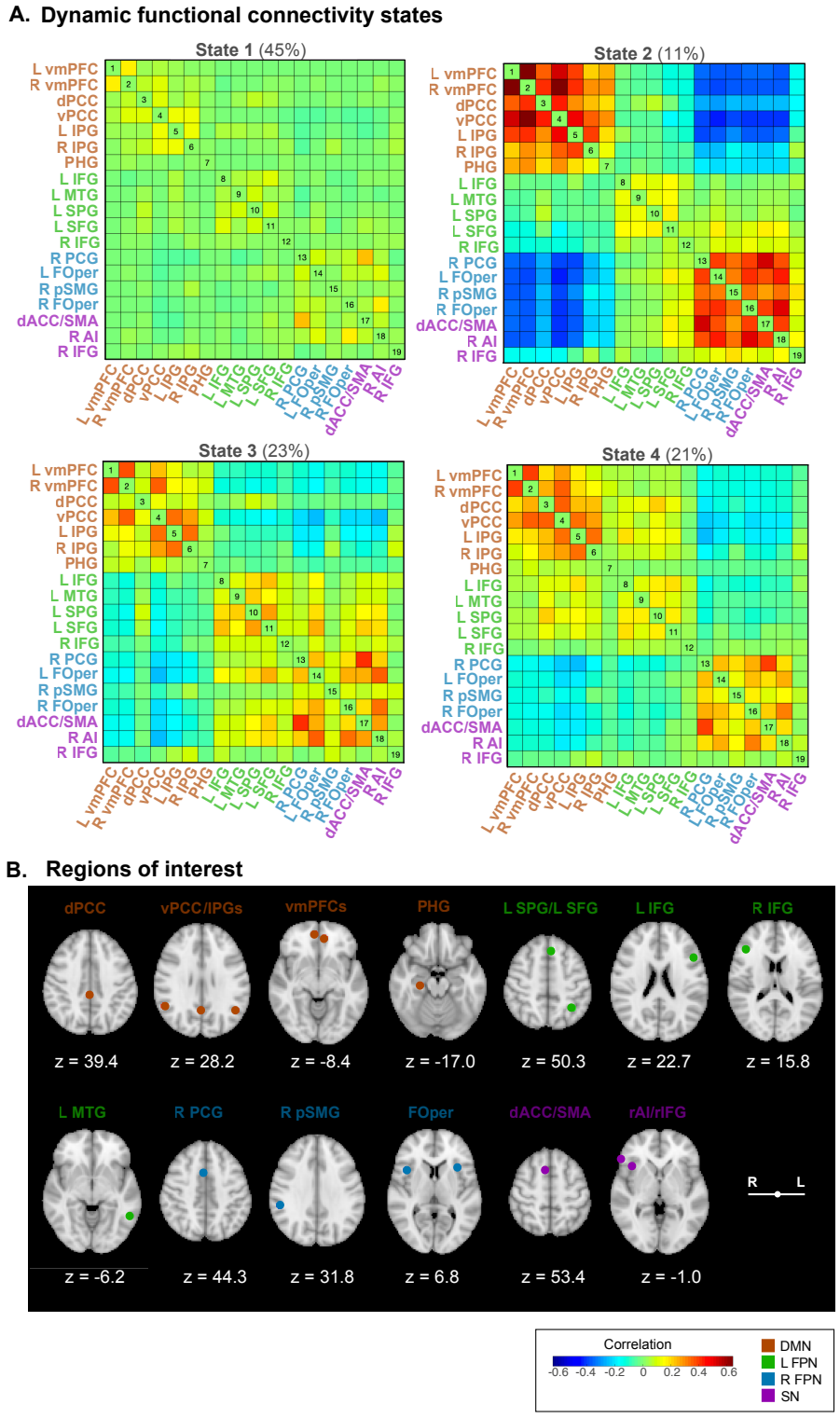


Figure 4.2: Dynamic functional connectivity states: (A) Four dynamic functional connectivity states were found in the clustering analysis. State 1 is an undifferentiated state which likely results from a the average of less frequent clusters. State 2 and State 3 show an anticorrelation between DMN and the remaining networks. Finally, State 4 shows an anticorrelation between DMN and right FPN with some partly correlation between left FPN and DMN. Frequency of state is displayed on the top of each centroid. Regions selected from these networks are shown in (B).

small states involving connectivity patterns of other regions in the brain would be averaged in the undifferentiated state. The second and third state, accounting for 11% and 23% of windows, represent anticorrelation between DMN and cognitive control areas in SN, right FPN and left FPN. This anticorrelation is more pronounced in State 2. State 4 also shows an anticorrelation between DMN and both SN and right FPN, however there is not a clear anticorrelation between DMN and left FPNs as several DMN regions are positively correlated with regions of left FPN.

There were significant differences between groups on fraction and dwell time for the first three states after FDR correction (Figure 4.3 and Figure C.2 in Appendix). Patients spent significantly more time in the undifferentiated state and significantly less time in the states showing a clear anticorrelation between DMN and cognitive control areas. Patients also had significantly fewer transitions between states when compared with controls (Figure 4.3B). The time spent in each state over an infinite time was also estimated as the stationary distribution of the transition matrices of each subject (Figure 4.3C).

We quantified the ability to transition between states by calculating the entropy of the stationary distribution. Significant differences in entropy were found between our groups with controls having greater entropy than patients (Figure 4.3D). Within patients, we investigate the association of entropy with a set of clinical characteristics available for the majority of patients at subacute phase, namely presence of contusion or intracerebral haemorrhage (ICH), loss of consciousnes (LOC) and PTA. Entropy was not associated with any of these clinical characteristics (p-values > 0.05) (Figure C.3 in Appendix). Furthermore, we investigated the association with hospital duration, a characteristic available for 97.3% of patients. We found that patients spending more time in the hospital had significantly lower entropy, an indication of less functional flexibility across our states (Figure C.4A in Appendix).

4.3.3 Blood biomarkers of injury associated with entropy

Entropy was next compared with GFAP, NFL, UCHL-1, serum S100 calcium binding protein B (S100B) and T-Tau concentrations at subacute (Figure 4.4). With the exception of NFL, all biomarkers had an early peak following the injury which then reduced over time

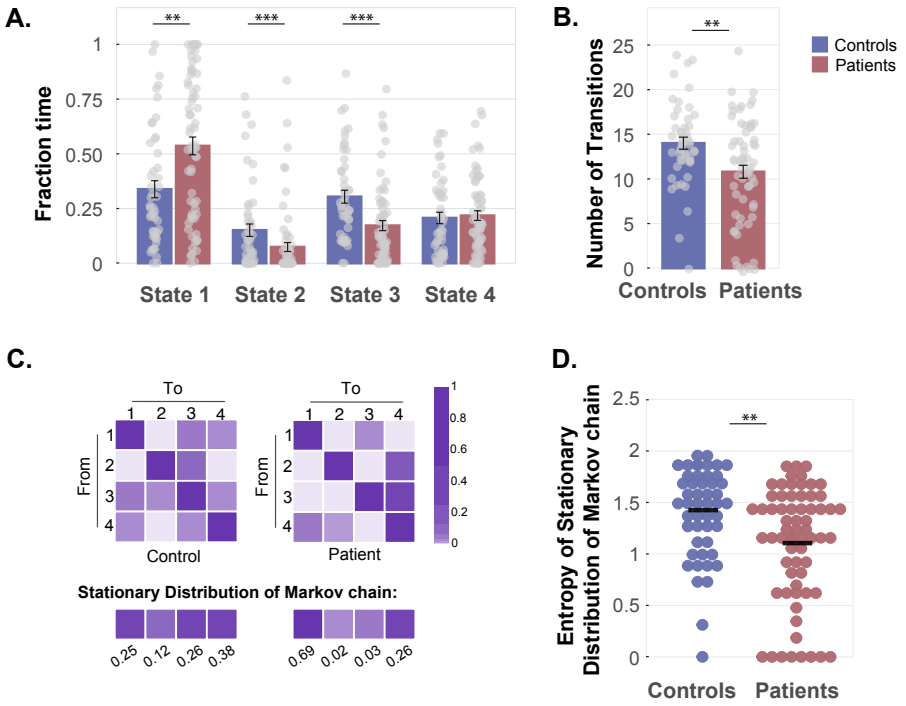


Figure 4.3: Temporal characteristics of states at subacute: Mean and standard error for the (A) fraction time and (B) number of transitions per group. Significant differences were found after FDR correction between groups for the time spent on State 1, 2 and 3, with patients spending more time on State 1 than both anticorrelation states 2 and 3. Patients also showed significantly less number of transitions in comparison to controls. Stationary distribution of Markov chain was estimated from transitions matrices as showed in (C) for one control and one patient. (D) Entropy of the discrete stationary distribution of Markov chain was also estimated. Patients showed a significantly reduction of entropy following TBI when compared with controls. FDR p-value: * 0.05 - 0.01; ** 0.01 - 0.001; *** 0.001 - 0.0001

(Figure 4.4A). Plasma NFL concentration increased over the time until the subacute scan. Entropy in patients was significantly correlated after FDR correction with concentration of GFAP, NFL, UCHL-1 and T-Tau. No significant correlation was observed between controls' entropy and their blood biomarkers concentration (FDR corrected p-values $>$ 0.05).

4.3.4 Relationship with structural organisation

Figure 4.5A shows significant differences after FDR correction in white matter organisation over a set of tracts between patients and controls. Mean FA of left frontal aslant tract (FAT) and both genu and body of corpus callosum had an AUC greater than 0.70 in discriminating controls and patients (Figure 4.5A). Using a multivariate measure combining mean FA of all tracts (eg. Mahalanobis distance), we were able to better discriminate our groups with an AUC of 0.77 than any individual tract.

We next examined whether greater white matter injury was associated with lower entropy (Figure 4.5B). Mahalanobis distance, where greater values represent worse white matter organisation, was not significantly correlated with entropy. A set of tracts were found to be significantly correlated with entropy, and right FAT, which is part of the salience network, was the individual tract most correlated with entropy. FAT tract in this study refers to the tract from right anterior insula to dorsal ACC/preSMA from Bonnelle et al. (2012), which partly overlaps with frontal aslant tract described by Catani et al. (2012).

4.3.5 Longitudinal characteristics

We reran the K-means clustering algorithm on the fMRI scans acquired at 6 and 12 months. Four optimal states were found using the elbow method, visually matching the states observed in the subacute scan (Figure C.5 in Appendix). Next, we investigated if longitudinal changes in blood biomarkers were associated with longitudinal changes in entropy over a period of 6 months. There was a significant correlation (r=-0.62, FDR, p-value=0.005) between longitudinal changes in T-Tau and entropy over this period (Figure 4.6). An increase in entropy was significantly associated with a decrease in T-Tau

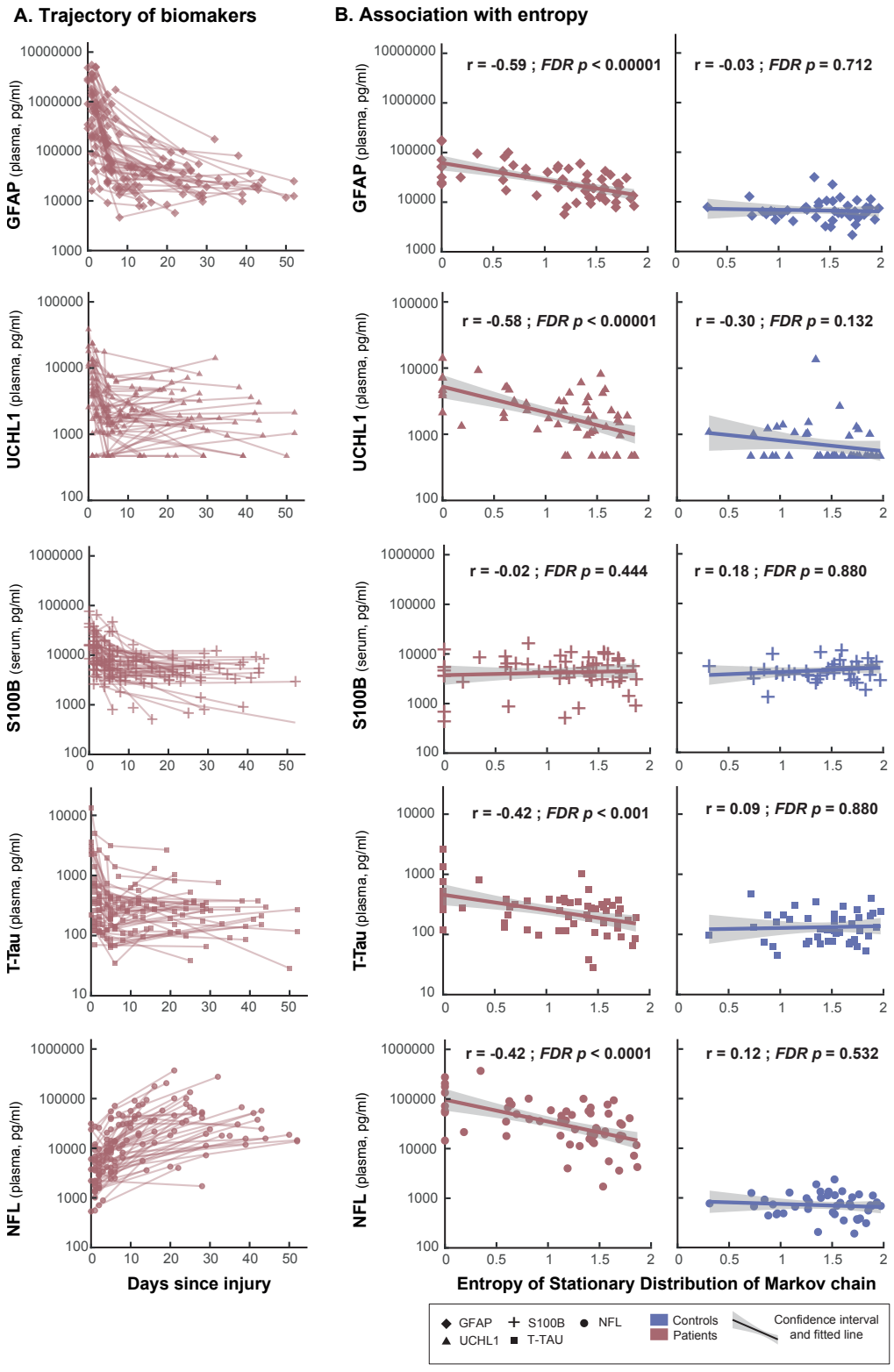


Figure 4.4: Association of blood biomarkers and entropy of stationary distribution of Markov chain at subacute: Trajectory of blood biomarker concentrations following TBI upto the first scan is showed in (A). Entropy was associated with the concentration of blood biomarkers at the time of the scan. A negative and significant Spearman's correlation was found for GFAP, UCHL-1, T-Tau and NFL. No association was found between entropy and blood biomarkers in controls

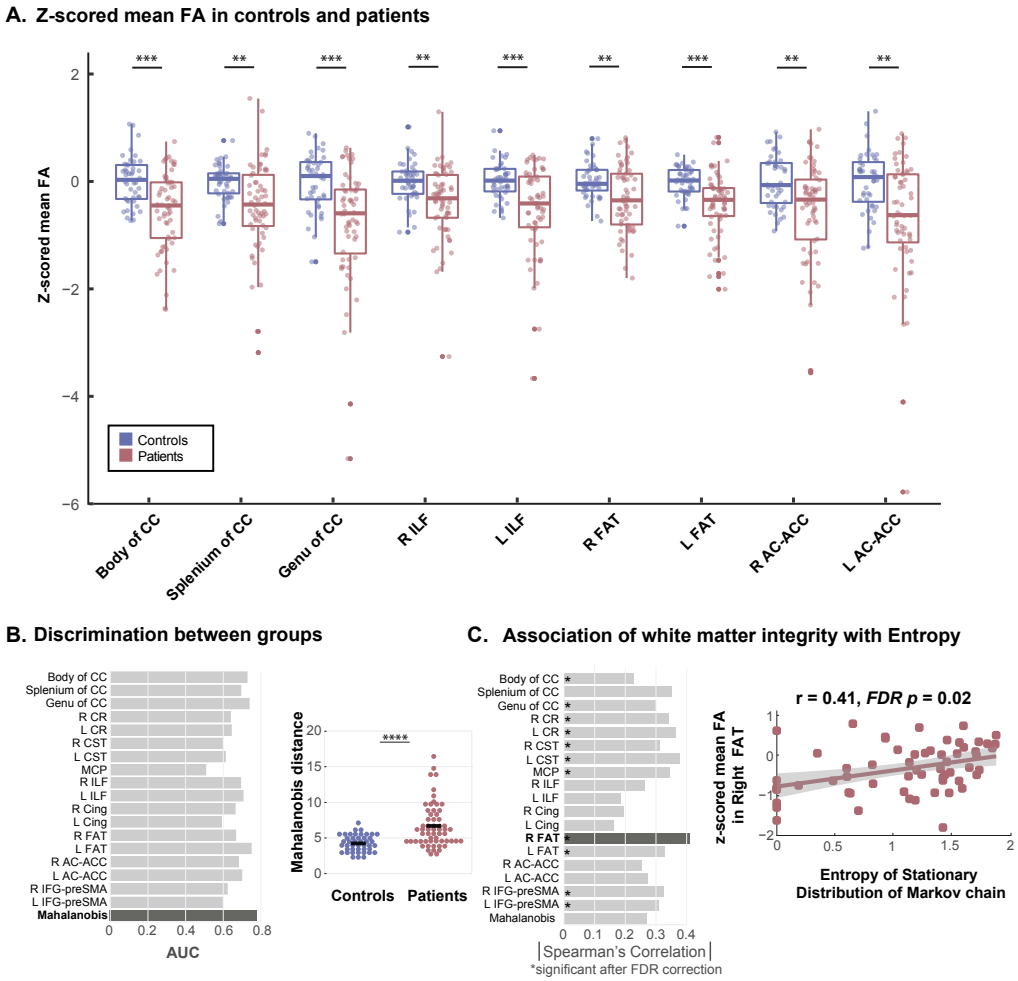


Figure 4.5: White matter organisation: FA z-scored in reference to controls of corresponding sites was estimated for a set of tracts. Significant differences after FDR correction were found between patients and controls for the set of tracts in (A). For visualisation purposes, only the set of tracts with significant differences between groups and with Cohen-D above 0.7 are showed. Significant differences were also found for right ventro-basal tract and both left and right corona radiata. (B) Mahalanobis distance was the most discriminative measure of white matter organisation between patients and controls. (C) We compared the different measures of white matter organisation with entropy. FA in right FAT showed the higher and significant correlation with entropy. FDR p-value: * 0.05 - 0.01; ** 0.01 - 0.001; *** 0.001 - 0.0001; **** <0.0001; Tracts: CC - corpus callosum; CR - corona radiata; CST - corticospinal; MCP - middle cerebellar Peduncle; ILF - Inferior longitudinal fasciculus; Cing - Cingulum; FAT - Frontal Aslant; AC-ACC - anterior caudate to anterior cingulum; IFG-preSMA - inferior fronal gyris to pre-supplementary motor area

concentration. By using a linear-mixed model with initial concentration of T-Tau as additional independent variable, we found that entropy and blood biomarker relationship remained significant (estimate of regression coefficient for T-Tau: β = -0.1602, p-value = 0.002 ; estimate of regression coefficient for initial concentration of T-Tau: β = 0.1403, p-value= 0.03). This result suggests that changes in T-Tau explains changes in entropy over a period of 6 months beyond that explained by the initial concentration of T-Tau alone.

No significant correlation after FDR correction between changes in entropy and changes in other blood biomarkers was found. Changes in T-Tau were not correlated with changes in white matter organisation, as measured by Mahalanobis distance (r = 0.11, p-value = 0.593). This finding suggests that a possible link between the evolution of T-Tau and brain function following TBI is stronger than longitudinal changes in white matter organisation.

4.3.6 Sedation

Thirteen severe TBI patients were sedated during the subacute scan. After removing these patients from the subacute analysis, there were no significant differences in entropy between patients and controls. However, patients still spent significantly less time than controls in State 3 (Figure C.6 in Appendix), the most frequent state showing the anticorrelation between DMN and both SN and FPNs. Entropy was still significantly correlated with hospital duration, with patients with less entropy spending more time in hospital (Figure C.4B in Appendix). There was still a significant correlation between entropy and GFAP, NFL and UCHL-1 of blood biomarkers during the subacute phase (Figure C.7 in Appendix). None of the patients who were sedated during the subacute scan returned for further scans at 6 or 12 months, therefore our main finding showing a link between the evolution of T-Tau and entropy following TBI as shown in Figure 4.6 was not affected by this potential confound.

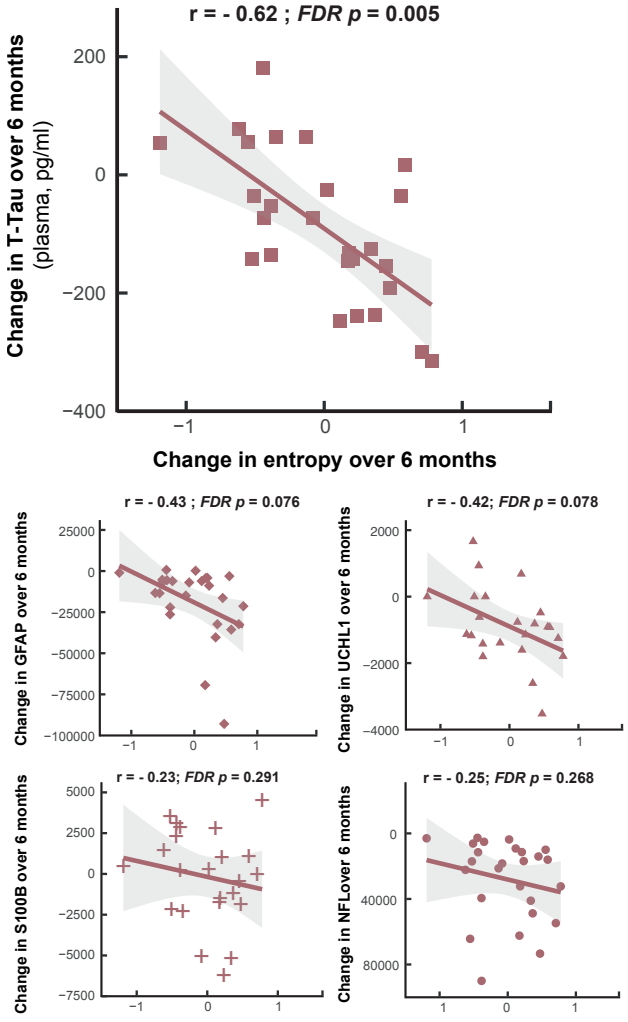


Figure 4.6: Association of entropy and blood biomarkers over 6 months following injury: A negative and significant association between changes in T-Tau concentration over 6 months after injury and changes in entropy over the same time period was found. This finding remained significant after controlling for the initial concentration of T-Tau. No significant association between entropy and other blood biomarkers was found. However, there is a trend between GFAP concentration and entropy which did not survived FDR correction.

4.4 Discussion

In this study, we show a disruption in the functional flexibility to transition between regions of DMN and cognitive-control networks following TBI which is related to plasma T-Tau. To our knowledge, this study investigates for the first time the relationship of T-Tau and other fluid blood biomarkers with functional connectivity disruption following TBI in humans. The major findings of our study reveal the existence of distinct patterns of functional connectivity between regions of DMN, FPNs and SN at rest and secondly, it reveals that reduced ability to transition between functional patterns is strongly associated with increased T-Tau concentrations over a period of 6 months after injury. The increase in T-Tau was specific to functional changes, as no association was found with white matter organisation.

4.4.1 Distinct cognitive-related functional states following moderate-severe TBI

Human cognition depends on complex interactions across DMN and cognitive-control networks to integrate information (Murphy et al. (2020)). Since TBI survivors frequently suffer from long-lasting cognitive impairments, we performed a dFNC analysis to investigate the dynamic interactions across cognitive-related functional networks. We found two expected states showing an anticorrelation between regions of DMN and cognitive-control networks, namely FPNs and SN. Previous studies have already shown an anticorrelation between DMN and both FPNs and SN (Kelly et al. (2008); Murphy et al. (2020); Sharp et al. (2014); Bonnelle et al. (2012)). In high working memory load tasks "task-negative" DMN and both "task-positive" FPNs and SN are in competition, with better cognitive performance linked to greater activation of cognitive-control networks and DMN deactivation (Li et al. (2019b)). In this study, we observed subacute TBI patients spending significantly less time in the anticorrelation states in comparison to controls. Bonnelle et al. (2012) showed a link between disruption of the anticorrelation between DMN and SN with disruption of white matter organisation of a SN tract connecting the right anterior insulae to the presupplementary motor area and dorsal anterior cingulate cortex, the tract named as FAT in our study. We also found significantly reduced FA in patients at

the subacute stage in comparison to controls in this tract. This may explain the lack of anticorrelation states or their infrequency in our subacute patients. We also found one unexpected state, showing dorsal PCC , left inferior frontal gyrus and, to a lesser extent, ventral PCC , all from DMN, correlated with some regions of left FPN. The anticorrelation between DMN and both right FPN and SN was still present. Recently, Murphy et al. (2020) found that the frontoparietal system can be separated into two novel subnetworks, where one is correlated with dynamics of DMN, and the other is anticorrelated. This suggests that some frontoparietal regions can be linked with introspective processes of DMN (Dixon et al. (2018)) as seen in our State 4. No differences in the time spent in this state was found between our groups, suggesting that the contribution of frontoparietal networks to introspective processes is not disrupted following moderate-severe TBI.

The brain must be able to flexibly transition between functional network states in order to respond appropriately to external or internal demands (Hou et al. (2019)). The temporal variations across all states were combined, as measured by entropy, to estimate functional flexibility between distinct networks. Subacute patients showed lower entropy in comparison to controls. In a cohort of mild-moderate TBI patients of which 92% had mTBI, Horn et al. (2020) also observed a lower functional flexibility by estimating travelling-distance between meta-states and meta-state transitions. It is known that structural connections shape neural dynamics (Honey et al. (2010); Sharp et al. (2014)). Lower entropy in our patients was not significantly associated with a disruption of white matter organisation, as measured by Mahalanobis distance, but was associated with a reduction of FA in right FAT. A measure of widespread white matter organisation might capture brain structural alterations beyond those with an impact on cognition. Thus, integrity of FAT which is responsible for the modulation of the anticorrelation between DMN and SN for cognitive processes (Bonnelle et al. (2012); Li et al. (2019b)) may better explain subtle differences in the interactions between cognitive-related networks. Future studies should also investigate how alterations in FAT and the remaining subset of white matter tracts found to be significantly associated with entropy, relate to T-Tau. With longitudinal data available for both DWI and fMRI sequences, we should also investigate, in future, how functional flexibility given by entropy might be altered by hyperconnectivity patterns often observed

after TBI.

4.4.2 Fluid blood biomarkers associated with functional flexibility

In the period from 6 days to 10 weeks after injury, we found an increase in multiple fluid blood biomarkers, namely UCHL-1, GFAP, NFL and T-Tau, associated with a reduction in the flexibility of functional coordination between DMN, FPNs and SN. This association was not seen in controls. Previous studies have shown that UCHL-1 and GFAP are promising biomarkers for neuronal and astroglial injuries (Zetterberg and Blennow (2016)) respectively, and are related to injury severity and outcome (Takala et al. (2016); Bogoslovsky et al. (2017); Vos et al. (2010)). Both NFL and T-Tau are sensitive biomarkers of axonal injury (Zetterberg and Blennow (2016)), and relate to patient outcome (Shahim et al. (2016, 2020); Zemlan et al. (2002); Ost et al. (2006)). Our findings suggest that distinct injury mechanisms may have an effect on functional flexibility at the subacute injury stage. However within the limits of our study it is not possible to disentangle the effect of specific injury mechanisms within a cohort heterogeneous for injury mechanism from severity.

Pathological tau leads to cognitive deficits by silencing neural circuits in mice. Therefore, we investigated if persistent functional deficits in TBI patients were correlated with presence of tau. Changes in functional flexibility over the first 6 months following injury were strongly associated with changes in T-Tau over the same time period but not with other blood fluid biomarkers. This finding remained significant after controlling for the initial concentration of T-Tau. This result provides novel insight into the impact of pathological neural mechanisms of tau on brain function in humans. To our knowledge, an association between functional connectivity and T-Tau has been shown previously in mice models but not in humans (Busche et al. (2019); Marinković et al. (2019); Menkes-Caspi et al. (2015)). Recently, it was shown that soluble tau can impair neuronal activity by silencing neurons, which can be reversed by a therapeutic intervention (Rubenstein et al. (2019)). Green et al. (2019) investigated the effect of human tau with pro- or anti-aggregant mutations in transgenic mouse models of Alzheimer's disease. They looked at functional and structural connectivity using diffusion-sensitized structural MRI and rs-fMRI. Over

a period of 12-months, mice with both pro- and anti-aggregant mutations showed a reduction of functional connectivity, suggesting for the first time that soluble tau induces functional deficits rather than fibrillary tau. After 12 months, transgenic human tau was supressed by doxycycline treatment for 8 weeks and soluble tau disappeared. Functional connectivity was restored to values equivalent to wildtype litter-mates. This evidence suggests that effects of tau pathology might not be irreversible but instead a temporary blocker for brain function. Our results suggest an early distortion of functional flexibility after TBI, likely due to the injury itself, which worsens over 6 months associated with an increase in tau concentration. Early functional flexibility deficits have been related with chronic incomplete recovery (Horn et al. (2020)). By blocking functional flexibility, tau might be suppressing functional reorganisation required following TBI and thus, patients experience persistent deficits. Our results present further evidence of the neural mechanisms for persistent functional deficits following TBI. It is consistent with other evidence suggesting therapeutic intervention to reverse tau suppression could improve long-term outcomes in patients.

We also investigated an association between subacute entropy and its change over 6 months with GOSE at 6-months and MOCA scores at 12-months. Entropy in the subacute phase showed an acceptable discrimination of GOSE groups at 6 months (AUC=0.71). However, no discrimination was found when severe patients sedated during scan were removed from the analysis. No discrimination was found with 12-months MOCA scores and entropy at the subacute phase or its change over time. In this study, we used a subset of patients from a larger study where it an association between T-Tau and MOCA was shown ($r = 0.17$, p-value = 0.0003) (Graham et al. (2020a)). We were not able to replicate this finding as we are limited by a smaller dataset with less severe patients. These limitations may also explain the lack of association seen between entropy and both GOSE and MOCA. In addition, phosphorylated tau (P-Tau) might be more sensitive to severity and cognitive performance than T-Tau. Yang et al. (2017) reported that levels of P-Tau, and not T-Tau, were correlated with TBI severity and cognitive deficits in patients with moderate-severe TBI.

4.4.3 Limitations

There were several limitations in this study. The sample-size was smaller at 6 and 12 months which limits our longitudinal findings. Our main longitudinal finding includes a correlation of -0.62 between changes in tau with changes in entropy over 6 months after injury. To reach a statistical power of 80% with a significance of 0.05, at least 18 patients would be required to observe a correlation of 0.62. Our sample-size of patients with both longitudinal fMRI and fluid blood biomarkers exceeded the required number of patients by 31% (18 vs 26). Next, in a multi-site study there might be differences between scanners that can result in false positives. In this study, we reduced scanner differences by removing differences in structured noise across scanners using ICA-AROMA and secondly, by including site as confound to regress out differences in the amplitude of BOLD signal. Feis et al. (2015) showed that structured noise differences can be reduced by an ICA-based clean up approach. In their study they applied a different ICA-based approach, which, as opposed to ICA-AROMA, also regresses out 24 motion parameters. In order to account for this difference we also regress the 24 motion parameters. Additionally, by manually labelling ICA-AROMA components we also confidently assured the removal of structured noise differences across scanners as well as removal of motion. Regarding our protocol for rs-fMRI scans, longer acquisition times can potentially increase the detection power of dFNC (Hindriks et al. (2016)). However, other studies were able to identify dFNC using an acquisition of 10 min, as in this study, or even lower (Bonkhoff et al. (2020); Fong et al. (2019); Hou et al. (2019); Schumacher et al. (2019); Horn et al. (2020)). Regarding DWI preprocessing, more advanced reconstruction techniques could have been used which can correctly represent complex white matter fibre configurations, such as crossing fibers, as opposed to DTI model. Finally, in this study we assessed T-Tau concentration which includes phosphorylated and unphosphorylated forms of tau. Rubenstein et al. (2017) showed that P-Tau and P-Tau:T-Tau rate may be more robust for determination of TBI severity and neurotrauma than T-Tau. However, Olivera et al. (2015) showed that T-Tau may be of pathophysiological relevance as military personnel with history of TBI had long-term elevations of plasma T-Tau correlated with post-concussive symptoms. In addition, while assessing a relationship between T-Tau with entropy, mixel-linear models should be

used in future to account for the heterogeneity of clinical characteriscts of TBI patients.

Chapter 4: High Concentration of T-Tau Following TBI Related to Network Functional Inflexibility: a Longitudinal Study

Chapter 5. Conclusion and Future Directions

The aim of this thesis was to better characterise the induced longitudinal effects of injury either as result of traumatic brain injury (TBI) or resective surgery on brain structure and function. By making use of graph theory, machine learning and imaging this has been achieved. A summary of the main findings and some potential future directions are presented below.

5.1 Summary of Work

Network reorganisation following ATLR and its relation with seizure relapse
In Chapter 2 we show substantial longitudinal diffusion changes in topology and within white matter fasciculus after surgery. Both alterations were found beyond the site of resection. By comparing with a "null" model, we show that induced alterations in network topology were beyond that expected from the surgery itself, suggesting a reorganisation response by the residual brain. Postoperative seizure freedom was not associated with alterations in topology. In contrast, postoperative seizure-free patients had a significantly larger reduction of quantitative anisotropy (QA) in inferior fronto-occipital fasciculus (IFOF), uncinate fasciculus (UF) and extreme capsule (EMC), a result maintained even after controlling for volume of resection.

Changes in network structure following mTBI and its association with cognitive recovery
In Chapter 3 we show significant longitudinal network changes over one year after mild TBI (mTBI) mainly in fronto-temporal regions, cingulum and some basal ganglia structures. Topological alterations in a set of those regions were predictive of alterations in cognitive performance over the same time period, with alterations in medial superior frontal, anterior cingulum and middle temporal cortices being the more relevant.

High concentration of T-Tau following TBI related to network functional inflexibility: a longitudinal study

In Chapter 4 we show an alteration in functional coordination between cognitive-related intrinsic connectivity networks (ICNs), with moderate-severe patients showing a more "rigid" brain early after injury. In comparison to controls, patients spent significantly less time in an anticorrelated state, known for its relevance in cognitive function, and more time in an undifferentiated state. Reduction in T-Tau concentration over 6 months was associated with improvements in dynamic functional connectivity over the same time period. Changes in the coordination between functional ICNs and T-Tau were not related with patients' outcome.

5.2 General Considerations

The impact of resective surgery on network topology has previously been inferred in Taylor et al. (2018) by the removal of transected connections in preoperative networks, the so called null model in this thesis. However, inferring surgery-induced changes in brain topology without including postoperative data does not allow assessment of secondary degeneration and/or brain reorganisation or even investigate if these mechanisms occur. Using longitudinal data with postoperative scans, we show for the first time evidence of secondary degeneration and/or brain reorganisation following anterior temporal lobe resection (ATLR) in temporal lobe epilepsy (TLE) patients. Our results confirm previous findings of widespread alterations after epilepsy surgery including primary degeneration proximal to the resection and in more distant areas (McDonald et al. (2010); Yogarajah et al. (2010); Winston et al. (2014)). We extended these studies by showing that these alterations are potentially secondary adaptive changes. Using a null model of surgery, as in Taylor et al. (2018), we showed these changes to be above and beyond those expected through the removal of connections alone. We found evidence of possible further degeneration and strengthening of specific white matter tracts beyond what was expected. Moreover, greater QA reductions in interhemispheric connections and in the vicinity of resection were related to postoperative seizure freedom in left TLE suggesting a greater impact of local tract properties, a finding not shown previously to our knowledge. Thus,

we can conclude that our work in Chapter 2 contributes to an improved understanding of how brain networks and white matter fasciculi change in response to surgery.

Longitudinal alterations in brain networks and white matter fasciculi in response to moderate-severe TBI have been widely reported, as opposed to mTBI. At the time the study in Chapter 3 was conducted, we knew of a single longitudinal study on structural brain network changes and cognitive function in mTBI (Dall'Acqua et al. (2017)), which focused on individual connections between brain regions. We hypothesised that a graph-theoretical perspective on the connectivity of regions which accounts for wider network connectivity (rather than individual connections which do not) is also likely to be informative (Fagerholm et al. (2015); Rubinov and Sporns (2010)). Thus, we extended their study by investigating topological differences over 1 year following mTBI at a regional level. Our findings demonstrate a longitudinal relationship between changes in structural brain connectivity and changes in cognitive functions following TBI. Dall'Acqua et al. (2017) reported structural hyperconnectivity in a subnetwork involving anterior cingulum cortex (ACC) at an early phase, which normalised chronically, suggesting a possible temporary and compensatory mechanism. Similarly we observed an early increase of ACC strength which normalised later in the majority of patients. Our regression model suggests that normalisation of ACC's strength is positively associated with cognitive recovery. This normalisation and further alterations in frontal and temporal regions were the major explanators for cognitive changes. Thus, a detailed graph theoretical analysis on connectivity of regions can also contribute to an improved understanding of how brain networks change in response to mTBI. Moreover, combining different network metrics in distinct brain regions in a multivariate way using machine learning also allow one to characterise longitudinal variance in cognitive performance.

Alterations in cognition or behaviour are often described as the result of alterations to the cost-effective architecture of brain networks, making graph theoretical analysis a powerful tool to characterise patients' behaviour or cognition over time. Recently, Rubenstein et al. (2019) showed a link between high concentrations of tau in plasma with behaviour and cognitive deficits in mice models for repetitive mTBI. As mentioned in Chapter 1, TBI can result in the release of tau from microtubules during axonal injury. However, Ruben-

stein et al. (2019) showed that the behaviour and cognitive deficits were restored after supressing tau. Green et al. (2019) also showed that tau induces functional deficits and when supressed functional connectivity is restored. These findings suggest that deficits seen following injury are not just a consequence of axonal injury. The presence of tau can itself drive cognitive and behaviour deficits, making one consider that graph theoretical analysis should be complemented by this additional factor when characterising patients' behaviour or cognition over time. In Chapter 4 we show for the first time an association of T-Tau with alterations in functional connectivity in humans. More specifically, we showed that T-Tau might supress the ability of ICNs to cooperate. Thus, our study provide further evidence of the neural mechanisms for persistent functional deficits in TBI.

5.3 Clinical Implications

In this thesis, we characterise longitudinal effects of injury on brain structure and function following an injury. Using graph theory, machine learning and medical imaging analysis, we identified potential biomarkers associated with injury recovery and severity.

Identification of biomarkers specific to injury recovery and/or function impairment, such as topological features, white matter organisation assessments or fluid blood biomarkers, are essential to define trajectories of injury progression, which can potentially be used at an individual level in future. For instance, we identified topological features in mild TBI patients which were associated with better cognitive performance including a potential early compensatory mechanism, also described in (Dall'Acqua et al. (2017)). By assessing structural networks over time, one can possibly estimate the trajectory of an individual in terms of structural alterations/biomarkers in specific brain regions and assess how those trajectories fit with function recovery, as seen in group-level analysis. However, given the heterogeneous behaviour of TBI, more single subject analyses are likely needed to personalise medicine approaches and therapies (Chamberland et al. (2020)).

Processing imaging data with more sophisticated methods is not always feasible in a clinical setting, especially when those methods are computationally expensive and time consuming. Alternatively, fluid blood biomarkers can be easily used in clinical practise.

Little is still known how some fluid blood biomarkers relate to neurodegeneration, a better understanding on how brain function is related with those biomarkers might help in future prognosis and therapy stratification.

5.4 Future Directions

An improved understanding of how brain networks and white matter fasciculi change in response to surgery might allow us to fit better models in future when predicting seizure-freedom. Although we did not observe an association between postoperative seizure freedom and alterations in topology, we only explored this association in a univariate way and further studies would be needed to clarify this point. In Chapter 2 we show evidence of secondary degeneration following resective surgery. The impact of secondary degeneration itself on seizure-freedom should be further investigated. Increased levels of P-Tau in mice models and TLE patients suggest that epilepsy might involve tauopathy (Xi et al. (2011); Yan et al. (2012); Puvenna et al. (2016); Liu et al. (2017)), so one could argue that tau pathology exacerbated by transection of tracts could lead to further degeneration and atrophy, and possibly contribute to seizure relapse. Following ATLR, patients can experience seizure relapse from early to years after surgery. Do patients with early relapse reach a "critical point" of atrophy quicker than other patients who only reach it years after? It has been shown that patients with longer epilepsy duration have poorer outcomes following surgery. Is that related with higher levels of atrophy which would be further exacerbated by surgery? Modelling atrophy propagation with longitudinal data could possibly allow us to find this "critical point" and investigate its existence. Nevertheless, one needs to consider that epilepsy is a complex disorder that cannot be fully explained in just one scale or in just one perspective (spatial vs temporal). Moreover, as mentioned in Chapter 1, fractional anisotropy (FA) is sensitive to white matter pathology but not specific to axonal damage or demyelination, so surgery-induced changes should be further investigated with other diffusion metrics such as radial diffusivity (RD) and axial diffusivity (AD).

In Chapter 3, we showed the existence of topological alterations following mTBI at a regional level and suggested possible mechanisms underlying those changes. A better un-

derstanding on the underlying mechanisms following mTBI can potentially help clinicians in prognostication. By following a similar approach to the one in Chapter 2, we could potentially disentangle the effect of different mechanisms in future studies. Without a pre-injured network to create a "null model", one could create such model by removing the affected tracts at the time of the impact from brain networks of a cohort of X controls. This will result on a set of X "null models" per patient. Connectometry, which detects subtle differences within fasciculi and can be performed at an individual level, is a useful tool to identify the injured tracts at an early phase in each patient. Differences in topological metrics between postoperative data at additional time points and distribution of those metrics on null models could potentially help disentangle the effects of neurodegeneration from temporary compensatory mechanisms, especially when combined with longitudinal assessments of patients' cognitive and behavioural outcomes. This analysis could also enable personalized predictions of recovery trajectories and optimal rehabilitation strategies based on network metric changes at higher temporal resolution.

In Chapter 4, we showed an association between T-Tau in plasma and a more "rigid" functional brain following moderate-severe TBI. Although, elevated concentrations of Tau have been related with cognitive and behavioural deficits in mice models, we did not find an association of tau with cognitive performance. P-Tau might be a preferred choice to quantify effects of tau pathology in human brain in future, especially in smaller sample sizes. There is still a lack of understanding on how tau blocks neuronal activity. Future studies are needed to investigate tau mechanisms to suppress neuronal activity at a cellular scale. It is also unknown how tau leads to cognitive and behaviour deficits and how its suppression restores these deficits. Longitudinal studies using graph theoretical analysis, complemented by repetitive assessments of tau, could better characterise causal relationships between tau and changes in structural and functional networks. If tau suppression in mice models restores cognitive deficits, one could argue that tau suppression might improve brain flexibility/coordination among subnetworks and thus, increase the ability for the human brain to reorganise and thus recover. Future clinical trials should be also conducted to investigate if individuals would recover more quicker with a tau therapy.

Appendix A. Supplementary Material - Alterations following ATLR

Additional tables, figures and information for Chapter 2 are presented below.

A.1 Additional Tables

	Left temporal lobe epilepsy (TLE)	Right TLE	Controls	Significance
Subjects (n)	8	5	17	-
Sex (Male/Female)	3/5	0/5	8/6	Chi2 (Left TLE; Controls) = 0.786 p = 0.375 Chi2 (Right TLE; Controls) = 4.935 p = 0.026
Age at baseline scan	38.43±11.56	35.60±11.56	38.14±10.09	t (Left TLE; Controls) = 0.060 p = 0.953 t (Right TLE; Controls) = -0.466 p = 0.647
Onset	15.38±9.41	13.20±3.56	-	-
Age at surgery	38.68±11.49	36.72±11.61	-	-
Epilepsy Duration	23.30±17.19	23.52±10.88	-	-
Status Epilepticus (n)	2	0	-	-
Secondary generalised seizures (n)	7	3	-	-
Hippocampal Sclerosis (n)	6	3	-	-
Seizure-Free for 5 years (n)	4	0	-	-
Seizure recurrence (n)	3	3	-	-

Table A.1: Demographic and clinical data of patients and controls with imaging available 12 months after surgery.

IDP	Sex	Side	Onset	Surg	Dur.	Bas.	SE	SGS	HS	ILAE Y1	ILAE Y2	ILAE Y3	ILAE Y4	ILAE Y5	SF	Rel.
1	F	L	2	19.1	17.1	18.5	N	Y	Y	1	2	3	1	5	N	Y
2	F	L	13	20.3	7.3	19.8	Y	Y	Y	1	1	1	1	-	N	N
3	F	L	0.9	27.3	26.4	26.8	N	Y	N	1	1	1	1	1	Y	N
4	M	L	16	52.9	36.9	51.3	N	Y	Y	1	1	1	1	1	Y	N
5	M	L	32	40.6	8.6	40.6	N	N	N	1	1	1	1	-	N	N
6	F	L	34	38.6	4.6	37.9	N	Y	Y	2	2	2	2	1	N	Y
7	M	L	22	33.9	11.9	32.6	N	Y	N	1	1	4	1	-	N	Y
8	M	L	2	39.1	37.1	38.2	N	Y	Y	1	1	1	1	1	Y	N
9	M	L	8	40.3	32.3	38.9	N	Y	Y	2	1	1	1	-	N	Y
10	F	L	17	29.3	12.3	27.4	N	Y	Y	1	1	-	-	-	N	N
11	F	L	21	42.3	21.3	40.9	N	N	Y	4	4	4	4	1	N	Y
12	F	L	38	43.2	5.2	43.1	N	N	N	1	1	1	1	1	Y	N
13	M	L	31	46	15	45.9	N	Y	Y	1	2	3	3	1	N	Y
14	F	L	3	49.1	46.1	48.8	N	Y	Y	1	1	1	1	1	Y	N
15	M	L	23	28.6	5.6	28.2	Y	Y	N	1	1	1	1	1	Y	N
16	F	L	7	46	39	45.8	N	Y	Y	1	1	1	1	1	Y	N
17	M	L	12	45.1	33.1	44.9	N	Y	Y	1	1	1	1	1	Y	N
18	F	L	11	47.7	36.7	47.6	N	Y	Y	5	5	5	5	5	N	Y
19	F	L	16	31	15	30.8	Y	Y	Y	1	1	1	1	1	Y	N
20	M	L	7	26.4	19.4	26.3	N	N	Y	1	1	1	-	-	N	N
21	F	L	23	26.6	3.6	26.5	N	N	N	2	4	2	2	2	N	Y
22	M	L	17	32.5	15.5	32.1	N	N	Y	1	1	1	1	1	Y	N
23	M	L	1	47.3	46.3	46.2	N	Y	Y	1	1	1	1	1	Y	N
24	M	L	20	35.2	15.2	33.7	N	Y	N	1	1	4	3	3	N	Y
25	F	L	31	39.9	8.9	38.9	N	Y	N	1	2	1	1	1	N	Y
26	M	L	13	21.1	8.1	20.8	N	Y	Y	1	1	1	1	3	N	Y
27	F	R	14	22.2	8.2	21.1	N	Y	Y	2	3	4	4	4	N	Y
28	M	R	31	42.6	11.6	41.6	-	-	Y	1	1	1	1	1	Y	N
29	F	R	15	20.2	5.2	19.9	N	Y	N	1	1	1	2	4	N	Y
30	F	R	10	41.9	31.9	40.5	-	-	N	1	1	1	1	-	N	N
31	F	R	17	39.2	22.2	38.2	N	Y	Y	1	1	1	-	-	N	N
32	F	R	23	44.7	21.7	42.3	N	N	N	2	1	1	4	-	N	Y
33	F	R	7	48.1	41.1	46.7	N	Y	Y	1	1	1	-	-	N	N
34	F	R	50	68.2	18.2	66.8	Y	Y	N	4	4	4	4	4	N	Y
35	M	R	14	47.7	33.7	44.9	N	N	N	4	4	2	2	2	N	Y
36	F	R	22	48	26	46.8	N	Y	Y	1	1	1	1	1	Y	N
37	F	R	1.5	31.7	30.2	30.3	N	N	Y	1	1	1	1	1	Y	N
38	F	R	10	32.4	22.4	31.2	N	N	N	1	1	-	-	-	N	N
39	F	R	7	25.3	18.3	24.8	N	Y	N	1	1	1	1	1	Y	N
40	F	R	3	54.5	51.5	53.2	N	Y	Y	2	3	3	-	-	N	Y
41	F	R	18	47	29	45.3	N	Y	N	4	4	4	-	-	N	Y
42	F	R	12	48.2	36.2	47.3	N	Y	Y	1	1	1	-	-	N	N
43	F	R	15	23.4	8.4	22.6	N	Y	N	1	1	1	3	3	N	Y
44	F	R	23	36.6	13.6	35.7	N	N	N	2	1	2	2	1	N	Y
45	F	R	9	42.5	33.5	41.9	N	Y	Y	1	1	1	1	1	Y	N
46	F	R	2	57.3	55.3	57	N	Y	Y	1	1	1	3	1	N	Y
47	F	R	16	51.8	35.8	50.9	N	Y	Y	3	3	2	2	2	N	Y
48	F	R	9	28.5	19.5	27.3	N	N	N	2	1	4	4	4	N	Y

Table A.2: Complete preoperative clinical information of all patients with postoperative ILAE seizure outcomes and relapse data. *Abbreviations:* Sex: male (M)/female (F);); Side: side of surgery left (L) or right (R); Onset: epilepsy onset age in years; Surg.: age at surgery in years; Dur.: epilepsy duration in years; Bas.: age at baseline scan; SE: history of status epilepticus in yes (Y) or no (N); SGS: evidence of secondary generalised seizures in yes (Y) or no (N); ILAE Y1, Y2, Y3, Y4,Y5: post-surgery seizure outcome at year 1, 2, 3, 4 and 5; SF: seizure-free for 5 years in yes (Y) or no (N); Rel.: seizure-recurrence over 5 years in yes (Y) or no (N).

Properties	Metrics
Segregation	Average Clustering Coefficient
	Local Clustering Coefficient
	Local Efficiency
	Small-worldness
Integration	Characteristic Path Length
	Global Efficiency
	Small-worldness
Centrality	Closeness
	Betweenness
	Eigenvector
	Strength

Table A.3: List of network metrics used to quantify network segregation, integration and centrality.

Bundles	**No streamlines**	**Mean length±STD**	**Cohen's d**	**Finding**
AC	174	30.4 ± 8.51	-2.24	Reduction
AF_L	38	23.4 ± 2.56	-1.72	Reduction
AF_R	4	20.5 ± 0.87	-0.27	Reduction
AR_L	2	21.0 ± 1.00	-0.78	Reduction
AR_R	2	21.0 ± 1.00	-0.5	Reduction
C_L	25	27.5 ± 7.00	-1.05	Reduction
C_R	3	24.0 ± 5.66	-0.97	Reduction
CC	389	30.1 ± 9.33	-0.91	Reduction
CS_L	19	23.7 ± 3.57	-1.72	Reduction
CS_R	15	24.0 ± 2.42	-0.46	Reduction
CST_L	57	25.6 ± 4.38	-1.46	Reduction
CST_R	91	30.7 ± 8.81	-0.46	Reduction
CT_L	81	27.7 ± 6.89	-2.87	Reduction
CT_R	15	26.0 ± 5.16	-0.45	Reduction
EMC_L	5	24.8 ± 5.00	-2.19	Reduction
F_L	82	32.4 ± 10.95	-2.45	Reduction
F_R	5	22.0 ± 1.26	-1.37	Reduction

FPT_L	1	24.0 ± 0	-0.38	Reduction
FPT_R	59	29.7 ± 8.52	-0.5	Reduction
IFOF_L	667	41.3 ± 9.93	-2.94	Reduction
IFOF_R	36	25.4 ± 5.33	-0.44	Reduction
ILF_L	65	25.1 ± 4.24	-2.24	Reduction
ILF_R	2	21.0 ± 1.00	-0.37	Reduction
MdLF_L	27	23.5 ± 2.41	-1.87	Reduction
MdLF_R	3	24.7 ± 0.94	-0.5	Reduction
OPT_L	5	23.6 ± 1.50	-1.71	Reduction
OPT_R	23	25.3 ± 3.76	-0.38	Reduction
OR_L	4	22.0 ± 1.41	-0.94	Reduction
OR_R	1	22.0 ± 0	-0.26	Reduction
PPT_L	90	25.6 ± 3.69	-1.56	Reduction
PPT_R	49	28.4 ± 6.95	-0.44	Reduction
SLF_L	9	23.1 ± 2.13	-0.9	Reduction
SLF_R	2	20.0 ± 0	-0.28	Reduction
TPT_R	1	20.0 ± 0	-0.4	Reduction
UF_L	26	29.0 ± 5.30	-2.82	Reduction
all bundles	**2077**	**32.54 ± 10.61**	**-2.3**	**Reduction**
CC	37	24.0 ± 3.90	0.33	Increase
CS_L	77	23.7 ± 3.58	1.12	Increase
CS_R	1	20.0 ± 0	0.15	Increase
CST_L	76	24.3 ± 4.54	0.94	Increase
CST_R	2	20.0 ± 0	0.14	Increase
CT_L	24	23.5 ± 4.21	0.39	Increase
EMC_L	14	23.3 ± 1.62	0.84	Increase
FAT_L	1	20.0 ± 0	0.19	Increase
FPT_L	52	23.9 ± 4.29	1.12	Increase

FPT_R	2	20.0 ± 0	0.14	Increase
PPT_L	81	25.0 ± 4.79	0.92	Increase
PPT_R	2	20.0 ± 0	0.14	Increase
all bundles	**369**	**24.0 ± 4.24**	**0.87**	**Increase**

Table A.4: White matter changes significantly different between left TLE patients and controls 3 months after surgery. The subsections were grouped in the set of bundles of the connectome atlas. Cohen's d between groups, number of altered streamlines (No streamlines) and mean length for each bundle is presented below. The Cohen's d between groups taking into account all the subsections found by connectometry without any grouping is also presented with the label "all bundles".

Bundles	**No streamlines**	**Mean length±STD**	**cohen-D**	**Finding**
AC	255	35.21 ± 10.5	-3.63	Reduction
AF_L	2	21.00 ± 1.0	-0.58	Reduction
AF_R	37	25.51 ± 8.8	-1.3	Reduction
C_L	5	23.60 ± 2.9	-0.86	Reduction
C_R	119	33.98 ± 11.5	-0.81	Reduction
CC	650	27.77 ± 6.4	-1.19	Reduction
CS_L	14	22.00 ± 2.4	-0.64	Reduction
CS_R	61	22.56 ± 2.4	-1.95	Reduction
CST_L	4	26.50 ± 2.8	-0.73	Reduction
CST_R	136	24.93 ± 3.6	-1.76	Reduction
CT_L	12	24.83 ± 7.1	-0.78	Reduction
CT_R	198	26.55 ± 6.4	-3.12	Reduction
EMC_R	6	22.00 ± 1.2	-2.32	Reduction
F_L	3	23.33 ± 3.4	-1.04	Reduction
F_R	76	27.84 ± 5.9	-2.34	Reduction
FAT_L	5	22.40 ± 1.5	-0.96	Reduction
FAT_R	33	21.58 ± 1.4	-1.71	Reduction
FPT_L	17	23.53 ± 2.5	-0.99	Reduction

FPT_R	85	23.34 ± 2.9	-2.38	Reduction
IFOF_R	513	34.41 ± 10.6	-3.22	Reduction
ILF_R	8	36.25 ± 10.5	-1.88	Reduction
MdLF_R	50	24.64 ± 3. 2	-1.55	Reduction
OPT_R	31	24.13 ± 2.9	-1.6	Reduction
OR_R	2	23.00 ± 1.0	-0.72	Reduction
PPT_L	6	26.00 ± 4.8	-0.57	Reduction
PPT_R	89	25.44 ± 3.6	-1.5	Reduction
SLF_R	70	23.31 ± 3.5	-1.8	Reduction
U_R	6	22.33 ± 2.1	-1.54	Reduction
UF_R	100	35.78 ± 10.4	-4.97	Reduction
all bundles	**2593**	**29.4 ± 9.04**	**-2.76**	**Reduction**

Table A.5: White matter changes significantly different between right TLE patients and controls 3 months after surgery. The subsections were grouped in the set of bundles of the connectome atlas. Cohen's d between groups, number of altered streamlines (No streamlines) and mean length for each bundle is presented below. The Cohen's d between groups taking into account all the subsections found by connectometry without any grouping is also presented with the label "all bundles".

!

Bundles	**No streamlines**	**Mean length±STD**	**Cohen's d**	**Finding**
AC	17	24.82 ± 3.0	-1.14	Reduction
AF_R	3	27.33 ± 5.3	-0.18	Reduction
C_L	6	23.67 ± 3.4	-0.66	Reduction
CC	263	25.29 ± 6.1	-0.29	Reduction
CS_L	13	25.09 ± 5.2	-0.86	Reduction
CST_R	26	22.77 ± 2.9	-0.03	Reduction
CT_R	25	22.63 ± 2.3	-0.08	Reduction
EMC_L	1	21.71 ± 0.7	-1.92	Reduction
IFOF_L	137	24.00 ± 4.1	-2.93	Reduction
IFOF_R	12	22.75 ± 3.5	-0.2	Reduction

ILF_L	1	22.88 ± 2.3	-0.37	Reduction
ILF_R	1	26.00 ± 0	-0.17	Reduction
OPT_R	4	23.00 ± 1.7	-0.08	Reduction
OR_R	3	22.38 ± 2.4	-0.01	Reduction
PPT_R	31	30.60 ± 7.6	-0.06	Reduction
SLF_L	5	24.00 ± 2.8	-0.23	Reduction
SLF_R	3	20.00 ± 0	-0.1	Reduction
U_R	1	20.00 ± 0	-0.17	Reduction
UF_L	1	22.00 ± 0	-1.96	Reduction
UF_R	1	21.50 ± 1.7	-0.1	Reduction
all bundles	**554**	**23.3 ± 1.89**	**-1.24**	**Reduction**

Table A.6: White matter changes significantly different between left TLE patients with different surgical outcomes over 5 years. The subsections were grouped in the set of bundles of the connectome atlas. Cohen's d between groups, number of altered streamlines (No streamlines) and mean length for each bundle is presented below. The Cohen's d between groups taking into account all the subsections found by connectometry without any grouping is also presented with the label "all bundles".

Regions	**Abbr.**
Precental gyrus	PreC
Superior frontal gyrus, dorsolateral	SF
Superior frontal gyrus, orbital part	ORBsup
Middle frontal gyrus	MF
Middle frontal gyrus, orbital part	ORBmid
Inferior frontal gyrus, opercular part	IFOper
Inferior frontal gyrus, triangular part	IFTrian
Inferior frontal gyrus, orbital part	ORBinf
Rolandic operculum	ROL
Supplementary motor area	SMA
Olfactory cortex	OLF
Superior frontal gyrus, medial	SFMed
Superior frontal gyrus, medial orbital	ORBsupmed
Gyrus rectus	REC
Insula	insula (INS)
Anterior cingulate and paracingulate gyri	ACC
Median cingulate and paracingulate gyri	MCC
Posterior cingulate gyrus	PCC
Hippocampus	HIP
Parahippocampal gyrus	PHIP
Amygdala	AMY
Calcarine fissure and surrounding cortex	CAL
Cuneus	CUN
Lingual gyrus	lingual (LIN)
Superior occipital gyrus	SO
Middle occipital gyrus	MO
Inferior occipital gyrus	IO
Fusiform gyrus	FFG
Postcentral gyrus	postcentral (PoC)
Superior parietal gyrus	SP
Inferior parietal, but supramarginal and angular gyri	IP
Supramarginal gyrus	SMG
Angular gyrus	ANG
Precuneus	PCUN
Paracentral lobule	PCL
Caudate nucleus	CAU
Lenticular nucleus, putamen	putamen (PUT)
Lenticular nucleus, pallidun	PAL
Thalamus	THA
Heschl gyrus	HES
Superior temporal gyrus	ST
Temporal pole: superior temporal gyrus	TPOsup
Middle temporal gyrus	MT
Temporal pole: middle temporal gyrus	TPOmid
Inferior temporal gyrus	IT

Table A.7: AAL regions and their abbreviation included in the study.

Classification	**Bundles**	**Abbr.**
Association	Arcuate Fasciculus	AF
	Cingulum	C
	Extreme Capsule	EMC
	Frontal Aslant Tract	FAT
	Inferior Fronto Occipital Fasciculus	IFOF
	Inferior Longitudinal Fasciculus	ILF
	Middle Longitudinal Fasciculus	MdLF
	Superior Longitudinal Fasciculus	SLF
	U-fiber	U
	Uncinate Fasciculus	UF
	Vertical Occipital Fasciculus	VOF
Commissural	Anterior Commissure	AC
	Corpus Callosum	CC
	Posterior Commissure	PC
Projection	Acoustic Radiation	AR
	Corticostriatal Pathway	CS
	Corticospinal Tract	CST
	Corticothalamic Pathway	CT
	Fornix	F
	Frontopontine Tract	FPT
	Occipitopontine Tract	OPT
	Optic Radiation	OR
	Parietopontine Tract	PPT
	Temporopontine Tract	TPT

Table A.8: Tracts from the connectome atlas and their abbreviations.

A.2 Additional Figures

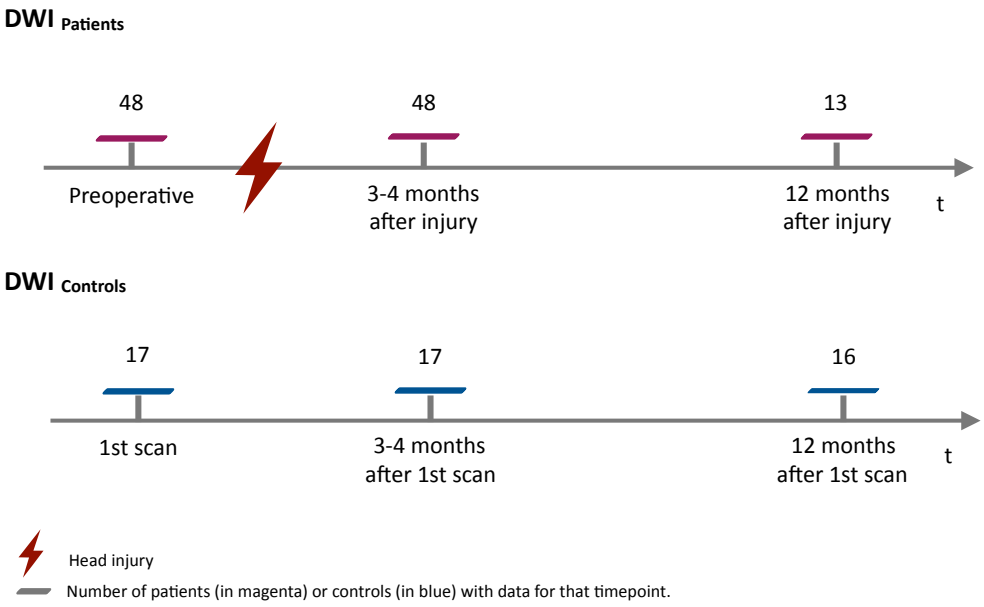


Figure A.1: Diagram of available longitudinal DWI data for both controls and patients. There was loss of data for the last timepoint due to patient dropout. In addition, data are still being collected.

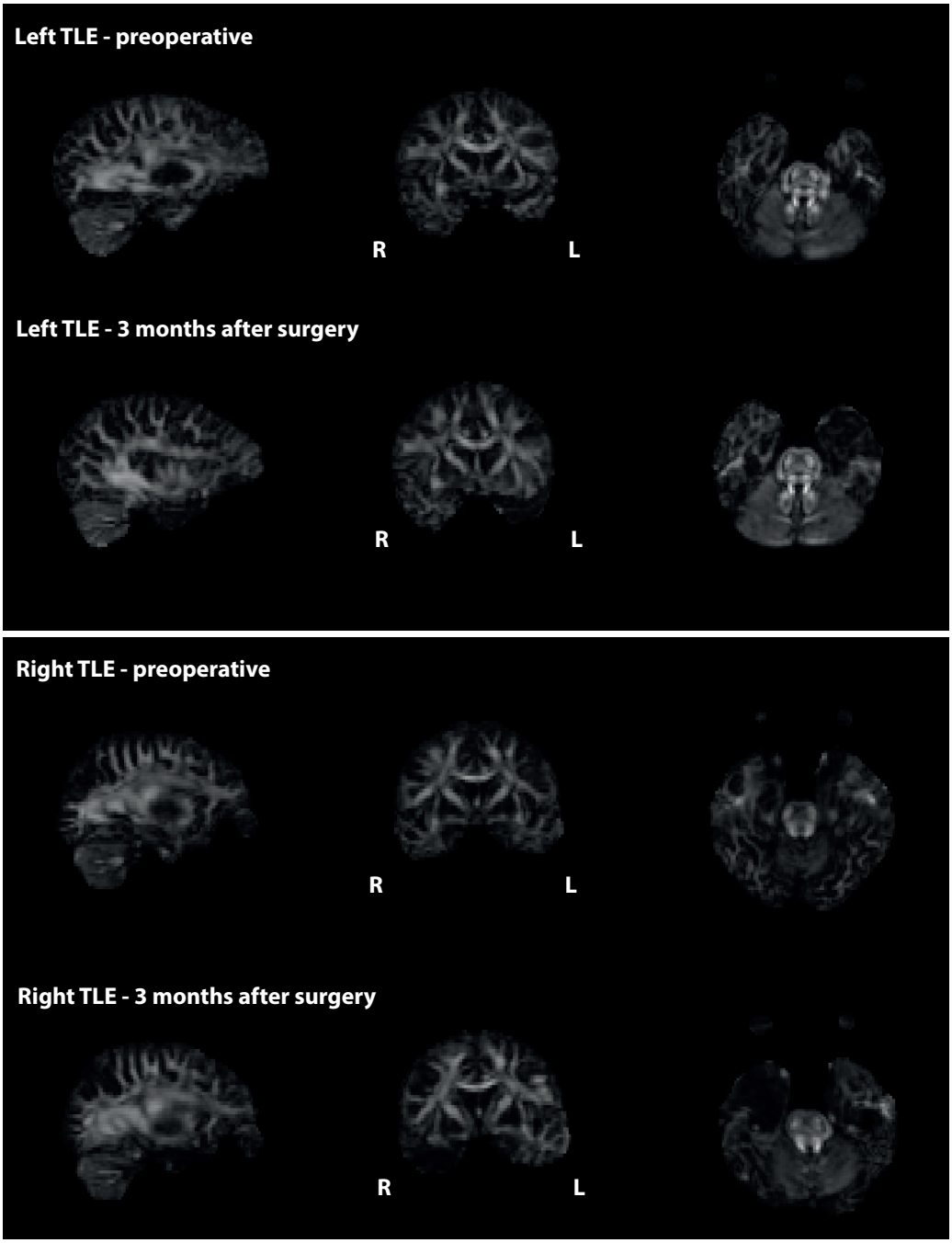


Figure A.2: Raw QA image for left and right TLE patients, preoperatively and 3 months after surgery.

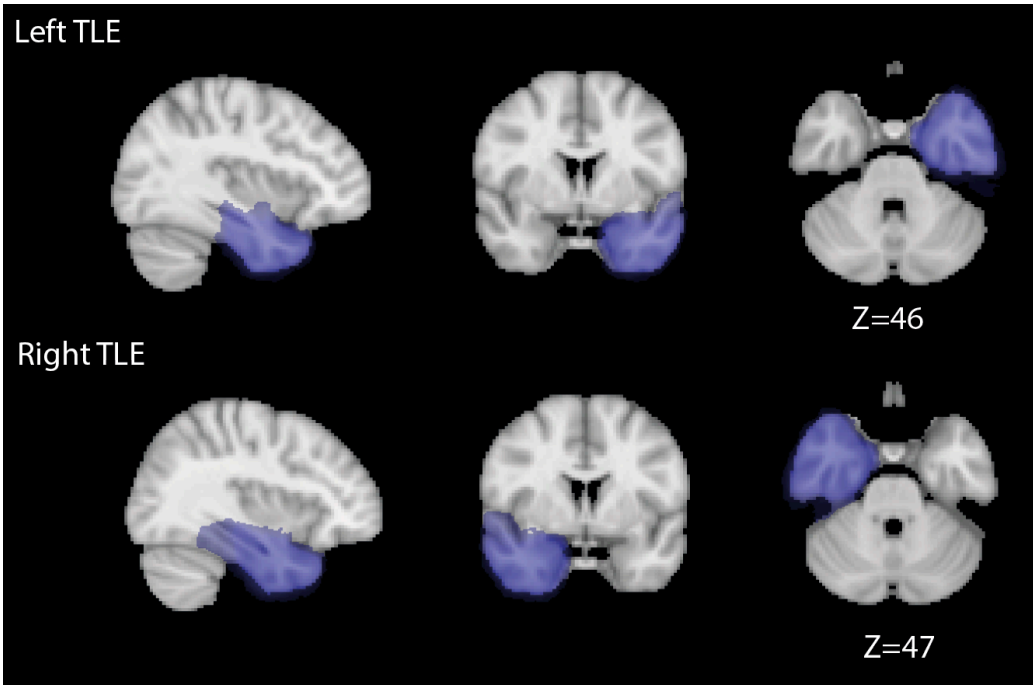


Figure A.3: Overlaid resection masks across all left and right TLE patients.

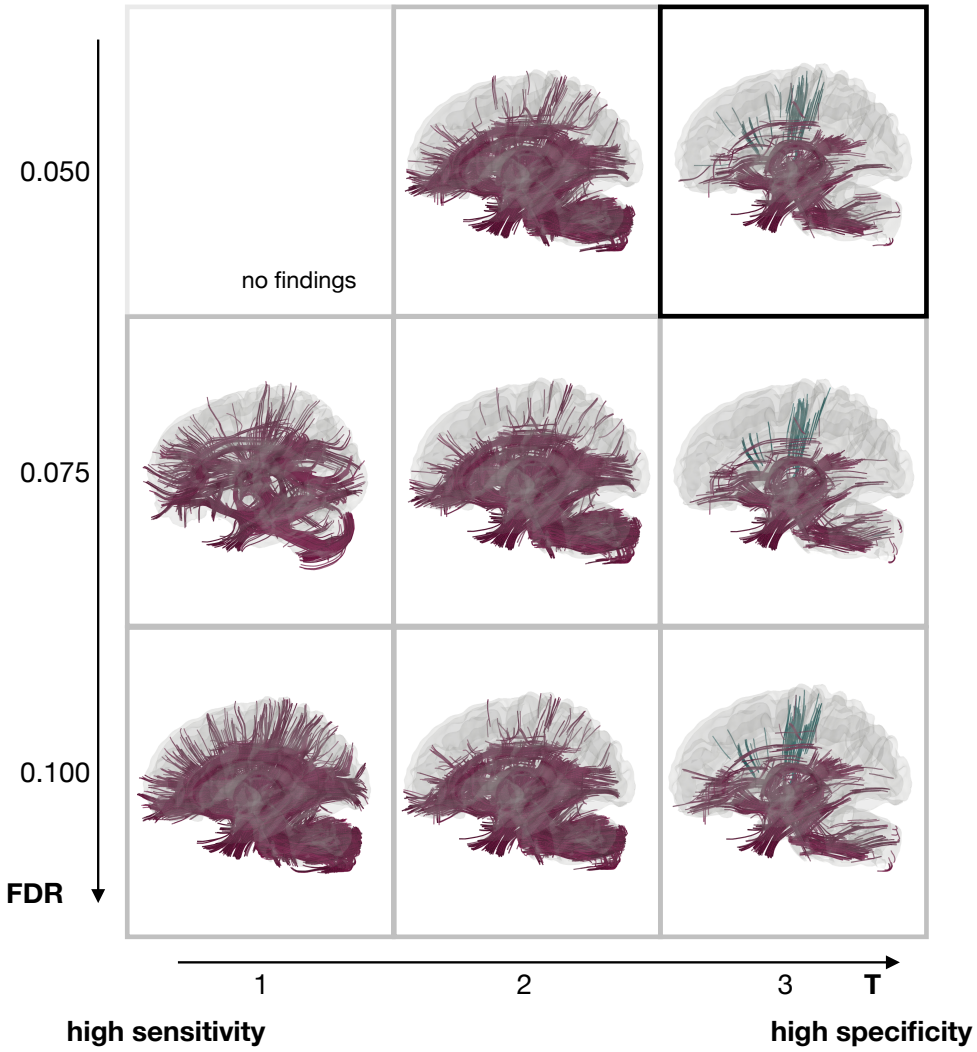


Figure A.4: QA changes over 3 months between controls and left TLE patients: We ran connectometry analysis with different t-score thresholds to select local connectomes (T-score: 1, 2 and 3) at different significance levels (FDR: 0.05, 0.075 and 0.1). Higher values of t-score give more specific and confirmatory results, whereas lower values give more sensitive results, which are useful for exploratory studies. The square with black borders indicates the grid search point selected for further analysis in the study.

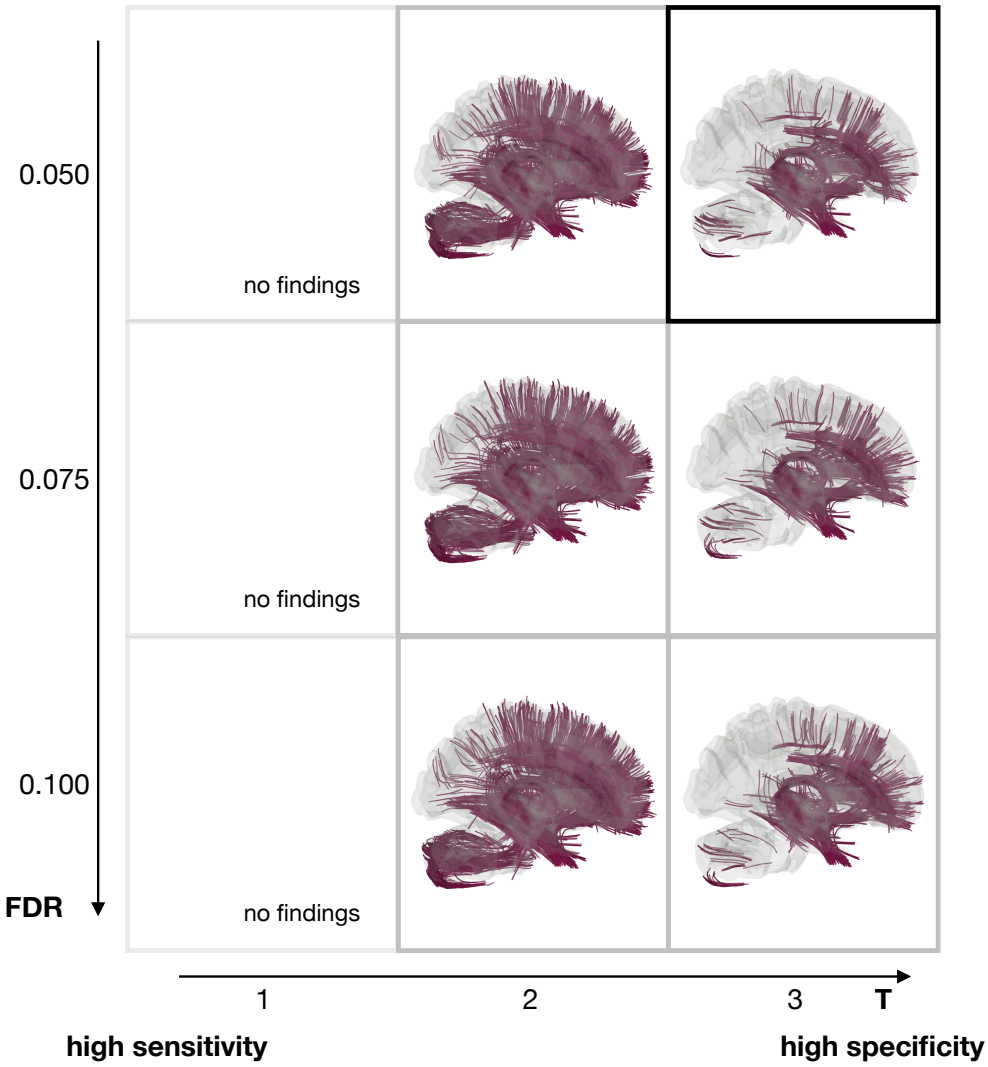


Figure A.5: QA changes over 3 months between controls and right TLE patients: We ran connectometry analysis with different t-score thresholds to select local connectomes (T-score: 1, 2 and 3) at different significance levels (FDR: 0.05, 0.075 and 0.1). Higher values of t-score give more specific and confirmatory results, whereas lower values give more sensitive results, which are useful for exploratory studies. The square with black borders indicates the grid search point selected for further analysis in the study.

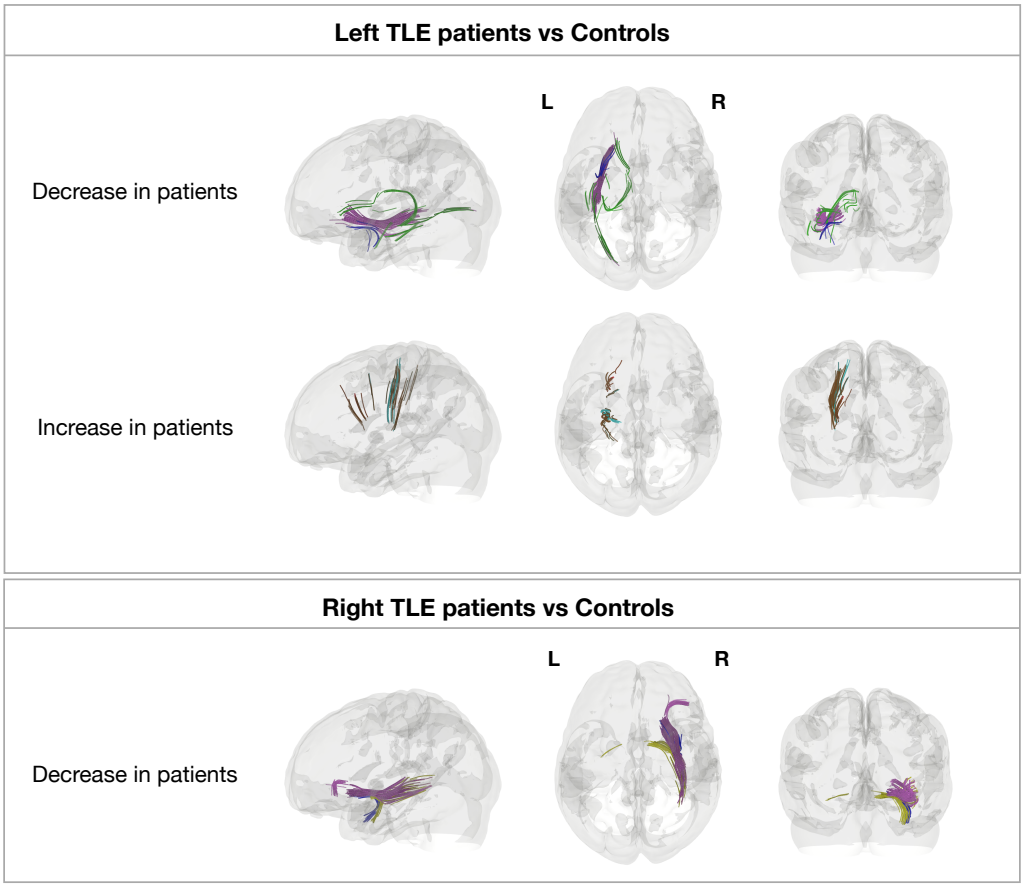


Figure A.6: Subsections of the bundles with greater changes over 3 months in TLE patients: For left TLE patients, greater reductions were seen in ipsilateral IFOF, UF and CT. Left TLE patients also showed greater increase in QA over 3-4 months in ipsilateral CS, FPT and CST. Right TLE patients showed greater reduction in IFOF, UF and AC. In both left and right patients, the affected subsections in IFOF extend to the frontal cortex superiorly to UF. Purple – IFOF; Blue – UF; Green – CT, Cyan - CST; Brown - CS; Red – FPT; Yellow – AC. L - Left; R - Right.

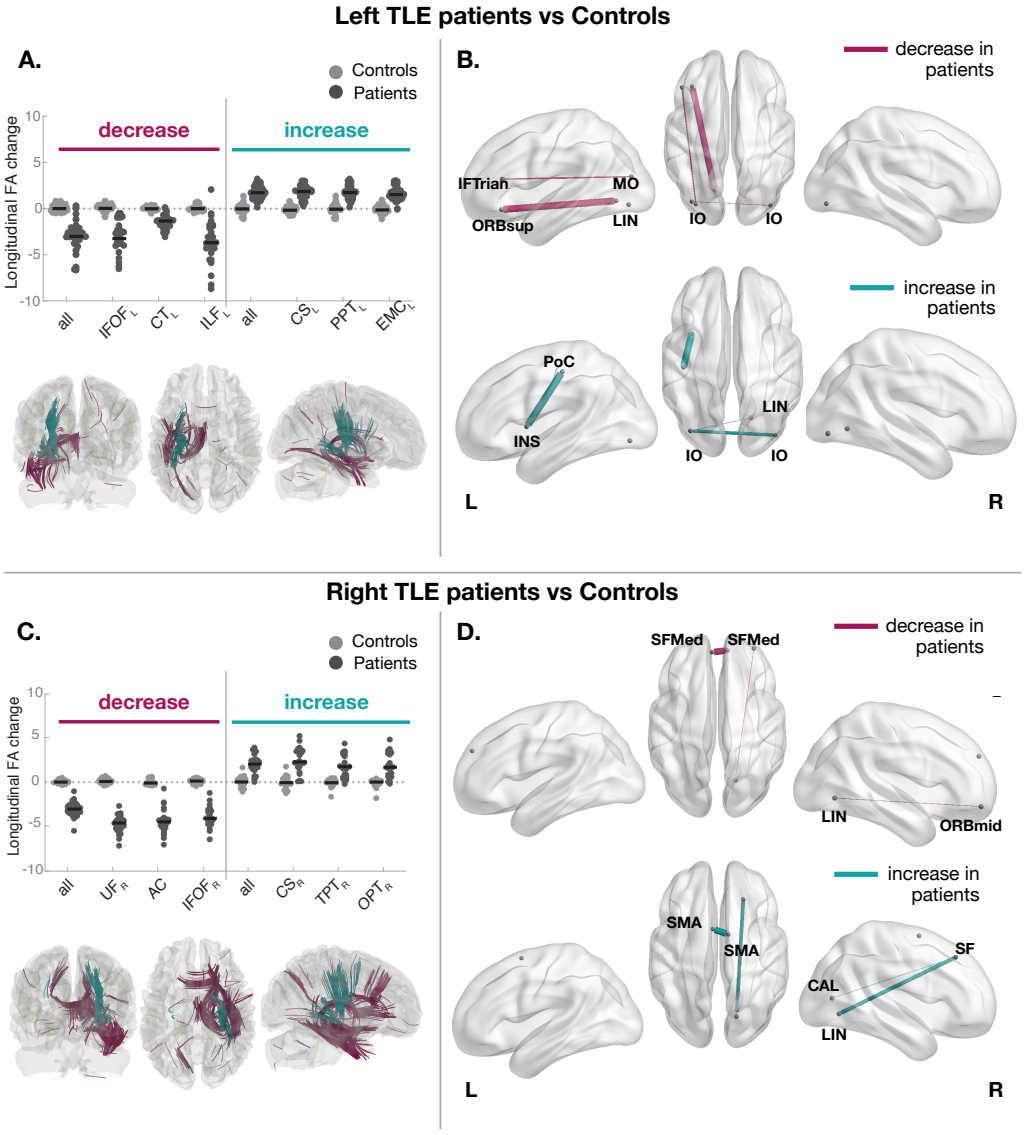


Figure A.7: Significant FA changes between controls and TLE patients, before and after surgery, in parts of tracts revealed by connectometry: Significant FA changes in subsections of bundles were found between groups (FDR<0.05; T-score=3). Subsections of tracts in which patients had a significant FA reduction or increase relative to controls are coloured in purple and green, respectively (A,C). Left and right TLE patients had a greater decrease of FA in ipsilateral IFOF. Greater reductions in FA were also observed in ipsilateral CT and ILF in left TLE patients. Right TLE patients also showed greater reduction in AC and UF. Left TLE showed a greater increase of FA in ipsilateral CS, parietopontine tract (PPT) and EMC. Right TLE showed a greater increase in CS, temporopontine (TPT) and occipitopontine (OPT). The beeswarm plots show the longitudinal changes in FA between groups for all subsections found by connectometry (label all in the plot) and the bundles with greater difference between groups. Each datapoint indicates a single subject. For visualisation purposes, only the three bundles with highest values of cohen-D are presented in the beeswarm plot. (B,D) The tract bundles where subsections were found to be significantly different by connectometry were determined to estimate the AAL regions those subsections are connecting to. The weight of the connections/edges is proportional to the amount of tracts with altered subsections. For visualisation, only the top 70% of strongest connections are shown. Cal - Calcarine; ORBsup - Superior frontal, orbital;IFTrian - Inferior frontal, triangular; IO - Inferior occipital; INS - Insula; LIN - Lingual; ORBmid - Middle frontal, orbital; MO - Middle occipital; SF - Superior frontal, dorsolateral; SFMed - Superior frontal, medial; SMA - Supplementary Motor Area. PoC – Postcentral

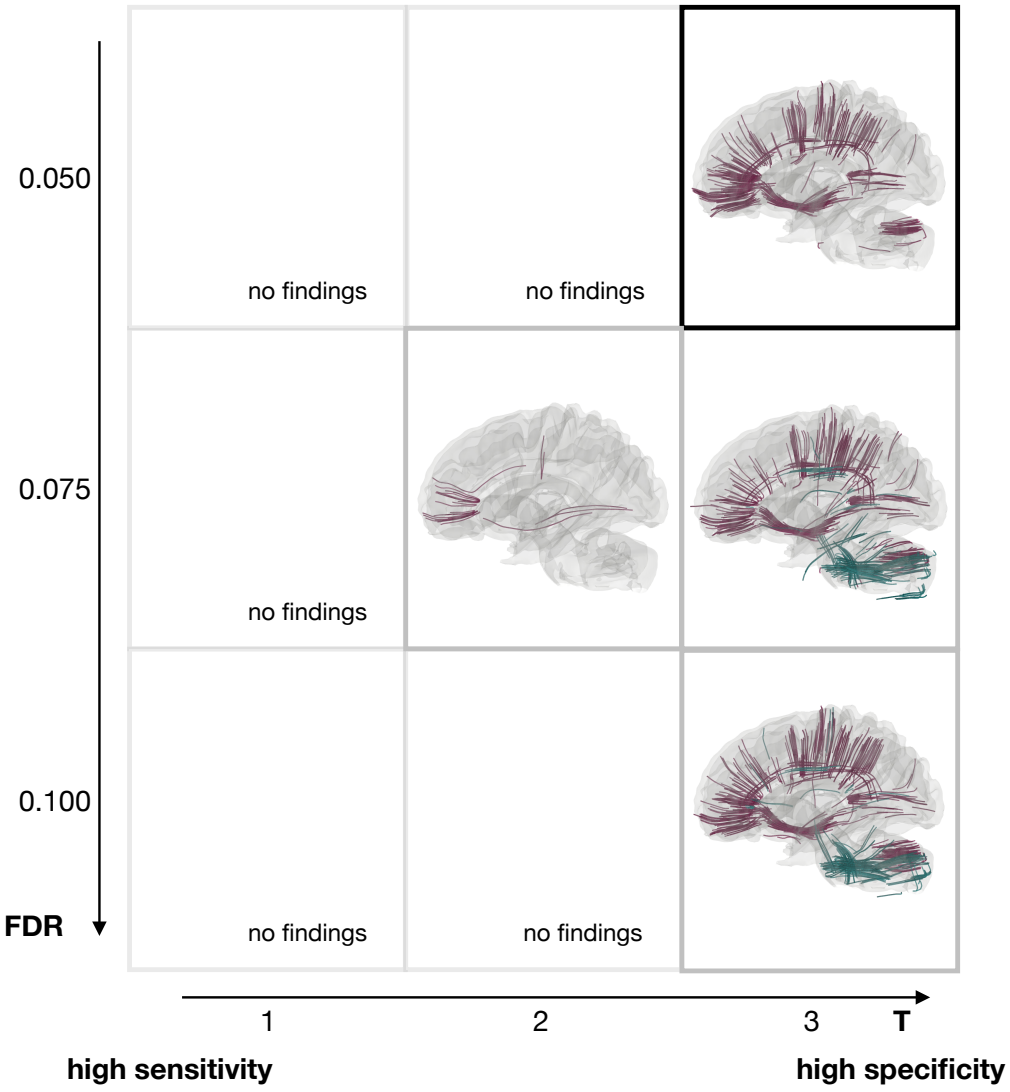


Figure A.8: QA changes over 3 months between left TLE patients seizure-free over 5 years and left TLE patients with relapse: We ran connectometry analysis with different t-score thresholds to select local connectomes (T-score: 1, 2 and 3) at different significance levels (FDR: 0.05, 0.075 and 0.1). Higher values of t-score give more specific and confirmatory results, whereas lower values give more sensitive results, which are useful for exploratory studies. The square with black borders indicates the grid search point selected for further analysis in the study.

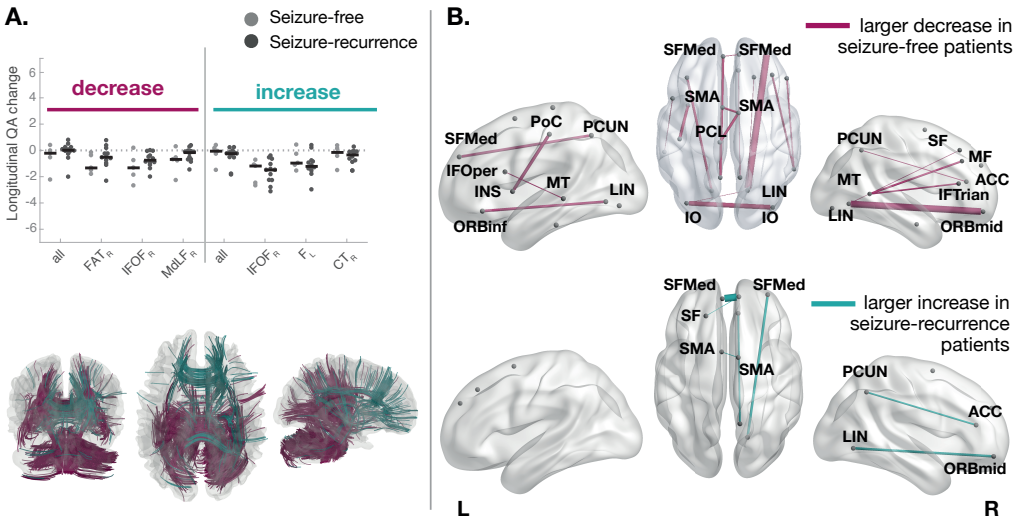


Figure A.9: Tract sections with QA changes over 3 months that are associated with postoperative seizure freedom in patients with right TLE: Significant QA changes in subsections of bundles were found between outcome groups (FDR < 0.05; T-score $= 3$). (A) Subsections of tracts where seizure-free patients had a significantly larger QA reduction over 3 months in comparison to patients with seizure-recurrence are coloured in purple. Subsections of tracts where seizure-recurrence patients had a significantly larger QA reduction over 3 months in comparison to seizure-free patients are coloured in green. The beesswarm plot shows the longitudinal changes in QA between groups for all subsections found by connectometry (label all in the plot) and the bundles with greater reductions. For visualisation purposes, only the three bundles with the highest Cohen's d are displayed. (B) The tract bundles where subsection were found to be significant different by connectometry were determined to estimate the AAL regions those subsections are connecting to. The weight of the connections/edges is proportional to the amount of tracts with altered subsections. For visualisation purposes, a threshold was applied to hide the edges with a weight less than 30% of the strongest connection. A table with the names and abbreviations of all regions and bundles can be found in Tables A.7 and A.8.

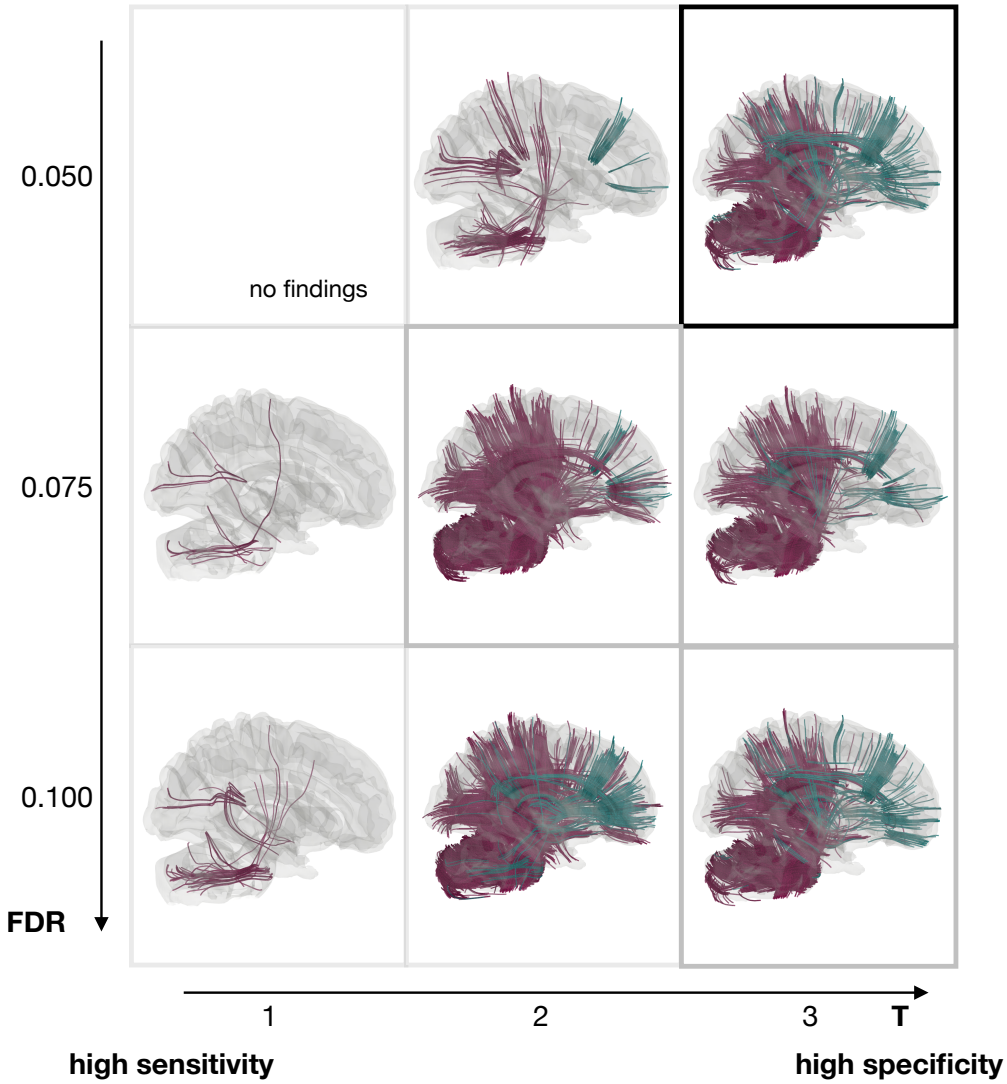


Figure A.10: QA changes over 3 months between right TLE patients seizure-free over 5 years and right TLE patients with relapse: We ran connectometry analysis with different t-score thresholds to select local connectomes (T-score: 1, 2 and 3) at different significance levels (FDR: 0.05, 0.075 and 0.1). Higher values of t-score give more specific and confirmatory results, whereas lower values give more sensitive results, which are useful for exploratory studies. The square with black borders indicates the grid search point selected for further analysis in the study.

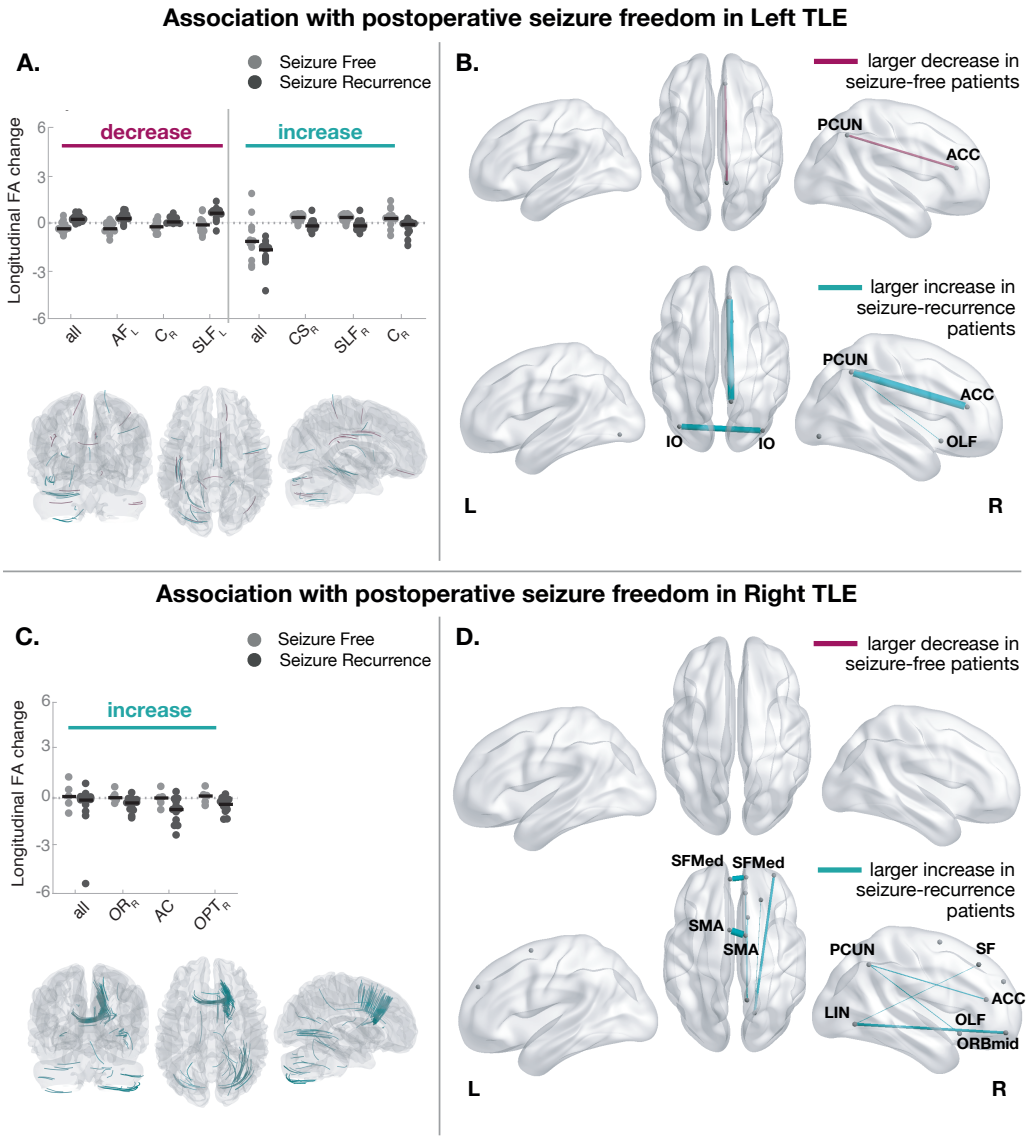


Figure A.11: Tract sections with FA changes over 3 months that are associated with postoperative seizure freedom in patients with left and right TLE: Significant FA changes in subsections of bundles were found between outcome groups (FDR < 0.05; T-score $= 3$). (A) Subsections of tracts where seizure-free patients had a significantly larger FA reduction over 3 months in comparison to patients with seizure-recurrence are coloured in purple. Subsections of tracts where seizure-recurrence patients had a significantly larger FA reduction over 3 months in comparison to seizure-free patients are coloured in green. The beesswarm plot shows the longitudinal changes in QA between groups for all subsections found by connectometry (label all in the plot) and the bundles with greater reductions. For visualisation purposes, only the three bundles with the highest Cohen's d are displayed. (B) The tract bundles where subsection were found to be significant different by connectometry were determined to estimate the AAL regions those subsections are connecting to. The weight of the connections/edges is proportional to the amount of tracts with altered subsections. For visualisation purposes, a threshold was applied to hide the edges with a weight less than 30% of the strongest connection. A table with the names and abbreviations of all regions and bundles can be found in Tables A.7 and A.8.

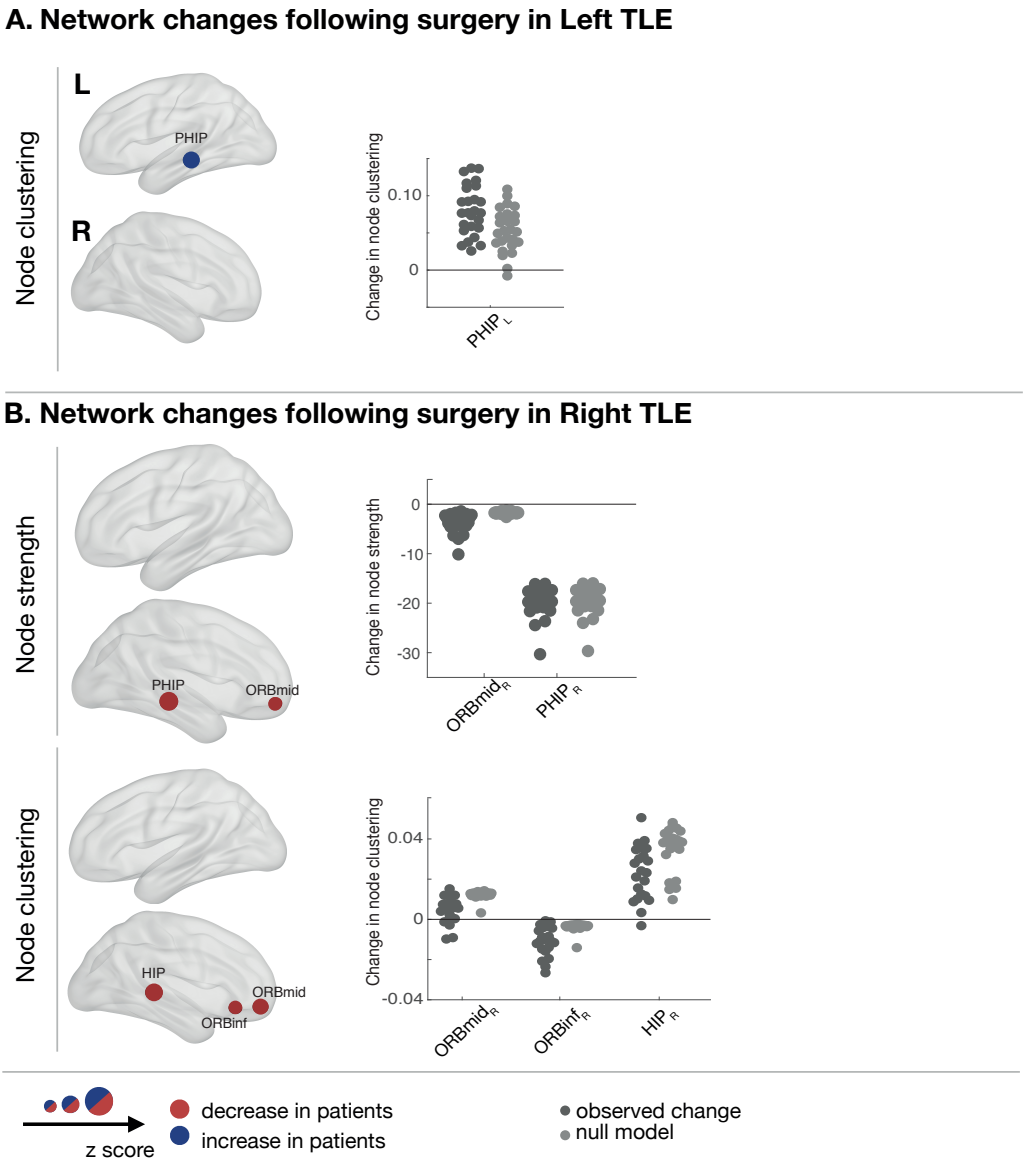


Figure A.12: Changes over 3 months in node clustering and node strength patients and controls: The AAL regions that showed significant differences in node clustering and node strength between patients and controls over 3 months are represented by a node/circle and overlaid within a brain volume. Nodes coloured in blue show the AAL regions where patients had an increase in node clustering in comparison to controls over 3 months. Nodes coloured in red show the AAL regions in which patients had a significant reduction in strength or clustering in comparison to controls. Scatter plots show the observed and predicted (null model) change in patients after surgery for those AAL regions. Positive values suggest an increase of node strength or clustering following surgery. The scatter plots therefore compare the impact on network measures of the surgical resection alone with the overall changes seen post-operatively. No significant differences in node efficiency were observed between patients and controls HIP – Hippocampus; ORBinf - Inferior frontal, orbital; ORBmid - Middle frontal, orbital; PHIP – Parahippocampal.

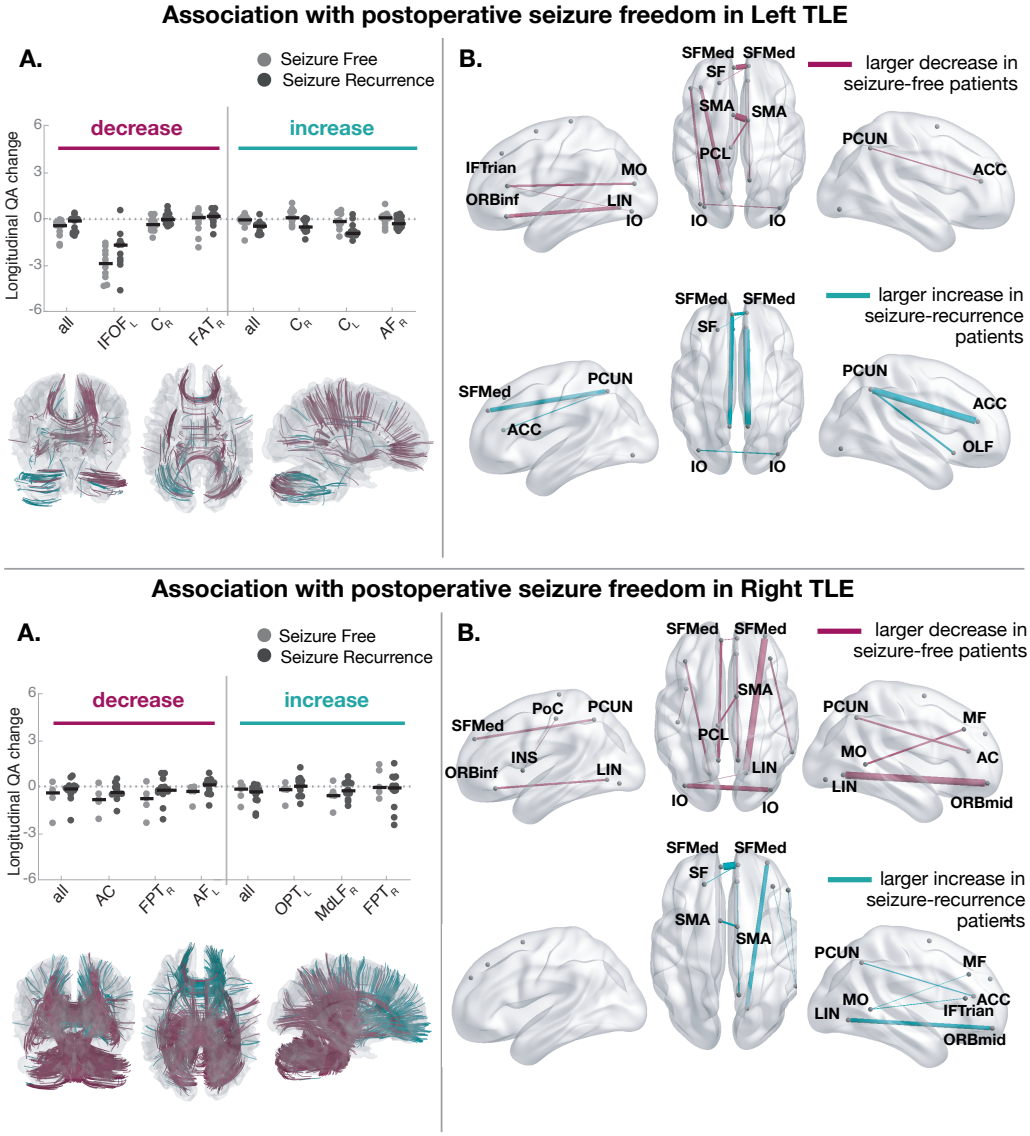


Figure A.13: Tract sections with QA changes over 3 months that are associated with postoperative seizure freedom in patients with left and right TLE after regressing out the resection volume: Significant QA changes in subsections of bundles were found between outcome groups (FDR < 0.05; T-score $= 3$). (A) Subsections of tracts where seizure-free patients had a significantly larger QA reduction over 3 months in comparison to patients with seizure-recurrence are coloured in purple. Subsections of tracts where seizure-recurrence patients had a significantly larger QA reduction over 3 months in comparison to seizure-free patients are coloured in green. The beesswarm plot shows the longitudinal changes in QA between groups for all subsections found by connectometry (label all in the plot) and the bundles with greater reductions. For visualisation purposes, only the three bundles with the highest Cohen's d are displayed. (B) The tract bundles where subsection were found to be significant different by connectometry were determined to estimate the AAL regions those subsections are connecting to. The weight of the connections/edges is proportional to the amount of tracts with altered subsections. For visualisation purposes, a threshold was applied to hide the edges with a weight less than 30% of the strongest connection. A table with the names and abbreviations of all regions and bundles can be found in Tables A.7 and A.8.

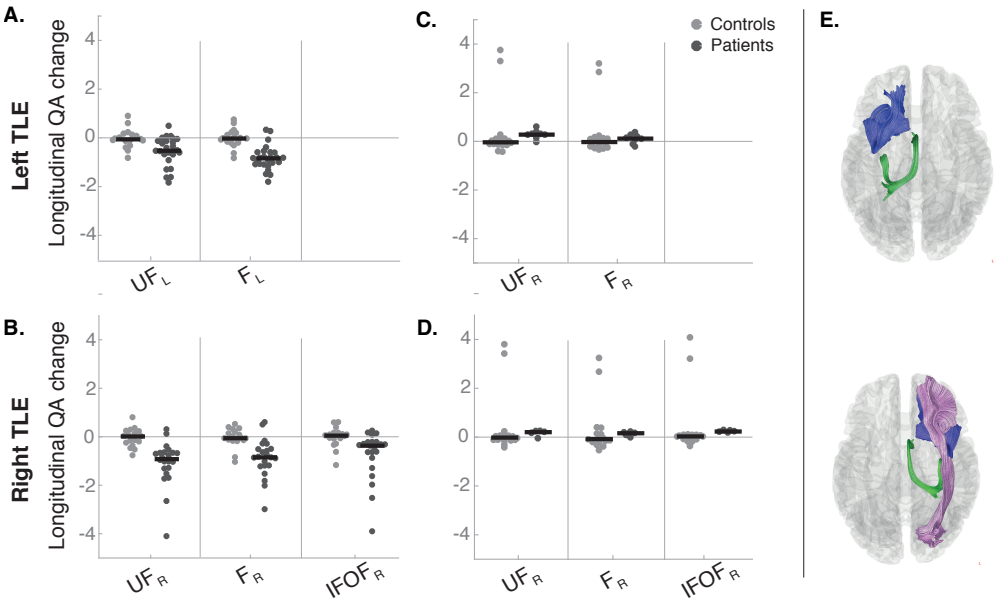


Figure A.14: Reduced QA after surgery over 3 months: Bundles from the connectome atlas which showed statistical significance after FDR correction between groups over 3 months (A,C) and over 12 months (B,D). Longitudinal QA change is the difference between post-operative and pre-operative mean QA after regressing out age and sex for left TLE (A,B) and right TLE (C,D). Each data point represents a subject and the black line the median across subjects. (E) Location of the tracts. F – Fornix (green); IFOF – Inferior fronto occipital fasciculus (lilac); UF – Uncinate fasciculus (blue); L- Left; R – Right.

A.3 Imaging Protocols

All participants were presented for magnetic resonance imaging (MRI) scanning on a 3T GE Signa HDx scanner (General Electric, Waukesha, Milwaukee, WI) using a body coil for transmission and 8-channel phased array coil for reception. Standard imaging gradients with a maximum strength of 40 mTm-1 and slew rate 150 Tm-1s-1 were used. The study protocol consisted of a coronal 3D T1-weighted volumetric acquisition (matrix, 256x256x170; in-plane resolution, 0.9375x0.9375x1.1 mm) and diffusion weighted images (b-value =1200 s mm^{-2} [δ=21ms, Δ=29 ms using full gradient strength of 40 mTm-1], 60 axial slices with 2.4mm thickness, 52 noncollinear directions, 6 non-diffusion weighted scans). Diffusion MRI data were acquired using a cardiac-triggered single-shot spin-echo planar imaging sequence (Wheeler-Kingshott et al. (2002)) with echo time = 73 ms. The gradient directions were estimated and ordered as described in Cook et al. (2007). The field of view was 24 x 24 cm and the acquisition matrix size was 96x96, zero filled to 128x128 during reconstruction, resulting in a voxel size of 1.875 x 1.875 x 2.4 mm. These imaging protocols are identical to our previous study (Taylor et al. (2018)).

A.4 Atlas-based Approach: Diffusion Changes in Whole White Matter Bundles

To investigate white matter alterations after resective surgery and their association with postoperative seizure-freedom, we employed an atlas-based/whole-tract approach to investigate changes in entire fasciculi. In comparison to connectometry, this approach is less sensible to focal changes within bundles. Nevertheless it is commonly employed by its simplicity and low computational cost. White matter degeneration in the vicinity of the resected tissue may adversely affect fiber tractography-based approaches, leading to false negative connections. Therefore, the population-average atlas of the connectome (Yeh et al. (2018)) was preferred. This atlas identifies 550,000 white matter tracts verified manually by experienced neuroanatomists (Yeh et al. (2018)), which are grouped in 80 bundles. Cranial nerves, cerebellum and brainstem bundles were not considered in this study. For each subject and timepoint, we estimated the mean QA for each bundle. We constrained the analysis to the non-resected area using the resection masks. After obtain-

ing the mean QA for each participant and timepoint, we computed the longitudinal change over 3-4 months and over the following 8-9 months. We compared the longitudinal changes between patient and control groups using inference statistical tests. To study the association of longitudinal changes with postoperative seizure-freedom, we grouped patients in 2 classes as follows: Class 1:Seizure-free, if the patient remained ILAE1 throughout the 5 years of follow up, and class 2:Seizure-recurrence, if the patient had ILAE>1 at any time during the five-years follow up. Longitudinal changes between both groups or classes were compared using inference statistical tests.

After temporal lobe resection, there were significant reductions in QA located in the ipsilateral fornix (F) (Left TLE: FDR p-value < 0.001; Right TLE: FDR p-value $= 0.005$) and UF (Left TLE: FDR p-value $= 0.047$; Right TLE: FDR p-value $= 0.001$) (Figure A.14). There was also a significant reduction of QA in the ipsilateral IFOF for right TLE patients (FDR p-value $= 0.035$). As expected, controls showed longitudinal QA changes around zero over 3-4 months after surgery. No significant changes were found between 3 and 12 months after surgery between groups, including the bundles with significant reductions in QA over 3-4 months after surgery. Longitudinal QA changes after the surgery were not significantly different between TLE patients with different outcomes (Ranksum test, $p > 0.05$ for all tract bundles).

A.5 Group Subsections from Connectometry

The subsections of tracts found to be significantly different between patients and controls were grouped as in the population-average atlas of the connectome (Yeh et al. (2018)), which comprise 550,000 white matter tracts grouped in 80 bundles. Cranial nerves, cerebellum and brainstem bundles were not considered in this study. We imported the coordinates of the subsections of tracts found by connectometry and the tracts of each bundle of the connectome atlas into MATLAB. Only subsections at 1mm or less from a tract in the connectome atlas were considered. Any other subsections were considered as false positives. As in the connectome atlas, the subsections were grouped and labelled by the bundle name of the closest tract of the connectome atlas.

To study what grey matter regions these subsections of tracts were connecting, we estimate

their entire length. To this purpose, we saved the closest tract of the connectome atlas to each subsection. After estimating the entire length of the subsections, we computed a connectivity matrix using AAL parcellation scheme. The area of the AAL regions overlapping with the resection tissue was labelled as a new ROI termed RT.

A.6 Association with Postoperative Outcome for Right TLE Patients

In right TLE, we found widespread differences between outcome groups in subsections of tracts (Figure A.9). Similarly to left TLE patients, we found greater QA reductions relate to greater chances of postoperative seizure freedom in the vicinity of resection area, between LIN and orbitofrontal cortices and in interhemispheric connections in frontal and occipital lobes. Interhemispheric connections with reduction in QA associated with seizure-freedom were mostly seen in the occipital lobe and to a less extent in frontal lobe as opposed to left TLE. Nevertheless, we also observed greater reduction in some interhemispheric connections in frontal lobe associated to seizure-recurrence.

Although we observed significant changes over 3-4 months for right TLE patients, we caution against overinterpretation of this result given the small sample size, particularly for seizure-free group. Only 5 patients were seizure-free for the 5-year follow up period, which may not represent properly the variability within group.

A.7 Consistency of Resection Masks

In order to verify if the resections were consistent across patients, the resective masks were inspected by visual inspection and Dice overlap was computed to quantity masks' similarity. As described in Moreira da Silva et al. (2017) and Traynor et al. (2010), Dice overlap was computed for all possible pairs of masks across patients, as explained below:

$$overlap = \frac{\sum_m 2\alpha N(A \cap B)}{\sum_m \alpha(N(A)+N(B))}$$

where m represents every combination of pairs between patients, α the weight, N the number of voxels and A and B the resection masks of the pair m. We used two different weights, 1, in which bigger masks contribute more to the similarity index and 1/V, in

Weight	Left	Right
1	0.77	0.71
1/V	0.74	0.72

Table A.9: Similarity of the resection masks across patients. The similarity was computed by Dice Overlap which ranges between 0 (no overlap) and 1 (full overlap). Both weighting approaches suggest a similar resection across patients with some variations, likely on the boundary of the resection.

which masks contribute equally. V is the mean volume of number of voxels in A and B. As described in Table A.9, the similarity of the resections masks across patients is high.

We additionally investigated if resection volumes differed between groups. As expected, right temporal lobe epilepsy patients had larger resection volumes than left sided patients. These volumes were not significantly related to outcomes of seizure freedom however (Table A.10) .

	Volume mean (std)	p-value
Left TLE volume (ILAE1/ILAE>1)	50878 mm3/ 44294mm3 (8769 mm3/ 14905 mm3)	0.212
Right TLE volume (ILAE1/ILAE>1)	54630 mm3/ 47740 mm3 (6760 mm3/ 7370 mm3)	0.104

Table A.10: Comparison of resection volumes between patients with ILAE equals to 1 and ILAE higher than 1.

Appendix B. Supplementary Material - Alterations following mTBI

Additional tables and figure for Chapter 3 are presented below.

B.1 Additional Tables

Test	Controls	Subacute	Chronic	Chronic vs Controls	Subacute vs Controls	Subacute vs Chronic
SOIP	Med = 75.9	Med = 57.7	Med = 70.2	p = 0.294	p = 0.009	p = 0.004
(motor speed adjusted)	IQR = 61.1-92.1	IQR = 45.6-70.8	IQR = 56.9-79.4	FDR p = 0.665	**FDR p = 0.030**	**FDR p = 0.010**
PASAT (2 second intervals,	Med = 57	Med = 45	Med = 48	p = 0.532	p = 0.006	p = 0.059
percentage correct)	IQR = 44.3-68.0	IQR = 4.0-58.5	IQR = 45.0-58.5	FDR p = 0.665	**FDR p = 0.030**	FDR p = 0.118
List Learning	Med = 12	Med = 10	Med = 11	p = 0.498	p = 0.004	p = 0.002
(final trial score)	IQR = 10-13	IQR = 5.5-12.0	IQR = 9.5-13.0	FDR p = 0.665	**FDR p = 0.030**	**FDR p = 0.010**
Digit Span Backwards	Med = 7	Med = 6	Med = 6	p = 0.116	p = 0.101	p = 0.569
(sequence length)	IQR = 6-8	IQR = 5.0-8.5	IQR = 5-8	FDR p = 0.627	FDR p = 0.168	FDR p = 0.632
Spatial Span Backwards	Med = 8	Med = 7	Med = 7	p = 0.379	p = 0.161	p = 0.397
(sequence length)	IQR = 7-9	IQR = 6.0-8.5	IQR = 6-8.5	FDR p = 0.665	FDR p = 0.179	FDR p = 0.567
Verbal Letter Fluency	Med = 40.5	Med = 36	Med = 40	p = 0.927	p = 0.146	p = 0.086
(Total correct)	IQR = 34.0-47.3	IQR = 27.0-46.5	IQR = 32-45	FDR p = 0.927	FDR p = 0.179	FDR p = 0.143
Category Fluency	Med = 43.5	Med = 41	Med = 41	p = 0.188	p = 0.129	p = 0.512
(Total correct)	IQR = 39.8-45.3	IQR = 35.5-45.0	IQR = 33.5-44.5	FDR p = 0.627	FDR p = 0.179	FDR p = 0.632
C-WIT (colour naming,	Med = 27	Med = 32	Med = 29	p = 0.175	p = 0.019	p = 0.015
completion time)	IQR = 25.8-30.5	IQR = 27.5-36.5	IQR = 26.5-37.5	FDR p = 0.627	**FDR p = 0.048**	**FDR p = 0.038**
C-WIT (word naming,	Med = 21.5	Med = 24	Med = 22	p = 0.497	p = 0.024	p = 0.010
completion time)	IQR = 19.0-25.0	IQR = 22-28	IQR = 20-25	FDR p = 0.665	**FDR p = 0.048**	**FDR p = 0.033**
C-WIT (inhibition,	Med = 55	Med = 54	Med = 51	p = 0.684	p = 0.865	p = 0.976
completion time)	IQR = 48.8-58.5	IQR = 43.5-60.0	IQR = 44-66	FDR p = 0.760	FDR p = 0.865	FDR p = 0.976
1st Component principal components analysis (PCA)	Med = 0.55	Med = -0.64	Med = 0.34	p = 0.268	p = 0.001	p <0.001
	IQR = -0.34-1.26	IQR = -2.57-0.13	IQR = -1.08-1.00	FDR p = 0.268	**FDR p = 0.001**	**FDR p <0.001**

Table B.1: Results of neuropsychological tests and first component of PCA of controls and patients in the early (subacute) or late post-injury (chronic) phase. The results of inferential statistical tests, to compare groups cognitive performance, are presented in the last columns.

Patient	Age	Sex	Level of Education	NART	TBI	Injury cause	GCS	LOC	PTA
1	24	M	9	81	moderate	Unclear	10	1	1
2	53	M	9	105	moderate	Assault	12	15	4
3	23	F	9	105	moderate	Fall	12	0	1
4	38	M	14	105	moderate	Fall	12	3	336
5	65	F	14	122	moderate	Fall	9	10	240
6	65	M	14	127	mild	Fall	14	5	2
7	18	M	9	126	mild	Accident	14	5	0
8	22	M	9	84	mild	RTA	15	0	0
9	64	M	9	90	mild	Fall	14	10	0
10	40	F	14	118	mild	Fall	14	0	2
11	47	M	9	106	mild	Assault	15	3	0
12	36	M	9	102	mild	Assault	14	5	0
13	24	M	11	105	mild	Assault	15	1	0
14	35	F	15	117	mild	Fall	13	5	30
15	33	F	9	90	mild	Fall	15	1	1
16	22	M	9	84	mild	RTA	14	0	1
17	66	M	9	106	mild	Fall	15	0	0
18	46	M	11	111	mild	Accident	15	1	0
19	34	M	9	92	mild	Assault	15	1	0
20	26	M	14	94	mild	Assault	14	0	7
21	49	M	9	97	mild	Fall	15	0	0
22	58	M	14	117	mild	Fall	14	1	1
23	29	M	17	113	mild	Sport	14	0.5	6

Table B.2: Clinical data of each patient assessed in this study. RTA - Road Traffic Accident

Control	**Age**	**Sex**	**Level of Education**	**NART**
1	19	M	9	86
2	66	M	9	105
3	28	F	15	113
4	30	M	14	123
5	35	M	9	115
6	63	M	9	107
7	25	M	16	107
8	59	M	11	115
9	54	F	9	121
10	59	M	9	106
11	22	F	11	97
12	48	M	9	117
13	45	M	11	107
14	21	F	9	107
15	19	M	11	112
16	65	M	9	115
17	36	M	14	115
18	35	M	14	117
19	28	M	14	113
20	54	M	9	115
21	37	M	9	112
22	50	M	9	100
23	38	F	9	96
24	19	M	14	121
25	48	M	14	117
26	20	M	14	106
27	41	M	9	113
28	42	F	11	111

Table B.3: Clinical data of each control assessed in this study.

Segregation	Transitivity
	Average Clustering Coefficient
	Local Clustering Coefficient
	Local Efficiency
	Small-worldness
Integration	Characteristic Path Length
	Global Efficiency
	Small-worldness
Resilience	Assortativity Coefficient
	Local Assortativity
Centrality	Closeness
	Betweenness
	Eigenvector
	Page-Ranks
	Eccentricity
Basic	Strength
	Diameter

Table B.4: List presenting the network metrics used in this study to quantify network segregation, integration, resilience and centrality.

AAL Region	Network metric	Coefficient	p-value	Dice Overlap
Right Anterior Cingulum	Strength	-1.89	<0.001	0.06
Right Orbital Superior Frontal	Clustering Coefficient	0.74	0.003	0.11
Left Medial Superior Frontal	Local Efficiency	1.33	<0.001	0.15
Left Orbital Superior Frontal	Local Assortativity	0.96	<0.001	0.14
Left Olfactory	Local Assortativity	0.84	<0.001	0.01
Left Medial Superior Frontal	Local Assortativity	-2.02	<0.001	0.15
Left Rectus	Local Assortativity	-0.85	<0.001	0.14
Right Pallidum	Local Assortativity	0.47	0.005	0
Left Medial Superior Frontal	Betweenness centrality	0.46	0.02	0.15
Left Middle Temporal	Eigenvector centrality	1.96	<0.001	0.02
Left Orbital Medial Frontal	PageRanks centrality	0.36	0.004	0.14

Table B.5: Standardized coefficients and p-values of eleven network metrics between 9 different regions, which change was predictive of cognitive performance following mTBI. The last column present the Dice overlap of the Lesions Probability Map with the eleven network metrics.

B.2 Additional Figures

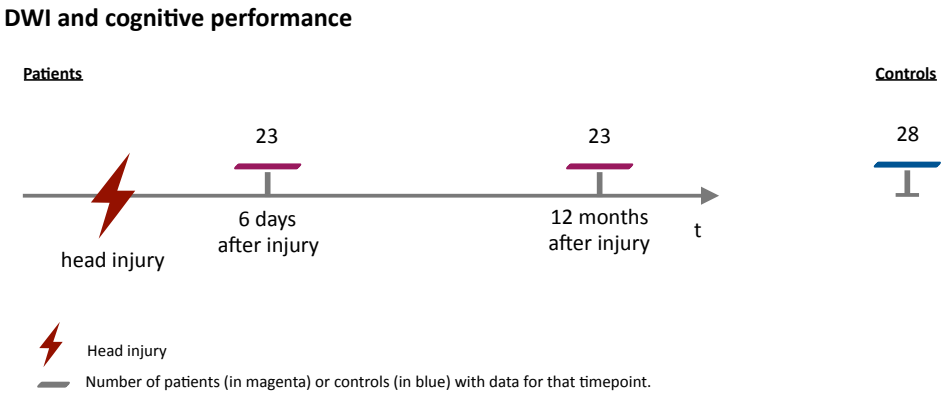


Figure B.1: Diagram of available longitudinal DWI data and cognitive score for patients. Controls were assessed once.

Appendix C. Supplementary Material - dFNC analysis

Additional tables and figures for Chapter 4 are presented below.

C.1 Additional Tables

	TBI				**Healthy controls**
fMRI dataset	**All**	**subacute**	**6 months**	**12 months**	
Total (N)	76	65	42	30	48
Age, median (IQR)	44.5(23.8)	45(24)	45(19.3)	46(15)	47(27.3)
Male, N (%)	63 (82.9)	55(84.6)	32(76.2)	25(83,3)	22(45.8)
has Diffusion MRI	**All**	**subacute**	**6 months**	**12 months**	
Total (N)	71	59	39	30	44
Age, median (IQR)	45(23.5)	45(24)	47(18.5)	46(15)	47.5(26.5)
Male, N (%)	60(84.5)	51(78.5)	29(74.4)	25(83.3)	21(47.7)
has Blood Biomarkers	**All**	**subacute**	**6 months**	**12 months**	
Total (N)	67	58	34	18	44
Age, median (IQR)	45(21)	45(20.8)	45(17.3)	43.5(15)	47.5(26.5)
Male, N (%)	56(83.6)	50(86.2)	24(70.6)	16(88.8)	21(47.7)

Table C.1: Sample size and clinical characteristics of participants.

Demographics		**Injury details**		**Clinical Characteristics**	
Total (N)	76	**Biophysics**		**Hospital Duration, median (IQR)**	13 (31.5)
Age, median (IQR)	44.5 (23.8)	High energy TBI	37 (48.7%)	**Initial GCS**	
Male	63 (82.9%)	Low energy TBI	34 (44.7)	3 to 8	7 (9.2%)
Premorbid employment		Unknown	3 (3.9%)	9 to 13	15 (19.7%)
Unfit for work	6 (7.9%)	**Injury cause**		14 to 15	32 (42.1%)
Home-maker	1 (1.3%)	Accidental	67 (88.2%)	unknown	22 (28.9%)
Retired	1 (1.3%)	Violence/assault	7 (1.3%)	**Lowset GCS first 24h, median (IQR)**	14 (3)
Student	6 (7.9%)	Self-harm	1 (1.3%)	**Pupils in ED**	
Jobseeker	7 (9.2%)	Other/unknown, N (%)	2 (2.6%)	bilaterally reactive	54 (71.1%)
Unknown	7 (9.2%)	**Occupational injury**	8 (10.5%)	unilaterally dilated/non-reactive	2 (2.6%)
Worker	48 (63.2%)	**Road traffic accident**	35 (46.1%)	unknown	20 (26.3%)
Ethnicity		Bicycle	14	**Loss of consciousness**	
Asian	5 (6.6%)	Car/Van	4	definite	35 (46.1%)
Black/African/Carribean	1 (1.3%)	Motorbike	5	suspected	23 (30.3%)
Unknown	10 (13.2%)	Other	1	absent	8 (10.5%)
White	60 (78.9%)	Pedestrian	11	unknown	10 (13.2%)
Education		**Blunt weapon**	2 (2.6%)	**Retrograde amnesia**	
University	30 (39.4%)	**Crush**	1 (1.3%)	definite	36 (47.4%)
Secondary education	15 (19.7%)			suspected	15 (19.7%)
Primary education	5 (6.6%)			absent	12 (15.8%)
Unknown	26 (34.2%)			unknown	13 (17.1%)
				Post traumatic amnesia	
				definite/suspected	60 (78.9%)
				duration 1-30 mins	4 (5.3%)
				duration 30-60 mins	1 (1.3%)
				duration 1-24 hours	9 (11.8%)
				duration 1-7 days	10 (13.2%)
				duration >7 days	12 (15.8%)
				duration unknown	5 (6.6%)
				absent	10 (13.2%)
				unknown	6 (7.9%)

Table C.2: Description of demographics, premorbid employment, ethnicity, education, injury details and clinical characteristics.

Neuroimaging reports		**Outcomes**		**Sedation MRI session**	
CT findings (acute)		**GOSE, subacute**		**Subacute (N=65)**	
DAI	7 (9.2%)	severe disability (3,4)	12 (15.8%)	Yes	13 (20%)
Extradural	15 (19.7%)	moderate disability (5,6)	26 (34.2%)	No	49 (75.4%)
SDH	48 (63.2%)	good recovery (7,8)	6 (7.9%)	Unknown	3 (4.6%)
SAH	47 (61.4%)	Unknown	32 (42.1%)	**6 months (N=42)**	
Contusion/ICH	35 (46.1%)	**GOSE, 6 months**		No	41 (97.6%)
Midline shift	6 (7.9%)	dead (1)	1 (1.31%)	Unknown	1 (2.4%)
CT Marshall classification (acute)		severe disability (3,4)	10 (13.2%)	**12 months (N=30)**	
I (DI, no vis. Pathology)	11 (14.5%)	moderate disability (5,6)	26 (34.2%)	No	30 (100%)
II (DI)	31 (40.8%)	good recovery (7,8)	27 (35.5%)	**Management and clinical course**	
III (DI, oedema)	8 (10.5%)	unknown	12 (15.8%)	Intubated & ventillated	34 (44.7%)
IV (DI, shift >5mm)	1 (1.3%)	**GOSE, 12 months**		Intracranial hypertension	23 (30.3%)
V (EML)	8 (10.5%)	dead (1)	1 (1.31%)	persistent	7 (30.4%)
VI (NEML)	12 (15.8%)	severe disability (3,4)	7 (9.2%)	Neurosurgery	
unknown	5 (6.6%)	moderate disability (5,6)	20 (26.3%)	evac of EDH	4 (5.3%)
MRI findings (10 days - 6 weeks)		good recovery (7,8)	28 (36.8%)	evac of SDH	3 (3.9%)
Subdural - acute	29 (38.2%)	unknown	20 (26.3%)	evac of parench. Haematoma	2 (2.6%)
Subdural - subacute	1 (1.3%)	**MOCA, 12 months, median (IQR)**	26 (3)	primary decompression	7 (9.2%)
Contusion	50 (65.8%)				
Intracerebral haemorrhage	8 (10.5%)				
Intraventricular haemorrhage	8 (10.5%)				
SAH	4 (5.3%)				
Extradural	23 (30.3%)				
Axonal injury	22 (28.9%)				
Oedema	11 (14.5%)				
Midline shift	9 (11.8%)				
Cisternal compression	1 (1.3%)				

Table C.3: Description of main findings on the neuroimaging reports, outcomes, sedation and management and clinical course.

	Max FD, median (IQR)	**% outliers, median (IQR)**	**% Agreement ICA-AROMA, median (IQR)**
Controls	0.52 (0.4)	0.33 (1.7)	80.0 (9.7)
Patients			
subacute	0.48 (0.6) p-value = 0.279	0 (1.0) p-value = 0.325	78.2 (11.8) p-value = 0.529
6 months	0.67 (0.8) p-value = 0.092	1 (2.0) p-value = 0.186	81.4 (7.5) p-value = 0.229
12 months	0.52 (0.4) p-value=0.709	0.33 (2.9) p-value = 0.778	82 (9.9) p-value=0.115

Table C.4: Maximum framewise displacement (FD), percentage of volumes with FD above 3 and percentage of agreement between automated and manual labelling of ICA-AROMA components. No significant differences were found for these measures between patients and controls.

	X	Y	Z
Default Mode Network			
Ventromedial prefrontal cortex (L)	-8	46	-8
Ventromedial prefrontal cortex (R)	6	52	-6
Dorsal posterior cingulum cortex	2	-34	40
Ventral posterior cingulum cortex	2	-58	28
Inferior parietal gyrus (L)	-48	-58	30
Inferior parietal gyrus (R)	54	-52	30
Parahippocampal gyrus	26	-22	-22
Left frontoparietal network			
Inferior frontal gyrus (L)	-48	18	24
Medial temporal gyrus (L)	-54	-52	-6
Superior parietal gyrus (L)	-34	-54	48
Superior frontal gyrus (L)	-4	28	48
Inferior frontal gyrus (R)	44	30	14
Right frontoparietal network			
Postcentral gyrus (R)	4	10	44
Frontal operculum (L)	-34	18	6
Posterior supramarginal (R)	54	-36	30
Frontal operculum (R)	42	14	8
Salience network			
Dorsal anterior cingulum cortex / Supplementary motor area	8	14	52
Anterior insula (R)	40	20	0
Inferior frontal gyrus (R)	56	30	-2

Table C.5: MNI coordinates (in mm) of spheres used in dFNC analysis.

	Subacute Entropy	**Change in entropy over 6 months**	**Subacute T-Tau**	**Change in T-Tau over 6 months**
GOSE 6 months				
N	53	33	52	26
AUC	0.71	0.57	0.59	0.63
Accuracy	0.68	0.67	0.56	0.65
MOCA 12 months				
N	40	27	32	25
R^2	0.1	-0.2	-0.004	-0.08
p-value	0.545	0.325	0.983	0.707

Table C.6: Patients' outcome is not associated with T-Tau or entropy.

C.2 Additional Figures

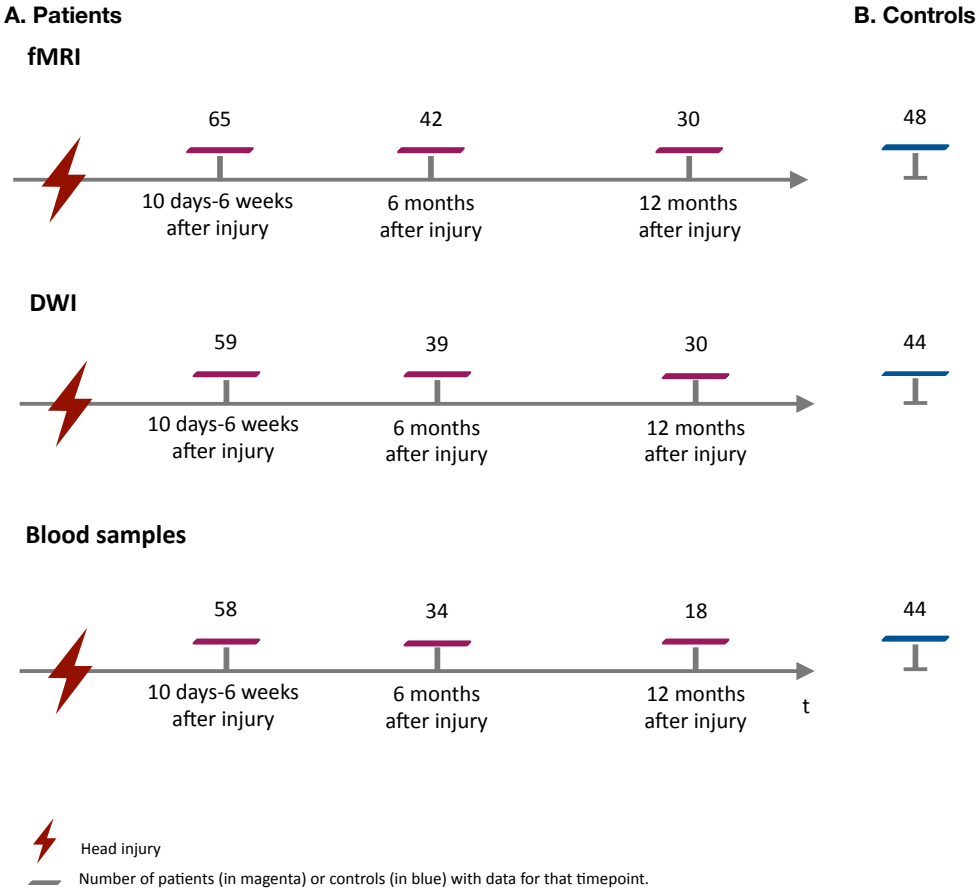


Figure C.1: Diagram of available longitudinal fMRI, DWI and blood biomarkers data for patients. Controls were assessed once. There was loss of data due to head movement, poor image quality due to major lesions, patients' dropout, death and COVID disruption. Some data is still being collected.

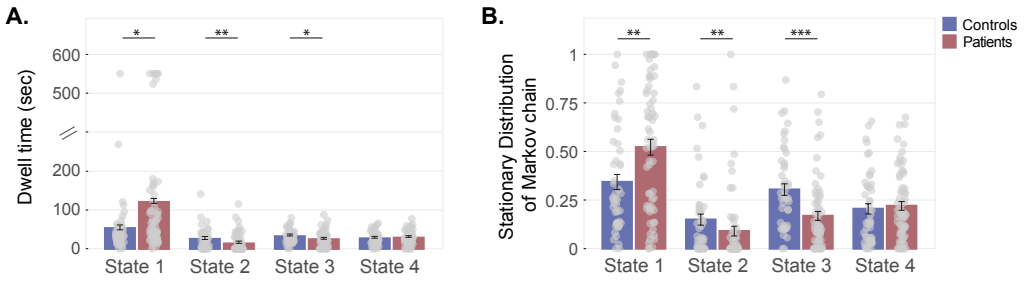


Figure C.2: Dwell time and stationary distribution of Markov chain: Mean and standard error of dwell time and stationary distribution of Markov chain for controls and subacute patients. FDR p-value: *** 0.0001 - 0.001, ** 0.001 - 0.01, * 0.01 - 0.05.

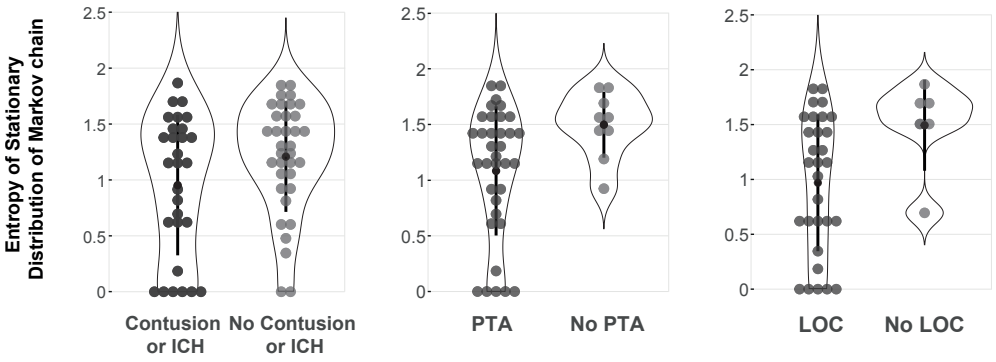


Figure C.3: Association between entropy and clinical characteristics: No significant differences were found between entropy and presence of contusion or ICH, PTA and LOC.

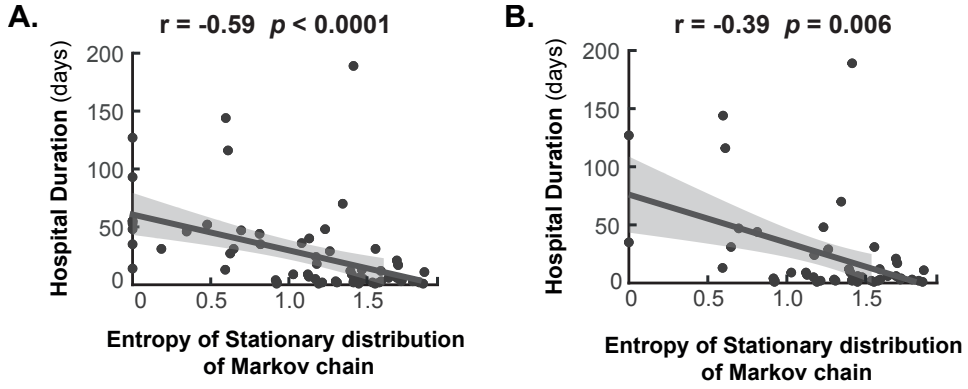


Figure C.4: Association between entropy and hospital duration: Entropy was correlated with hospital duration, where patients spending more time in the hospital having less entropy (A). This association was still present (B) after removing from the analysis the set of severe patients sedated at the time of the scan.

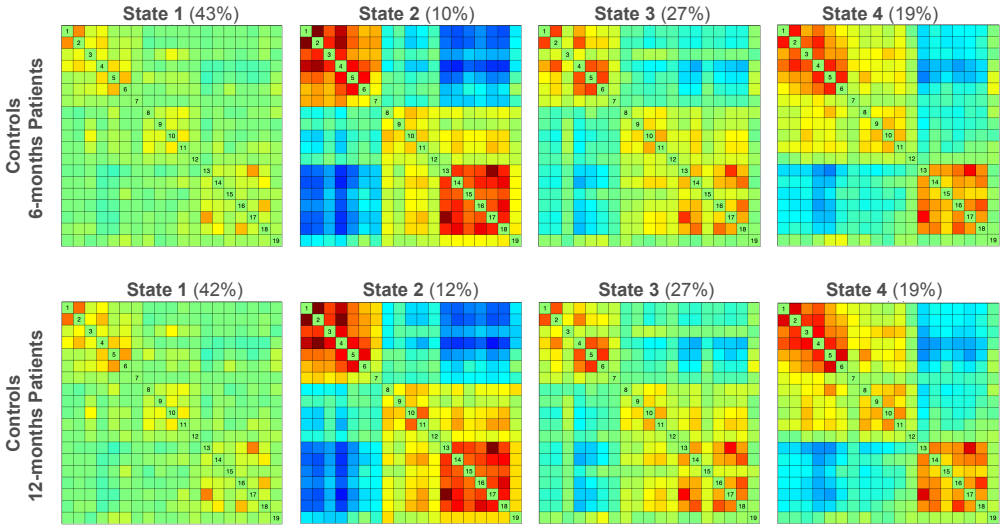


Figure C.5: States of dFNC at 6-months and 12-months: Centroids of each functional connectivity state obtained after clustering analysis on controls and patients 6 and 12-months after injury. States are equivalent to the ones obtained with subacute patients. Frequency of state is displayed on the top of each centroid.

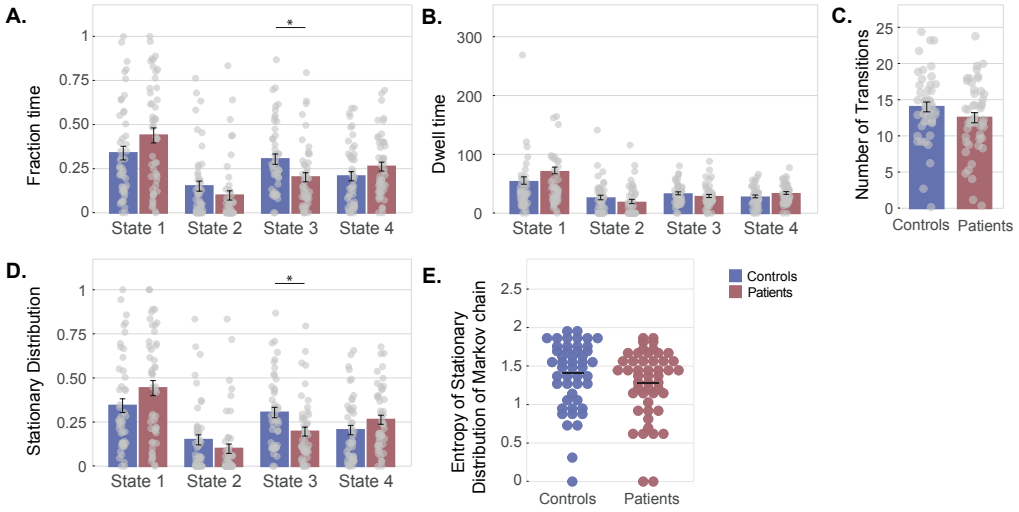


Figure C.6: Temporal characteristics in non-sedated patients: Mean and standard error of fraction time, dwell time, number of transitions, stationary distribution of Markov chain and entropy for controls and subacute patients not sedated during imaging acquisition. FDR p-value: * 0.01 - 0.05.

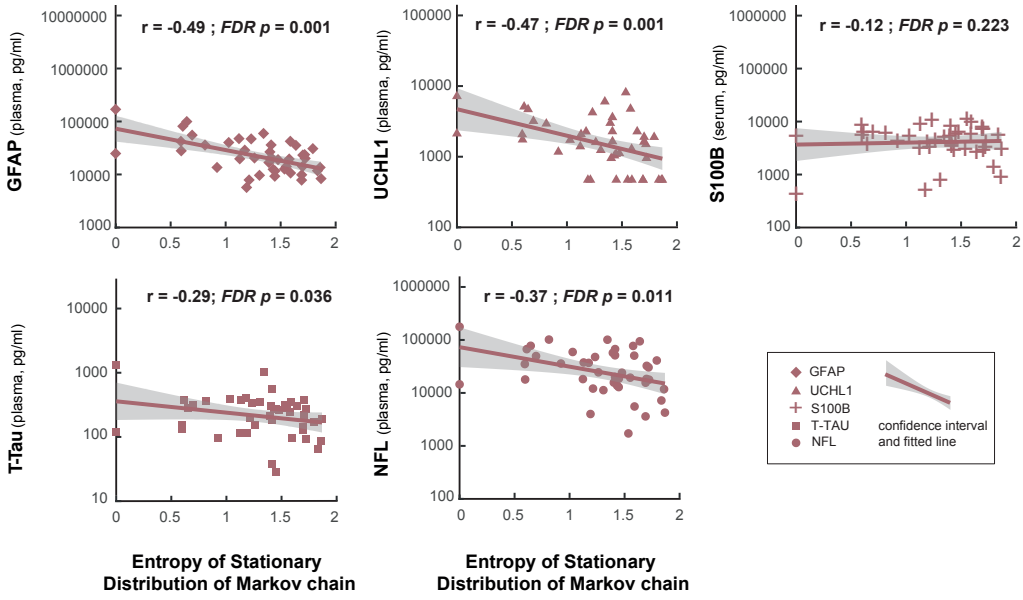


Figure C.7: Association of fluid blood biomarkers and entropy for the set of subacute patients non sedated during imaging scan.

Bibliography

Aerts, H., Fias, W., Caeyenberghs, K., and Marinazzo, D. (2016). Brain networks under attack: robustness properties and the impact of lesions. *Brain*, 139(12):3063–3083.

Ahmadi, M. E., Hagler, D., McDonald, C. R., Tecoma, E., Iragui, V., Dale, A. M., and Halgren, E. (2009). Side matters: diffusion tensor imaging tractography in left and right temporal lobe epilepsy. *American journal of neuroradiology*, 30(9):1740–1747.

Ahmadlou, M., Adeli, H., and Adeli, A. (2012). Graph theoretical analysis of organization of functional brain networks in ADHD. *Clinical EEG and neuroscience*, 43(1):5–13.

Alexander-Bloch, A. F., Vértes, P. E., Stidd, R., Lalonde, F., Clasen, L., Rapoport, J., Giedd, J., Bullmore, E. T., and Gogtay, N. (2012). The anatomical distance of functional connections predicts brain network topology in health and schizophrenia. *Cerebral cortex*, 23(1):127–138.

Alizadeh, M., Kozlowski, L., Muller, J., Ashraf, N., Shahrampour, S., Mohamed, F. B., Wu, C., and Sharan, A. (2019). Hemispheric regional based analysis of diffusion tensor imaging and diffusion tensor tractography in patients with temporal lobe epilepsy and correlation with patient outcomes. *Scientific Reports*, 9(1):1–8.

Allen, E. A., Damaraju, E., Plis, S. M., Erhardt, E. B., Eichele, T., and Calhoun, V. D. (2014). Tracking Whole-Brain Connectivity Dynamics in the Resting State. *Cerebral Cortex*, 24(3):663–676.

Alsaadi, T. M., Ulmer, J. L., Mitchell, M. J., Morris, G. L., Swanson, S. J., and Mueller, W. M. (2001). Magnetic resonance analysis of postsurgical temporal lobectomy. *Journal of Neuroimaging*, 11(3):243–247.

Andriessen, T. M., Jacobs, B., and Vos, P. E. (2010). Clinical characteristics and pathophysiological mechanisms of focal and diffuse traumatic brain injury. *Journal of cellular and molecular medicine*, 14(10):2381–2392.

Arenth, P. M., Russell, K. C., Scanlon, J. M., Kessler, L. J., and Ricker, J. H. (2014). Corpus callosum integrity and neuropsychological performance after traumatic brain injury: a diffusion tensor imaging study. *The Journal of head trauma rehabilitation*, 29(2):E1.

Arfanakis, K., Haughton, V. M., Carew, J. D., Rogers, B. P., Dempsey, R. J., and Meyerand, M. E. (2002). Diffusion tensor mr imaging in diffuse axonal injury. *American Journal of Neuroradiology*, 23(5):794–802.

Aribisala, B. S., Cowie, C. J., He, J., Wood, J., Mendelow, D. A., Mitchell, P., and Blamire, A. M. (2014). A Histogram-Based Similarity Measure for Quantitative Magnetic Resonance Imaging: Application in Acute Mild Traumatic Brain Injury. *Journal of Computer Assisted Tomography*, 38(6):915–923.

Arnold, T. C., Kini, L. G., Bernabei, J. M., Revell, A. Y., Das, S. R., Stein, J. M., Lucas, T. H., Englot, D. J., Morgan, V. L., Litt, B., et al. (2020). Remote effects of temporal lobe epilepsy surgery: long-term morphological changes after surgical resection. *medRxiv*.

Aung, W. Y., Mar, S., and Benzinger, T. L. (2013). Diffusion tensor MRI as a biomarker in axonal and myelin damage. *Imaging in medicine*, 5(5):427.

Bader-El-Den, M. and Gaber, M. (2012). GARF: Towards Self-optimised Random Forests. In Hutchison, D., Kanade, T., Kittler, J., Kleinberg, J. M., Mattern, F., Mitchell, J. C., Naor, M., Nierstrasz, O., Pandu Rangan, C., Steffen, B., Sudan, M., Terzopoulos, D., Tygar, D., Vardi, M. Y., Weikum, G., Huang, T., Zeng, Z., Li, C., and Leung, C. S., editors, *Neural Information Processing*, volume 7664, pages 506–515. Springer Berlin Heidelberg, Berlin, Heidelberg.

Barabási, A.-L. (2016). *Network Science*. Cambridge university press.

Barbey, A. K., Koenigs, M., and Grafman, J. (2011). Orbitofrontal Contributions to Human Working Memory. *Cerebral Cortex*, 21(4):789–795.

Barik, K., Daimi, S. N., Jones, R., Bhattacharya, J., and Saha, G. (2019). A machine learning approach to predict perceptual decisions: an insight into face pareidolia. *Brain Informatics*, 6(1):2.

Bartolomei, F., Bettus, G., Stam, C., and Guye, M. (2013). Interictal network properties in mesial temporal lobe epilepsy: a graph theoretical study from intracerebral recordings. *Clinical neurophysiology*, 124(12):2345–2353.

Bassett, D. S. and Bullmore, E. (2006). Small-world brain networks. *The neuroscientist*, 12(6):512–523.

Bazarian, J. J., Biberthaler, P., Welch, R. D., Lewis, L. M., Barzo, P., Bogner-Flatz, V., Brolinson, P. G., Büki, A., Chen, J. Y., Christenson, R. H., et al. (2018). Serum gfap and uch-l1 for prediction of absence of intracranial injuries on head ct (alert-tbi): a multicentre observational study. *The Lancet Neurology*, 17(9):782–789.

Bennett, R. E., Mac Donald, C. L., and Brody, D. L. (2012). Diffusion tensor imaging detects axonal injury in a mouse model of repetitive closed-skull traumatic brain injury. *Neuroscience letters*, 513(2):160–165.

Bernhardt, B. C., Bonilha, L., and Gross, D. W. (2015). Network analysis for a network disorder: the emerging role of graph theory in the study of epilepsy. *Epilepsy & Behavior*, 50:162–170.

Bernhardt, B. C., Chen, Z., He, Y., Evans, A. C., and Bernasconi, N. (2011). Graph-theoretical analysis reveals disrupted small-world organization of cortical thickness correlation networks in temporal lobe epilepsy. *Cerebral cortex*, 21(9):2147–2157.

Besson, P., Dinkelacker, V., Valabregue, R., Thivard, L., Leclerc, X., Baulac, M., Sammler, D., Colliot, O., Lehéricy, S., Samson, S., et al. (2014). Structural connectivity differences in left and right temporal lobe epilepsy. *Neuroimage*, 100:135–144.

Bogoslovsky, T., Wilson, D., Chen, Y., Hanlon, D., Gill, J., Jeromin, A., Song, L., Moore, C., Gong, Y., Kenney, K., and Diaz-Arrastia, R. (2017). Increases of Plasma Levels of Glial Fibrillary Acidic Protein, Tau, and Amyloid β up to 90 Days after Traumatic Brain Injury. *Journal of Neurotrauma*, 34(1):66–73.

Bonilha, L., Helpern, J. A., Sainju, R., Nesland, T., Edwards, J. C., Glazier, S. S., and Tabesh, A. (2013). Presurgical connectome and postsurgical seizure control in temporal lobe epilepsy. *Neurology*, 81(19):1704–1710.

Bonilha, L., Jensen, J. H., Baker, N., Breedlove, J., Nesland, T., Lin, J. J., Drane, D. L., Saindane, A. M., Binder, J. R., and Kuzniecky, R. I. (2015). The brain connectome as a personalized biomarker of seizure outcomes after temporal lobectomy. *Neurology*, 84(18):1846–1853.

Bonilha, L. and Keller, S. S. (2015). Quantitative MRI in refractory temporal lobe epilepsy: relationship with surgical outcomes. *Quantitative Imaging in Medicine and Surgery*, 5(2):204.

Bonilha, L., Nesland, T., Martz, G. U., Joseph, J. E., Spampinato, M. V., Edwards, J. C., and Tabesh, A. (2012). Medial temporal lobe epilepsy is associated with neuronal fibre loss and paradoxical increase in structural connectivity of limbic structures. *Journal of Neurology, Neurosurgery & Psychiatry*, 83(9):903–909.

Bonkhoff, A. K., Espinoza, F. A., Gazula, H., Vergara, V. M., Hensel, L., Michely, J., Paul, T., Rehme, A. K., Volz, L. J., Fink, G. R., Calhoun, V. D., and Grefkes, C. (2020). Acute ischaemic stroke alters the brain's preference for distinct dynamic connectivity states. *Brain*, 143(5):1525–1540.

Bonnelle, V., Ham, T. E., Leech, R., Kinnunen, K. M., Mehta, M. A., Greenwood, R. J., and Sharp, D. J. (2012). Salience network integrity predicts default mode network function after traumatic brain injury. *Proceedings of the National Academy of Sciences*, 109(12):4690–4695.

Bonnelle, V., Leech, R., Kinnunen, K. M., Ham, T. E., Beckmann, C. F., De Boissezon, X., Greenwood, R. J., and Sharp, D. J. (2011). Default mode network connectivity predicts sustained attention deficits after traumatic brain injury. *Journal of Neuroscience*, 31(38):13442–13451.

Broido, A. D. and Clauset, A. (2019). Scale-free networks are rare. *Nature communications*, 10(1):1–10.

Bubb, E. J., Metzler-Baddeley, C., and Aggleton, J. P. (2018). The cingulum bundle: Anatomy, function, and dysfunction. *Neuroscience & Biobehavioral Reviews*, 92:104–127.

Budde, M. D., Kim, J. H., Liang, H.-F., Russell, J. H., Cross, A. H., and Song, S.-K. (2008). Axonal injury detected by in vivo diffusion tensor imaging correlates with neurological disability in a mouse model of multiple sclerosis. *NMR in Biomedicine: An International Journal Devoted to the Development and Application of Magnetic Resonance In vivo*, 21(6):589–597.

Bullmore, E. and Sporns, O. (2009). Complex brain networks: graph theoretical analysis of structural and functional systems. *Nature Reviews Neuroscience*, 10(3):186–198.

Bullmore, E. T. and Bassett, D. S. (2011). Brain Graphs: Graphical Models of the Human Brain Connectome. *Annual Review of Clinical Psychology*, 7(1):113–140.

Busche, M. A., Wegmann, S., Dujardin, S., Commins, C., Schiantarelli, J., Klickstein, N., Kamath, T. V., Carlson, G. A., Nelken, I., and Hyman, B. T. (2019). Tau impairs neural circuits, dominating amyloid-β effects, in Alzheimer models in vivo. *Nature Neuroscience*, 22(1):57–64.

Byrne, L. M., Rodrigues, F. B., Blennow, K., Durr, A., Leavitt, B. R., Roos, R. A. C., Scahill, R. I., Tabrizi, S. J., Zetterberg, H., Langbehn, D., and Wild, E. J. (2017). Neurofilament light protein in blood as a potential biomarker of neurodegeneration in Huntington's disease: a retrospective cohort analysis. *The Lancet Neurology*, 16(8):601–609.

Caeyenberghs, K., Leemans, A., Geurts, M., Linden, C. V., Smits-Engelsman, B. C., Sunaert, S., and Swinnen, S. P. (2011). Correlations between white matter integrity and motor function in traumatic brain injury patients. *Neurorehabilitation and neural repair*, 25(6):492–502.

Carroll, L., Cassidy, J. D., Peloso, P., Borg, J., von Holst, H., Holm, L., Paniak, C., and Pépin, M. (2004). Prognosis for mild traumatic brain injury: results of the who collaborating centre task force on mild traumatic brain injury. *Journal of Rehabilitation Medicine*, 36(0):84–105.

Catani, M., Dell'Acqua, F., Vergani, F., Malik, F., Hodge, H., Roy, P., Valabregue, R., and De Schotten, M. T. (2012). Short frontal lobe connections of the human brain. *cortex*, 48(2):273–291.

Cazalis, F., Babikian, T., Giza, C., Copeland, S., Hovda, D., and Asarnow, R. F. (2011). Pivotal role of anterior cingulate cortex in working memory after traumatic brain injury in youth. *Frontiers in neurology*, 1:158.

Chamberland, M., Genc, S., Raven, E. P., Parker, G. D., Cunningham, A., Doherty, J., Bree, M. v. d., Tax, C. M., and Jones, D. K. (2020). Tractometry-based anomaly detection for single-subject white matter analysis. *arXiv preprint arXiv:2005.11082*.

Cole, J. H., Jolly, A., de Simoni, S., Bourke, N., Patel, M. C., Scott, G., and Sharp, D. J. (2018). Spatial patterns of progressive brain volume loss after moderate-severe traumatic brain injury. *Brain*, 141(3):822–836.

Concha, L., Beaulieu, C., Wheatley, B. M., and Gross, D. W. (2007). Bilateral white matter diffusion changes persist after epilepsy surgery. *Epilepsia*, 48(5):931–940.

Cook, P. A., Symms, M., Boulby, P. A., and Alexander, D. C. (2007). Optimal acquisition orders of diffusion-weighted MRI measurements. *Journal of Magnetic Resonance Imaging: An Official Journal of the International Society for Magnetic Resonance in Medicine*, 25(5):1051–1058.

Coughhlan, AK, Oddy, M, and Crawford, JR (2007). Birt Memory and Information Processing Battery London.

Croall, I. D., Cowie, C. J. A., He, J., Peel, A., Wood, J., Aribisala, B. S., Mitchell, P., Mendelow, A. D., Smith, F. E., Millar, D., Kelly, T., and Blamire, A. M. (2014). White matter correlates of cognitive dysfunction after mild traumatic brain injury. *Neurology*, 83(6):494–501.

Czeiter, E., Mondello, S., Kovacs, N., Sandor, J., Gabrielli, A., Schmid, K., Tortella, F., Wang, K. K., Hayes, R. L., Barzo, P., et al. (2012). Brain injury biomarkers may improve the predictive power of the impact outcome calculator. *Journal of neurotrauma*, 29(9):1770–1778.

Dall'Acqua, P., Johannes, S., Mica, L., Simmen, H.-P., Glaab, R., Fandino, J., Schwendinger, M., Meier, C., Ulbrich, E. J., Müller, A., et al. (2016). Connectomic and surface-based morphometric correlates of acute mild traumatic brain injury. *Frontiers in human neuroscience*, 10:127.

Dall'Acqua, P., Johannes, S., Mica, L., Simmen, H.-P., Glaab, R., Fandino, J., Schwendinger, M., Meier, C., Ulbrich, E. J., Müller, A., Baetschmann, H., Jäncke, L., and Hänggi, J. (2017). Functional and Structural Network Recovery after Mild Traumatic Brain Injury: A 1-Year Longitudinal Study. *Frontiers in Human Neuroscience*, 11:280.

De Simoni, S., Grover, P. J., Jenkins, P. O., Honeyfield, L., Quest, R. A., Ross, E., Scott, G., Wilson, M. H., Majewska, P., Waldman, A. D., et al. (2016a). Disconnection between the default mode network and medial temporal lobes in post-traumatic amnesia. *Brain*, 139(12):3137–3150.

De Simoni, S., Grover, P. J., Jenkins, P. O., Honeyfield, L., Quest, R. A., Ross, E., Scott, G., Wilson, M. H., Majewska, P., Waldman, A. D., Patel, M. C., and Sharp, D. J. (2016b). Disconnection between the default mode network and medial temporal lobes in post-traumatic amnesia. *Brain*, 139(12):3137–3150.

De Simoni, S., Jenkins, P. O., Bourke, N. J., Fleminger, J. J., Hellyer, P. J., Jolly, A. E., Patel, M. C., Cole, J. H., Leech, R., and Sharp, D. J. (2018). Altered caudate connectivity is associated with executive dysfunction after traumatic brain injury. *Brain*, 141(1):148–164.

De Tisi, J., Bell, G. S., Peacock, J. L., McEvoy, A. W., Harkness, W. F., Sander, J. W., and Duncan, J. S. (2011). The long-term outcome of adult epilepsy surgery, patterns of seizure remission, and relapse: a cohort study. *The Lancet*, 378(9800):1388–1395.

Delis, D. C., Kaplan, E., and Kramer, J. H. (2012). Delis-Kaplan Executive Function System. Technical report, American Psychological Association. type: dataset.

Dennis, E. L., Jin, Y., Villalon-Reina, J. E., Zhan, L., Kernan, C. L., Babikian, T., Mink, R. B., Babbitt, C. J., Johnson, J. L., Giza, C. C., et al. (2015). White matter disruption in moderate/severe pediatric traumatic brain injury: advanced tract-based analyses. *NeuroImage: Clinical*, 7:493–505.

Desmurget, M., Bonnetblanc, F., and Duffau, H. (2007). Contrasting acute and slow-growing lesions: a new door to brain plasticity. *Brain*, 130(4):898–914.

Dinkel, J., Drier, A., Khalilzadeh, O., Perlbarg, V., Czernecki, V., Gupta, R., Gomas, F., Sanchez, P., Dormont, D., Galanaud, D., et al. (2014). Long-term white matter changes after severe traumatic brain injury: a 5-year prospective cohort. *American Journal of Neuroradiology*, 35(1):23–29.

Dixon, M. L., De La Vega, A., Mills, C., Andrews-Hanna, J., Spreng, R. N., Cole, M. W., and Christoff, K. (2018). Heterogeneity within the frontoparietal control network and its relationship to the default and dorsal attention networks. *Proceedings of the National Academy of Sciences*, 115(7):E1598–E1607.

Edlow, B. L., Copen, W. A., Izzy, S., Bakhadirov, K., van der Kouwe, A., Glenn, M. B., Greenberg, S. M., Greer, D. M., and Wu, O. (2016). Diffusion tensor imaging in acute-to-subacute traumatic brain injury: a longitudinal analysis. *BMC neurology*, 16(1):2.

Edwards III, G., Zhao, J., Dash, P. K., Soto, C., and Moreno-Gonzalez, I. (2020). Traumatic brain injury induces tau aggregation and spreading. *Journal of neurotrauma*, 37(1):80–92.

Elderkin-Thompson, V., Hellemann, G., Pham, D., and Kumar, A. (2009). Prefrontal brain morphology and executive function in healthy and depressed elderly. *International Journal of Geriatric Psychiatry*, 24(5):459–468.

Elliott, C. A., Gross, D. W., Wheatley, B. M., Beaulieu, C., and Sankar, T. (2018). Longitudinal hippocampal and extra-hippocampal microstructural and macrostructural changes following temporal lobe epilepsy surgery. *Epilepsy research*, 140:128–137.

Faber, J., Schoene-Bake, J.-C., Trautner, P., von Lehe, M., Elger, C. E., and Weber, B. (2013). Progressive fiber tract affections after temporal lobe surgery. *Epilepsia*, 54(4):e53–e57.

Fagerholm, E. D., Hellyer, P. J., Scott, G., Leech, R., and Sharp, D. J. (2015). Disconnection of network hubs and cognitive impairment after traumatic brain injury. *Brain*, 138(6):1696–1709.

Fann, J. R., Ribe, A. R., Pedersen, H. S., Fenger-Grøn, M., Christensen, J., Benros, M. E., and Vestergaard, M. (2018). Long-term risk of dementia among people with traumatic brain injury in denmark: a population-based observational cohort study. *The Lancet Psychiatry*, 5(5):424–431.

Farahani, F. V., Karwowski, W., and Lighthall, N. R. (2019). Application of graph theory for identifying connectivity patterns in human brain networks: a systematic review. *frontiers in Neuroscience*, 13:585.

Faraji, A. H., Abhinav, K., Jarbo, K., Yeh, F.-C., Shin, S. S., Pathak, S., Hirsch, B. E., Schneider, W., Fernandez-Miranda, J. C., and Friedlander, R. M. (2015). Longitudinal evaluation of corticospinal tract in patients with resected brainstem cavernous malformations using high-definition fiber tractography and diffusion connectometry analysis: preliminary experience. *Journal of neurosurgery*, 123(5):1133–1144.

Farbota, K. D., Bendlin, B. B., Alexander, A. L., Rowley, H. A., Dempsey, R. J., and Johnson, S. C. (2012). Longitudinal diffusion tensor imaging and neuropsychological correlates in traumatic brain injury patients. *Frontiers in Human Neuroscience*, 6:160.

Feis, R. A., Smith, S. M., Filippini, N., Douaud, G., Dopper, E. G. P., Heise, V., Trachtenberg, A. J., van Swieten, J. C., van Buchem, M. A., Rombouts, S. A. R. B., and Mackay, C. E. (2015). ICA-based artifact removal diminishes scan site differences in multi-center resting-state fMRI. *Frontiers in Neuroscience*, 9.

Festoff, B. W., Sajja, R. K., van Dreden, P., and Cucullo, L. (2016). HMGB1 and thrombin mediate the blood-brain barrier dysfunction acting as biomarkers of neuroinflammation and progression to neurodegeneration in Alzheimer's disease. *Journal of Neuroinflammation*, 13(1):194.

Fong, A. H. C., Yoo, K., Rosenberg, M. D., Zhang, S., Li, C.-S. R., Scheinost, D., Constable, R. T., and Chun, M. M. (2019). Dynamic functional connectivity during task performance and rest predicts individual differences in attention across studies. *NeuroImage*, 188:14–25.

Forsyth, R. and Kirkham, F. (2012). Predicting outcome after childhood brain injury. *Canadian Medical Association Journal*, 184(11):1257–1264.

Friston, K. J., Harrison, L., and Penny, W. (2003). Dynamic causal modelling. *Neuroimage*, 19(4):1273–1302.

Galovic, M., Baudracco, I., Wright-Goff, E., Pillajo, G., Nachev, P., Wandschneider, B., Woermann, F., Thompson, P., Baxendale, S., McEvoy, A. W., et al. (2019). Association of piriform cortex resection with surgical outcomes in patients with temporal lobe epilepsy. *JAMA neurology*, 76(6):690–700.

Gardner, R. C., Burke, J. F., Nettiksimmons, J., Kaup, A., Barnes, D. E., and Yaffe, K. (2014). Dementia Risk After Traumatic Brain Injury vs Nonbrain Trauma: The Role of Age and Severity. *JAMA Neurology*, 71(12):1490.

Ghajari, M., Hellyer, P. J., and Sharp, D. J. (2017). Computational modelling of traumatic brain injury predicts the location of chronic traumatic encephalopathy pathology. *Brain*, 140(2):333–343.

Gilbert, N., Bernier, R. A., Calhoun, V. D., Brenner, E., Grossner, E., Rajtmajer, S. M., and Hillary, F. G. (2018). Diminished neural network dynamics after moderate and severe traumatic brain injury. *PLOS ONE*, 13(6):e0197419.

Graham, N. S. and Sharp, D. J. (2019). Understanding neurodegeneration after traumatic brain injury: from mechanisms to clinical trials in dementia. *Journal of Neurology, Neurosurgery & Psychiatry*, 90(11):1221–1233.

Graham, N. S., Zimmerman, K. A., Moro, F., Heslegrave, A., Maillard, S. A., Bernini, A., Miroz, J.-P., Donat, C., Lopez, M. Y., Bourke, N., Jolly, A., Mallas, E., Wilson, M., Fatania, G., Roi, D., Patel, M., Garbero, E., Nattino, G., Chieregato, A., Fainardi, E., Bacliou, C., Gradisek, P., Magnoni, S., Oddo, M., Zetterberg, H., Bertolini, G., and Sharp, D. J. (2020a). Advanced fluid and imaging biomarkers of axonal injury after traumatic brain injury: the prospective multi-centre BIO-AX-TBI study. *Submitted*.

Graham, N. S. N., Zimmerman, K. A., Bertolini, G., Magnoni, S., Oddo, M., Zetterberg, H., Moro, F., Novelli, D., Heslegrave, A., Chieregato, A., Fainardi, E., Fleming, J. M., Garbero, E., Abed-Maillard, S., Gradisek, P., Bernini, A., and Sharp, D. J. (2020b). Multicentre longitudinal study of fluid and neuroimaging BIOmarkers of AXonal injury after traumatic brain injury: the BIO-AX-TBI study protocol. *BMJ Open*, 10(11):e042093.

Green, C., Sydow, A., Vogel, S., Anglada-Huguet, M., Wiedermann, D., Mandelkow, E., Mandelkow, E.-M., and Hoehn, M. (2019). Functional networks are impaired by elevated tau-protein but reversible in a regulatable Alzheimer's disease mouse model. *Molecular Neurodegeneration*, 14(1):13.

Griffanti, L., Douaud, G., Bijsterbosch, J., Evangelisti, S., Alfaro-Almagro, F., Glasser, M. F., Duff, E. P., Fitzgibbon, S., Westphal, R., Carone, D., Beckmann, C. F., and Smith, S. M. (2017). Hand classification of fMRI ICA noise components. *NeuroImage*, 154:188–205.

Gronwall, D. M. A. (1977). Paced Auditory Serial-Addition Task: A Measure of Recovery from Concussion. *Perceptual and Motor Skills*, 44(2):367–373.

Gross, D. W. (2011). Diffusion tensor imaging in temporal lobe epilepsy. *Epilepsia*, 52:32–34.

Gross, D. W., Concha, L., and Beaulieu, C. (2006). Extratemporal white matter abnormalities in mesial temporal lobe epilepsy demonstrated with diffusion tensor imaging. *Epilepsia*, 47(8):1360–1363.

Gupta, R. and Sen, N. (2016). Traumatic brain injury: a risk factor for neurodegenerative diseases. *Reviews in the Neurosciences*, 27(1):93–100.

Haury, A.-C., Gestraud, P., and Vert, J.-P. (2011). The Influence of Feature Selection Methods on Accuracy, Stability and Interpretability of Molecular Signatures. *PLoS ONE*, 6(12):e28210.

Hiebert, J. B., Shen, Q., Thimmesch, A. R., and Pierce, J. D. (2015). Traumatic brain injury and mitochondrial dysfunction. *The American journal of the medical sciences*, 350(2):132–138.

Hillary, F., Slocomb, J., Hills, E., Fitzpatrick, N., Medaglia, J., Wang, J., Good, D., and Wylie, G. (2011). Changes in resting connectivity during recovery from severe traumatic brain injury. *International Journal of Psychophysiology*, 82(1):115–123.

Hindriks, R., Adhikari, M., Murayama, Y., Ganzetti, M., Mantini, D., Logothetis, N., and Deco, G. (2016). Can sliding-window correlations reveal dynamic functional connectivity in resting-state fMRI? *NeuroImage*, 127:242–256.

Hinton, G. E. (2011). Machine learning for neuroscience. *Neural systems & circuits*, 1(1):12.

Honey, C. J., Thivierge, J.-P., and Sporns, O. (2010). Can structure predict function in the human brain? *NeuroImage*, 52(3):766–776.

Horn, H. J., Vergara, V. M., Espinoza, F. A., Calhoun, V. D., Mayer, A. R., and Naalt, J. (2020). Functional outcome is tied to dynamic brain states after mild to moderate traumatic brain injury. *Human Brain Mapping*, 41(3):617–631.

Hou, W., Sours Rhodes, C., Jiang, L., Roys, S., Zhuo, J., JaJa, J., and Gullapalli, R. P. (2019). Dynamic Functional Network Analysis in Mild Traumatic Brain Injury. *Brain Connectivity*, 9(6):475–487.

Hubert, M., Rousseeuw, P., and Verdonck, T. (2009). Robust PCA for skewed data and its outlier map. *Computational Statistics & Data Analysis*, 53(6):2264–2274.

Imms, P., Clemente, A., Cook, M., D'Souza, W., Wilson, P. H., Jones, D. K., and Caeyenberghs, K. (2019). The structural connectome in traumatic brain injury: A meta-analysis of graph metrics. *Neuroscience & Biobehavioral Reviews*, 99:128–137.

Irimia, A., Wang, B., Aylward, S. R., Prastawa, M. W., Pace, D. F., Gerig, G., Hovda, D. A., Kikinis, R., Vespa, P. M., and Van Horn, J. D. (2012). Neuroimaging of structural pathology and connectomics in traumatic brain injury: Toward personalized outcome prediction. *NeuroImage: Clinical*, 1(1):1–17.

Jenkinson, M., Bannister, P., Brady, M., and Smith, S. (2002). Improved Optimization for the Robust and Accurate Linear Registration and Motion Correction of Brain Images. *NeuroImage*, 17(2):825–841.

Jenkinson, M., Beckmann, C. F., Behrens, T. E., Woolrich, M. W., and Smith, S. M. (2012). FSL. *NeuroImage*, 62(2):782–790.

Jenkinson, M. and Smith, S. (2001). A global optimisation method for robust affine registration of brain images. *Medical Image Analysis*, 5(2):143–156.

Johnson, V. E., Stewart, W., and Smith, D. H. (2013). Axonal pathology in traumatic brain injury. *Experimental neurology*, 246:35–43.

Jolly, A. E., Bălăeţ, M., Azor, A., Friedland, D., Sandrone, S., Graham, N. S. N., Zimmerman, K., and Sharp, D. J. (2020). Detecting axonal injury in individual patients after traumatic brain injury. *Brain*, page awaa372.

Jones, D. T., Knopman, D. S., Gunter, J. L., Graff-Radford, J., Vemuri, P., Boeve, B. F., Petersen, R. C., Weiner, M. W., and Jack Jr, C. R. (2016). Cascading network failure across the alzheimer's disease spectrum. *Brain*, 139(2):547–562.

Keller, S. S., Glenn, G. R., Weber, B., Kreilkamp, B. A., Jensen, J. H., Helpern, J. A., Wagner, J., Barker, G. J., Richardson, M. P., and Bonilha, L. (2017). Preoperative automated fibre quantification predicts postoperative seizure outcome in temporal lobe epilepsy. *Brain*, 140(1):68–82.

Kelly, A. C., Uddin, L. Q., Biswal, B. B., Castellanos, F. X., and Milham, M. P. (2008). Competition between functional brain networks mediates behavioral variability. *NeuroImage*, 39(1):527–537.

Kemmotsu, N., Girard, H. M., Bernhardt, B. C., Bonilha, L., Lin, J. J., Tecoma, E. S., Iragui, V. J., Hagler Jr, D. J., Halgren, E., and McDonald, C. R. (2011). MRI analysis in temporal lobe epilepsy: cortical thinning and white matter disruptions are related to side of seizure onset. *Epilepsia*, 52(12):2257–2266.

Kerschensteiner, M., Schwab, M. E., Lichtman, J. W., and Misgeld, T. (2005). In vivo imaging of axonal degeneration and regeneration in the injured spinal cord. *Nature medicine*, 11(5):572–577.

Khalil, M., Teunissen, C. E., Otto, M., Piehl, F., Sormani, M. P., Gattringer, T., Barro, C., Kappos, L., Comabella, M., Fazekas, F., et al. (2018). Neurofilaments as biomarkers in neurological disorders. *Nature Reviews Neurology*, 14(10):577–589.

Khazaee, A., Ebrahimzadeh, A., and Babajani-Feremi, A. (2015). Identifying patients with alzheimer's disease using resting-state fMRI and graph theory. *Clinical Neurophysiology*, 126(11):2132–2141.

Kim, J. H., Loy, D. N., Wang, Q., Budde, M. D., Schmidt, R. E., Trinkaus, K., and Song, S.-K. (2010). Diffusion tensor imaging at 3 hours after traumatic spinal cord injury predicts long-term locomotor recovery. *Journal of neurotrauma*, 27(3):587–598.

Kinnunen, K. M., Greenwood, R., Powell, J. H., Leech, R., Hawkins, P. C., Bonnelle, V., Patel, M. C., Counsell, S. J., and Sharp, D. J. (2010). White matter damage and cognitive impairment after traumatic brain injury. *Brain*, 134(2):449–463.

Kuceyeski, A., Maruta, J., Niogi, S. N., Ghajar, J., and Raj, A. (2011). The generation and validation of white matter connectivity importance maps. *NeuroImage*, 58(1):109–121.

Kuceyeski, A. F., Jamison, K. W., Owen, J. P., Raj, A., and Mukherjee, P. (2019). Longitudinal increases in structural connectome segregation and functional connectome integration are associated with better recovery after mild tbi. *Human brain mapping*, 40(15):4441–4456.

Lam, J., Cabeen, R., Tanna, R., Navarro, L., Heck, C. N., Liu, C. Y., Lee, B., Russin, J., Toga, A., and Lee, D. J. (2020). Gray matter atrophy: The impacts of resective surgery and vagus nerve stimulation for drug resistant epilepsy. *Neurosurgery*, 67(Supplement_1):nyaa447_661.

Lawrence, T., Helmy, A., Bouamra, O., Woodford, M., Lecky, F., and Hutchinson, P. J. (2016). Traumatic brain injury in England and Wales: prospective audit of epidemiology, complications and standardised mortality. *BMJ Open*, 6(11):e012197.

Leech, R., Kamourieh, S., Beckmann, C. F., and Sharp, D. J. (2011). Fractionating the Default Mode Network: Distinct Contributions of the Ventral and Dorsal Posterior Cingulate Cortex to Cognitive Control. *Journal of Neuroscience*, 31(9):3217–3224.

Leisman, G., Braun-Benjamin, O., and Melillo, R. (2014). Cognitive-motor interactions of the basal ganglia in development. *Frontiers in Systems Neuroscience*, 8.

Li, J., Li, X.-Y., Feng, D.-F., and Gu, L. (2011). Quantitative evaluation of microscopic injury with diffusion tensor imaging in a rat model of diffuse axonal injury. *European Journal of Neuroscience*, 33(5):933–945.

Li, L. M., Violante, I. R., Leech, R., Ross, E., Hampshire, A., Opitz, A., Rothwell, J. C., Carmichael, D. W., and Sharp, D. J. (2019a). Brain state and polarity dependent modulation of brain networks by transcranial direct current stimulation. *Human Brain Mapping*, 40(3):904–915.

Li, L. M., Violante, I. R., Zimmerman, K., Leech, R., Hampshire, A., Patel, M., Opitz, A., McArthur, D., Jolly, A., Carmichael, D. W., and Sharp, D. J. (2019b). Traumatic axonal injury influences the cognitive effect of non-invasive brain stimulation. *Brain*, 142(10):3280–3293.

Li, W., An, D., Tong, X., Liu, W., Xiao, F., Ren, J., Niu, R., Tang, Y., Zhou, B., Lei, D., Jiang, Y., Luo, C., Yao, D., Gong, Q., and Zhou, D. (2019c). Different patterns of white matter changes after successful surgery of mesial temporal lobe epilepsy. *NeuroImage: Clinical*, 21:101631.

Li, Y., Li, Y., Li, X., Zhang, S., Zhao, J., Zhu, X., and Tian, G. (2017). Head injury as a risk factor for dementia and alzheimer's disease: a systematic review and meta-analysis of 32 observational studies. *PloS one*, 12(1):e0169650.

Lindsey, H. M., Wilde, E. A., Caeyenberghs, K., and Dennis, E. L. (2019). Longitudinal neuroimaging in pediatric traumatic brain injury: current state and consideration of factors that influence recovery. *Frontiers in neurology*, 10:1296.

Liu, M., Gross, D. W., Wheatley, B. M., Concha, L., and Beaulieu, C. (2013). The acute phase of Wallerian degeneration: Longitudinal diffusion tensor imaging of the fornix following temporal lobe surgery. *NeuroImage*, 74:128–139.

Liu, X., Chen, L., and Chen, Y. (2017). N-methyl-d-aspartate receptors mediate epilepsy-induced axonal impairment and tau phosphorylation via activating glycogen synthase kinase-3β and cyclin-dependent kinase 5. *Discovery medicine*, 23(127):221–234.

Liu, X., Ward, B. D., Binder, J. R., Li, S.-J., and Hudetz, A. G. (2014). Scale-free functional connectivity of the brain is maintained in anesthetized healthy participants but not in patients with unresponsive wakefulness syndrome. *PLoS One*, 9(3):e92182.

Ljungqvist, J., Zetterberg, H., Mitsis, M., Blennow, K., and Skoglund, T. (2017). Serum neurofilament light protein as a marker for diffuse axonal injury: results from a case series study. *Journal of neurotrauma*, 34(5):1124–1127.

Lord, L.-D., Stevner, A. B., Deco, G., and Kringelbach, M. L. (2017). Understanding principles of integration and segregation using whole-brain computational connectomics: implications for neuropsychiatric disorders. *Philosophical Transactions of the Royal Society A: Mathematical, Physical and Engineering Sciences*, 375(2096):20160283.

Maas, A. I., Stocchetti, N., and Bullock, R. (2008). Moderate and severe traumatic brain injury in adults. *The Lancet Neurology*, 7(8):728–741.

Mac Donald, C. L., Dikranian, K., Bayly, P., Holtzman, D., and Brody, D. (2007). Diffusion tensor imaging reliably detects experimental traumatic axonal injury and indicates approximate time of injury. *Journal of Neuroscience*, 27(44):11869–11876.

Magnoni, S., Esparza, T. J., Conte, V., Carbonara, M., Carrabba, G., Holtzman, D. M., Zipfel, G. J., Stocchetti, N., and Brody, D. L. (2012). Tau elevations in the brain extracellular space correlate with reduced amyloid-β levels and predict adverse clinical outcomes after severe traumatic brain injury. *Brain*, 135(4):1268–1280.

Mai, J. K. and Majtanik, M. (2017). *Human Brain in Standard MNI Space: A Comprehensive Pocket Atlas*. Elsevier.

Mai, Jürgen K. and Paxinos, George (2012). *The Human Nervous System*. Elsevier.

Mallas, E.-J., De Simoni, S., Scott, G., Jolly, A. E., Hampshire, A., Li, L. M., Bourke, N. J., Roberts, S. A., Gorgoraptis, N., and Sharp, D. J. (2020). Abnormal dorsal attention network activation in memory impairment after traumatic brain injury. *Brain*.

Marinković, P., Blumenstock, S., Goltstein, P. M., Korzhova, V., Peters, F., Knebl, A., and Herms, J. (2019). *In vivo* imaging reveals reduced activity of neuronal circuits in a mouse tauopathy model. *Brain*, 142(4):1051–1062.

Mattsson, N., Andreasson, U., Zetterberg, H., Blennow, K., and for the Alzheimer's Disease Neuroimaging Initiative (2017). Association of Plasma Neurofilament Light With Neurodegeneration in Patients With Alzheimer Disease. *JAMA Neurology*, 74(5):557.

Mazrooyisebdani, M., Nair, V. A., Garcia-Ramos, C., Mohanty, R., Meyerand, E., Hermann, B., Prabhakaran, V., and Ahmed, R. (2020). Graph theory analysis of functional connectivity combined with machine learning approaches demonstrates widespread network differences and predicts clinical variables in temporal lobe epilepsy. *Brain connectivity*, 10(1):39–50.

McAllister, T. W. (2011). Neurobiological consequences of traumatic brain injury. *Dialogues in Clinical Neuroscience*, 13(3):287–300.

McDonald, C., Hagler, D., Girard, H., Pung, C., Ahmadi, M., Holland, D., Patel, R., Barba, D., Tecoma, E., Iragui, V., et al. (2010). Changes in fiber tract integrity and visual fields after anterior temporal lobectomy. *Neurology*, 75(18):1631–1638.

Menkes-Caspi, N., Yamin, H., Kellner, V., Spires-Jones, T., Cohen, D., and Stern, E. (2015). Pathological Tau Disrupts Ongoing Network Activity. *Neuron*, 85(5):959–966.

Merkley, T. L., Larson, M. J., Bigler, E. D., Good, D. A., and Perlstein, W. M. (2013). Structural and functional changes of the cingulate gyrus following traumatic brain injury: relation to attention and executive skills. *Journal of the International Neuropsychological Society: JINS*, 19(8):899.

Moore, E., Schaefer, R. S., Bastin, M. E., Roberts, N., and Overy, K. (2017). Diffusion tensor MRI tractography reveals increased fractional anisotropy (fa) in arcuate fasciculus following music-cued motor training. *Brain and Cognition*, 116:40–46.

Moreira da Silva, N., Ahmadi, S.-A., Tafula, S. N., Cunha, J. P. S., Bötzel, K., Vollmar, C., and Rozanski, V. E. (2017). A diffusion-based connectivity map of the gpi for optimised stereotactic targeting in dbs. *Neuroimage*, 144:83–91.

Murphy, A. C., Bertolero, M. A., Papadopoulos, L., Lydon-Staley, D. M., and Bassett, D. S. (2020). Multimodal network dynamics underpinning working memory. *Nature Communications*, 11(1):3035.

Mustafa, A. G. and Alshboul, O. A. (2013). Pathophysiology of traumatic brain injury. *Neurosciences (Riyadh)*, 18(3):222–234.

Nakai, T., Kato, C., and Matsuo, K. (2005). An fMRI Study to Investigate Auditory Attention: A Model of the Cocktail Party Phenomenon. *Magnetic Resonance in Medical Sciences*, 4(2):75–82.

Nakamura, T., Hillary, F. G., and Biswal, B. B. (2009). Resting network plasticity following brain injury. *PloS one*, 4(12):e8220.

Narayana, P. A. (2017). White matter changes in patients with mild traumatic brain injury: MRI perspective. *Concussion*, 2(2):CNC35.

Neselius, S., Brisby, H., Theodorsson, A., Blennow, K., Zetterberg, H., and Marcusson, J. (2012). Csf-biomarkers in olympic boxing: diagnosis and effects of repetitive head trauma. *PloS one*, 7(4):e33606.

Newcombe, V. F. J., Correia, M. M., Ledig, C., Abate, M. G., Outtrim, J. G., Chatfield, D., Geeraerts, T., Manktelow, A. E., Garyfallidis, E., Pickard, J. D., Sahakian, B. J., Hutchinson, P. J. A., Rueckert, D., Coles, J. P., Williams, G. B., and Menon, D. K. (2016). Dynamic Changes in White Matter Abnormalities Correlate With Late Improvement and Deterioration Following TBI: A Diffusion Tensor Imaging Study. *Neurorehabilitation and Neural Repair*, 30(1):49–62.

Nguyen, D., Vargas, M., Khaw, N., Seeck, M., Delavelle, J., Lovblad, K., and Haller, S. (2011). Diffusion tensor imaging analysis with tract-based spatial statistics of the white matter abnormalities after epilepsy surgery. *Epilepsy research*, 94(3):189–197.

Nordström, A. and Nordström, P. (2018). Traumatic brain injury and the risk of dementia diagnosis: A nationwide cohort study. *PLoS medicine*, 15(1):e1002496.

Obrocki, P., Khatun, A., Ness, D., Senkevich, K., Hanrieder, J., Capraro, F., Mattsson, N., Andreasson, U., Portelius, E., Ashton, N. J., et al. (2020). Perspectives in fluid biomarkers in neurodegeneration from the 2019 biomarkers in neurodegenerative diseases course—a joint phd student course at university college london and university of gothenburg. *Alzheimer's research & therapy*, 12(1):1–10.

Ofer, I., LeRose, C., Mast, H., LeVan, P., Metternich, B., Egger, K., Urbach, H., Schulze-Bonhage, A., and Wagner, K. (2019). Association between seizure freedom and default mode network reorganization in patients with unilateral temporal lobe epilepsy. *Epilepsy & Behavior*, 90:238–246.

Oh, A., Duerden, E. G., and Pang, E. W. (2014). The role of the insula in speech and language processing. *Brain and language*, 135:96–103.

Olde Dubbelink, K. T., Hillebrand, A., Stoffers, D., Deijen, J. B., Twisk, J. W., Stam, C. J., and Berendse, H. W. (2013). Disrupted brain network topology in Parkinson's disease: a longitudinal magnetoencephalography study. *Brain*, 137(1):197–207.

Olivera, A., Lejbman, N., Jeromin, A., French, L. M., Kim, H.-S., Cashion, A., Mysliwiec, V., Diaz-Arrastia, R., and Gill, J. (2015). Peripheral Total Tau in Military Personnel Who Sustain Traumatic Brain Injuries During Deployment. *JAMA Neurology*, 72(10):1109.

Olsson, B., Lautner, R., Andreasson, U., Öhrfelt, A., Portelius, E., Bjerke, M., Hölttä, M., Rosén, C., Olsson, C., Strobel, G., Wu, E., Dakin, K., Petzold, M., Blennow, K., and Zetterberg, H. (2016). CSF and blood biomarkers for the diagnosis of Alzheimer's disease: a systematic review and meta-analysis. *The Lancet Neurology*, 15(7):673–684.

Ost, M., Nylen, K., Csajbok, L., Ohrfelt, A. O., Tullberg, M., Wikkelso, C., Nellgard, P., Rosengren, L., Blennow, K., and Nellgard, B. (2006). Initial CSF total tau correlates with 1-year outcome in patients with traumatic brain injury. *Neurology*, 67(9):1600–1604.

O'brien, R. M. (2007). A Caution Regarding Rules of Thumb for Variance Inflation Factors. *Quality & Quantity*, 41(5):673–690.

Pandit, A. S., Expert, P., Lambiotte, R., Bonnelle, V., Leech, R., Turkheimer, F. E., and Sharp, D. J. (2013). Traumatic brain injury impairs small-world topology. *Neurology*, 80(20):1826–1833.

Peng, K., Steele, S. C., Becerra, L., and Borsook, D. (2018). Brodmann area 10: Collating, integrating and high level processing of nociception and pain. *Progress in Neurobiology*, 161:1–22.

Pisoni, A., Mattavelli, G., Casarotti, A., Comi, A., Riva, M., Bello, L., and Papagno, C. (2018). Object-action dissociation: A voxel-based lesion-symptom mapping study on 102 patients after glioma removal. *NeuroImage: Clinical*, 18:986–995.

Pläschke, R. N., Patil, K. R., Cieslik, E. C., Nostro, A. D., Varikuti, D. P., Plachti, A., Lösche, P., Hoffstaedter, F., Kalenscher, T., Langner, R., et al. (2020). Age differences in predicting working memory performance from network-based functional connectivity. *Cortex*, 132:441–459.

Poudel, G. R., Dominguez D, J. F., Verhelst, H., Vander Linden, C., Deblaere, K., Jones, D. K., Cerin, E., Vingerhoets, G., and Caeyenberghs, K. (2020). Network diffusion modeling predicts neurodegeneration in traumatic brain injury. *Annals of clinical and translational neurology*, 7(3):270–279.

Preti, M. G., Bolton, T. A., and Van De Ville, D. (2017). The dynamic functional connectome: State-of-the-art and perspectives. *NeuroImage*, 160:41–54.

Privault, N. (2013). Understanding markov chains. *Examples and Applications, Publisher Springer-Verlag Singapore*.

Pruim, R. H., Mennes, M., van Rooij, D., Llera, A., Buitelaar, J. K., and Beckmann, C. F. (2015). ICA-AROMA: A robust ICA-based strategy for removing motion artifacts from fMRI data. *NeuroImage*, 112:267–277.

Pustina, D., Doucet, G., Evans, J., Sharan, A., Sperling, M., Skidmore, C., and Tracy, J. (2014). Distinct types of white matter changes are observed after anterior temporal lobectomy in epilepsy. *PloS one*, 9(8):e104211.

Puvenna, V., Engeler, M., Banjara, M., Brennan, C., Schreiber, P., Dadas, A., Bahrami, A., Solanki, J., Bandyopadhyay, A., Morris, J. K., et al. (2016). Is phosphorylated tau unique to chronic traumatic encephalopathy? phosphorylated tau in epileptic brain and chronic traumatic encephalopathy. *Brain research*, 1630:225–240.

Raj, A., Kuceyeski, A., and Weiner, M. (2012). A network diffusion model of disease progression in dementia. *Neuron*, 73(6):1204–1215.

Raj, R., Kaprio, J., Korja, M., Mikkonen, E. D., Jousilahti, P., and Siironen, J. (2017). Risk of hospitalization with neurodegenerative disease after moderate-to-severe traumatic brain injury in the working-age population: A retrospective cohort study using the finnish national health registries. *PLoS medicine*, 14(7):e1002316.

Rigon, J., Burro, R., Guariglia, C., Maini, M., Marin, D., Ciurli, P., Bivona, U., and Formisano, R. (2017). Self-awareness rehabilitation after Traumatic Brain Injury: A pilot study to compare two group therapies. *Restorative Neurology and Neuroscience*, 35(1):115–127.

Riley, J. D., Franklin, D. L., Choi, V., Kim, R. C., Binder, D. K., Cramer, S. C., and Lin, J. J. (2010). Altered white matter integrity in temporal lobe epilepsy: association with cognitive and clinical profiles. *Epilepsia*, 51(4):536–545.

Rubenstein, R., Chang, B., Yue, J. K., Chiu, A., Winkler, E. A., Puccio, A. M., Diaz-Arrastia, R., Yuh, E. L., Mukherjee, P., Valadka, A. B., Gordon, W. A., Okonkwo, D. O., Davies, P., Agarwal, S., Lin, F., Sarkis, G., Yadikar, H., Yang, Z., Manley, G. T., Wang, K. K. W., and the TRACK-TBI Investigators, Cooper, S. R., Dams-O'Connor, K., Borrasso, A. J., Inoue, T., Maas, A. I. R., Menon, D. K., Schnyer, D. M., and Vassar, M. J. (2017). Comparing Plasma Phospho Tau, Total Tau, and Phospho Tau–Total Tau Ratio as Acute and Chronic Traumatic Brain Injury Biomarkers. *JAMA Neurology*, 74(9):1063.

Rubenstein, R., Sharma, D. R., Chang, B., Oumata, N., Cam, M., Vaucelle, L., Lindberg, M. F., Chiu, A., Wisniewski, T., Wang, K. K. W., and Meijer, L. (2019). Novel Mouse Tauopathy Model for Repetitive Mild Traumatic Brain Injury: Evaluation of Long-Term Effects on Cognition and Biomarker Levels After Therapeutic Inhibition of Tau Phosphorylation. *Frontiers in Neurology*, 10:124.

Rubinov, M. and Sporns, O. (2010). Complex network measures of brain connectivity: Uses and interpretations. *NeuroImage*, 52(3):1059–1069.

Salin, P., Tseng, G.-F., Hoffman, S., Parada, I., and Prince, D. A. (1995). Axonal sprouting in layer v pyramidal neurons of chronically injured cerebral cortex. *Journal of Neuroscience*, 15(12):8234–8245.

Schoene-Bake, J.-C., Faber, J., Trautner, P., Kaaden, S., Tittgemeyer, M., Elger, C. E., and Weber, B. (2009). Widespread affections of large fiber tracts in postoperative temporal lobe epilepsy. *Neuroimage*, 46(3):569–576.

Schumacher, J., Peraza, L. R., Firbank, M., Thomas, A. J., Kaiser, M., Gallagher, P., O'Brien, J. T., Blamire, A. M., and Taylor, J.-P. (2019). Dynamic functional connectivity changes in dementia with Lewy bodies and Alzheimer's disease. *NeuroImage: Clinical*, 22:101812.

Sedgwick, P. (2014). Cross sectional studies: advantages and disadvantages. *BMJ: British Medical Journal*, 348.

Seidenberg, M., Kelly, K. G., Parrish, J., Geary, E., Dow, C., Rutecki, P., and Hermann, B. (2005). Ipsilateral and contralateral MRI volumetric abnormalities in chronic unilateral temporal lobe epilepsy and their clinical correlates. *Epilepsia*, 46(3):420–430.

Shahim, P., Gren, M., Liman, V., Andreasson, U., Norgren, N., Tegner, Y., Mattsson, N., Andreasen, N., Öst, M., Zetterberg, H., Nellgård, B., and Blennow, K. (2016). Serum neurofilament light protein predicts clinical outcome in traumatic brain injury. *Scientific Reports*, 6(1):36791.

Shahim, P., Politis, A., van der Merwe, A., Moore, B., Chou, Y.-Y., Pham, D. L., Butman, J. A., Diaz-Arrastia, R., Gill, J. M., Brody, D. L., Zetterberg, H., Blennow, K., and Chan, L. (2020). Neurofilament light as a biomarker in traumatic brain injury. *Neurology*, 95(6):e610–e622.

Shahim, P., Zetterberg, H., Tegner, Y., and Blennow, K. (2017). Serum neurofilament light as a biomarker for mild traumatic brain injury in contact sports. *Neurology*, 88(19):1788–1794.

Shallice, T., Stuss, D. T., Alexander, M. P., Picton, T. W., and Derkzen, D. (2008). The multiple dimensions of sustained attention. *Cortex*, 44(7):794–805.

Shamim, S., Wiggs, E., Heiss, J., Sato, S., Liew, C., Solomon, J., and Theodore, W. H. (2009). Temporal lobectomy: resection volume, neuropsychological effects, and seizure outcome. *Epilepsy & Behavior*, 16(2):311–314.

Shannon, C. E. and Weaver, W. (1949). The mathematical theory of communication, 117 pp. *Urbana: University of Illinois Press*.

Sharp, D. J., Beckmann, C. F., Greenwood, R., Kinnunen, K. M., Bonnelle, V., De Boissezon, X., Powell, J. H., Counsell, S. J., Patel, M. C., and Leech, R. (2011). Default mode network functional and structural connectivity after traumatic brain injury. *Brain*, 134(8):2233–2247.

Sharp, D. J., Scott, G., and Leech, R. (2014). Network dysfunction after traumatic brain injury. *Nature Reviews Neurology*, 10(3):156–166.

Shipp, S. (2017). The functional logic of corticostriatal connections. *Brain Structure and Function*, 222(2):669–706.

Shively, S., Scher, A. I., Perl, D. P., and Diaz-Arrastia, R. (2012). Dementia resulting from traumatic brain injury: what is the pathology? *Archives of neurology*, 69(10):1245–1251.

Sinha, N., Wang, Y., da Silva, N. M., Miserocchi, A., McEvoy, A. W., de Tisi, J., Vos, S. B., Winston, G. P., Duncan, J. S., and Taylor, P. N. (2020). Structural brain network abnormalities and the probability of seizure recurrence after epilepsy surgery. *Neurology*.

Sinha, N., Wang, Y., Dauwels, J., Kaiser, M., Thesen, T., Forsyth, R., and Taylor, P. N. (2019). Computer modelling of connectivity change suggests epileptogenesis mechanisms in idiopathic generalised epilepsy. *NeuroImage: Clinical*, 21:101655.

Smith, D. H., Meaney, D. F., and Shull, W. H. (2003). Diffuse Axonal Injury in Head Trauma:. *Journal of Head Trauma Rehabilitation*, 18(4):307–316.

Smith, S. M., Fox, P. T., Miller, K. L., Glahn, D. C., Fox, P. M., Mackay, C. E., Filippini, N., Watkins, K. E., Toro, R., Laird, A. R., and Beckmann, C. F. (2009). Correspondence of the brain's functional architecture during activation and rest. *Proceedings of the National Academy of Sciences*, 106(31):13040–13045.

Smith, S. M., Jenkinson, M., Johansen-Berg, H., Rueckert, D., Nichols, T. E., Mackay, C. E., Watkins, K. E., Ciccarelli, O., Cader, M. Z., Matthews, P. M., and Behrens, T. E. (2006). Tract-based spatial statistics: Voxelwise analysis of multi-subject diffusion data. *NeuroImage*, 31(4):1487–1505.

Solem, R. C. (2015). Limitation of a cross-sectional study. *American Journal of Orthodontics and Dentofacial Orthopedics*, 148(2):205.

Song, S.-K., Sun, S.-W., Ju, W.-K., Lin, S.-J., Cross, A. H., and Neufeld, A. H. (2003). Diffusion tensor imaging detects and differentiates axon and myelin degeneration in mouse optic nerve after retinal ischemia. *Neuroimage*, 20(3):1714–1722.

Song, S.-K., Yoshino, J., Le, T. Q., Lin, S.-J., Sun, S.-W., Cross, A. H., and Armstrong, R. C. (2005). Demyelination increases radial diffusivity in corpus callosum of mouse brain. *Neuroimage*, 26(1):132–140.

Spencer, D. D., Spencer, S. S., Mattson, R. H., Williamson, P. D., and Novelly, R. A. (1984). Access to the posterior medial temporal lobe structures in the surgical treatment of temporal lobe epilepsy. *Neurosurgery*, 15(5):667–671.

Spencer, S. and Huh, L. (2008). Outcomes of epilepsy surgery in adults and children. *The Lancet Neurology*, 7(6):525–537.

Spira, M. E., Oren, R., Dormann, A., and Gitler, D. (2003). Critical calpain-dependent ultrastructural alterations underlie the transformation of an axonal segment into a growth cone after axotomy of cultured aplysia neurons. *Journal of Comparative Neurology*, 457(3):293–312.

Sporns, O. (2010). *Networks of the Brain*. MIT press.

Sporns, O. and Zwi, J. D. (2004). The small world of the cerebral cortex. *Neuroinformatics*, 2(2):145–162.

Squarcina, L., Bertoldo, A., Ham, T. E., Heckemann, R., and Sharp, D. J. (2012). A robust method for investigating thalamic white matter tracts after traumatic brain injury. *NeuroImage*, 63(2):779–788.

Stein, D. G. (2000). Brain injury and theories of recovery. In *International handbook of neuropsychological rehabilitation*, pages 9–32. Springer.

Taha, A. A. and Hanbury, A. (2015). Metrics for evaluating 3d medical image segmentation: analysis, selection, and tool. *BMC medical imaging*, 15(1):1–28.

Takala, R. S., Posti, J. P., Runtti, H., Newcombe, V. F., Outtrim, J., Katila, A. J., Frantzén, J., Ala-Seppälä, H., Kyllönen, A., Maanpää, H.-R., Tallus, J., Hossain, M. I., Coles, J. P., Hutchinson, P., van Gils, M., Menon, D. K., and Tenovuo, O. (2016). Glial Fibrillary Acidic Protein and Ubiquitin C-Terminal Hydrolase-L1 as Outcome Predictors in Traumatic Brain Injury. *World Neurosurgery*, 87:8–20.

Taylor, P. N., Han, C. E., Schoene-Bake, J.-C., Weber, B., and Kaiser, M. (2015). Structural connectivity changes in temporal lobe epilepsy: Spatial features contribute more than topological measures. *NeuroImage: Clinical*, 8:322–328.

Taylor, P. N., Moreira da Silva, N., Blamire, A., Wang, Y., and Forsyth, R. (2020). Early deviation from normal structural connectivity: A novel intrinsic severity score for mild TBI. *Neurology*, 94(10):e1021–e1026.

Taylor, P. N., Sinha, N., Wang, Y., Vos, S. B., de Tisi, J., Miserocchi, A., McEvoy, A. W., Winston, G. P., and Duncan, J. S. (2018). The impact of epilepsy surgery on the structural connectome and its relation to outcome. *NeuroImage: Clinical*, 18:202–214.

Thatcher, R., North, D., and Biver, C. (2005). EEG and intelligence: Relations between EEG coherence, EEG phase delay and power. *Clinical Neurophysiology*, 116(9):2129–2141.

Thedchanamoorthy, G., Piraveenan, M., Kasthuriratna, D., and Senanayake, U. (2014). Node Assortativity in Complex Networks: An Alternative Approach. *Procedia Computer Science*, 29:2449–2461.

Thelin, E. P., Johannesson, L., Nelson, D., and Bellander, B.-M. (2013). S100b is an important outcome predictor in traumatic brain injury. *Journal of neurotrauma*, 30(7):519–528.

Traynor, C., Heckemann, R. A., Hammers, A., O'Muircheartaigh, J., Crum, W. R., Barker, G. J., and Richardson, M. P. (2010). Reproducibility of thalamic segmentation based on probabilistic tractography. *NeuroImage*, 52(1):69–85.

Tzourio-Mazoyer, N., Landeau, B., Papathanassiou, D., Crivello, F., Etard, O., Delcroix, N., Mazoyer, B., and Joliot, M. (2002). Automated Anatomical Labeling of Activations in SPM Using a Macroscopic Anatomical Parcellation of the MNI MRI Single-Subject Brain. *NeuroImage*, 15(1):273–289.

Van den Heuvel, M. P. and Sporns, O. (2013). Network hubs in the human brain. *Trends in cognitive sciences*, 17(12):683–696.

Van Der Horn, H. J., Kok, J. G., De Koning, M. E., Scheenen, M. E., Leemans, A., Spikman, J. M., and Van Der Naalt, J. (2017). Altered wiring of the human structural connectome in adults with mild traumatic brain injury. *Journal of neurotrauma*, 34(5):1035–1044.

Vergara, V. M., Mayer, A. R., Kiehl, K. A., and Calhoun, V. D. (2018). Dynamic functional network connectivity discriminates mild traumatic brain injury through machine learning. *NeuroImage: Clinical*, 19:30–37.

Verhelst, H., Giraldo, D., Vander Linden, C., Vingerhoets, G., Jeurissen, B., and Caeyenberghs, K. (2019). Cognitive training in young patients with traumatic brain injury: a fixel-based analysis. *Neurorehabilitation and neural repair*, 33(10):813–824.

Vos, P. E., Jacobs, B., Andriessen, T. M. J. C., Lamers, K. J. B., Borm, G. F., Beems, T., Edwards, M., Rosmalen, C. F., and Vissers, J. L. M. (2010). GFAP and S100B are biomarkers of traumatic brain injury: An observational cohort study. *Neurology*, 75(20):1786–1793.

Wang, H.-L. S., Wang, N. Y.-H., and Yeh, F.-C. (2019). Specifying the diffusion MRI connectome in Chinese-speaking children with developmental dyslexia and auditory processing deficits. *Pediatrics & Neonatology*, 60(3):297–304.

Wang, J., Qiu, S., Xu, Y., Liu, Z., Wen, X., Hu, X., Zhang, R., Li, M., Wang, W., and Huang, R. (2014). Graph theoretical analysis reveals disrupted topological properties of whole brain functional networks in temporal lobe epilepsy. *Clinical Neurophysiology*, 125(9):1744–1756.

Wang, J. T., Medress, Z. A., and Barres, B. A. (2012). Axon degeneration: molecular mechanisms of a self-destruction pathway. *Journal of Cell Biology*, 196(1):7–18.

Werner, C. and Engelhard, K. (2007). Pathophysiology of traumatic brain injury. *British Journal of Anaesthesia*, 99(1):4–9.

Wheeler-Kingshott, C. A., Hickman, S. J., Parker, G. J., Ciccarelli, O., Symms, M. R., Miller, D. H., and Barker, G. J. (2002). Investigating cervical spinal cord structure using axial diffusion tensor imaging. *Neuroimage*, 16(1):93–102.

White, J. G., Southgate, E., Thomson, J. N., and Brenner, S. (1986). The structure of the nervous system of the nematode caenorhabditis elegans. *Philos Trans R Soc Lond B Biol Sci*, 314(1165):1–340.

Wieser, H. G., Blume, W. T., Fish, D., Goldensohn, E., Hufnagel, A., King, D., Sperling, M. R., and Lüders, H. (2003). Proposal for a New Classification of Outcome with Respect to Epileptic Seizures Following Epilepsy Surgery. *Epilepsia*, 42:282–286.

Winklewski, P. J., Sabisz, A., Naumczyk, P., Jodzio, K., Szurowska, E., and Szarmach, A. (2018). Understanding the physiopathology behind axial and radial diffusivity changes—what do we know? *Frontiers in neurology*, 9:92.

Winston, G. P., Stretton, J., Sidhu, M. K., Symms, M. R., and Duncan, J. S. (2014). Progressive white matter changes following anterior temporal lobe resection for epilepsy. *NeuroImage: Clinical*, 4:190–200.

Woolrich, M. W., Ripley, B. D., Brady, M., and Smith, S. M. (2001). Temporal Autocorrelation in Univariate Linear Modeling of FMRI Data. *NeuroImage*, 14(6):1370–1386.

Wu, J., Tan, S.-Y., Liu, Z., Tan, Y.-J., and Lu, X. (2017). Enhancing structural robustness of scale-free networks by information disturbance. *Scientific reports*, 7(1):1–13.

Wu, T. C., Wilde, E. A., Bigler, E. D., Yallampalli, R., McCauley, S. R., Troyanskaya, M., Chu, Z., Li, X., Hanten, G., Hunter, J. V., et al. (2010). Evaluating the relationship between memory functioning and cingulum bundles in acute mild traumatic brain injury using diffusion tensor imaging. *Journal of neurotrauma*, 27(2):303–307.

Xi, Z.-Q., Wang, X.-F., Shu, X.-F., Chen, G.-J., Xiao, F., Sun, J.-J., and Zhu, X. (2011). Is intractable epilepsy a tauopathy? *Medical hypotheses*, 76(6):897–900.

Xie, M., Wang, Q., Wu, T.-H., Song, S.-K., and Sun, S.-W. (2011). Delayed axonal degeneration in slow wallerian degeneration mutant mice detected using diffusion tensor imaging. *Neuroscience*, 197:339–347.

Xu, J., Rasmussen, I.-A., Lagopoulos, J., and Håberg, A. (2007). Diffuse axonal injury in severe traumatic brain injury visualized using high-resolution diffusion tensor imaging. *Journal of neurotrauma*, 24(5):753–765.

Xu, J., Wang, J., Fan, L., Li, H., Zhang, W., Hu, Q., and Jiang, T. (2016). Tractography-based Parcellation of the Human Middle Temporal Gyrus. *Scientific Reports*, 5(1):18883.

Yan, X.-X., Cai, Y., Shelton, J., Deng, S.-H., Luo, X.-G., Oddo, S., LaFerla, F. M., Cai, H., Rose, G. M., and Patrylo, P. R. (2012). Chronic temporal lobe epilepsy is associated with enhanced alzheimer-like neuropathology in 3× tg-ad mice. *PloS one*, 7(11):e48782.

Yang, W.-J., Chen, W., Chen, L., Guo, Y.-J., Zeng, J.-S., Li, G.-Y., and Tong, W.-S. (2017). Involvement of tau phosphorylation in traumatic brain injury patients. *Acta Neurologica Scandinavica*, 135(6):622–627.

Yeh, F.-C., Badre, D., and Verstynen, T. (2016). Connectometry: A statistical approach harnessing the analytical potential of the local connectome. *NeuroImage*, 125:162–171.

Yeh, F.-C., Panesar, S., Fernandes, D., Meola, A., Yoshino, M., Fernandez-Miranda, J. C., Vettel, J. M., and Verstynen, T. (2018). Population-averaged atlas of the macroscale human structural connectome and its network topology. *NeuroImage*, 178:57–68.

Yeh, F.-C., Tang, P.-F., and Tseng, W.-Y. I. (2013a). Diffusion MRI connectometry automatically reveals affected fiber pathways in individuals with chronic stroke. *NeuroImage: Clinical*, 2:912–921.

Yeh, F.-C., Verstynen, T. D., Wang, Y., Fernández-Miranda, J. C., and Tseng, W.-Y. I. (2013b). Deterministic Diffusion Fiber Tracking Improved by Quantitative Anisotropy. *PLoS ONE*, 8(11):e80713.

Yeh, F.-C., Wedeen, V. J., and Tseng, W.-Y. I. (2010). Generalized q-sampling imaging. *IEEE transactions on medical imaging*, 29(9):1626–1635.

Yogarajah, M., Focke, N. K., Bonelli, S. B., Thompson, P., Vollmar, C., McEvoy, A. W., Alexander, D. C., Symms, M. R., Koepp, M. J., and Duncan, J. S. (2010). The structural plasticity of white matter networks following anterior temporal lobe resection. *Brain*, 133(8):2348–2364.

Yuan, W., Wade, S. L., Quatman-Yates, C., Hugentobler, J. A., Gubanich, P. J., and Kurowski, B. G. (2017). Structural connectivity related to persistent symptoms after mild tbi in adolescents and response to aerobic training: preliminary investigation. *The Journal of head trauma rehabilitation*, 32(6):378.

Zalesky, A., Fornito, A., Cocchi, L., Gollo, L. L., van den Heuvel, M. P., and Breakspear, M. (2016). Connectome sensitivity or specificity: which is more important? *NeuroImage*, 142:407–420.

Zemlan, F. P., Jauch, E. C., Mulchahey, J., Gabbita, S., Rosenberg, W. S., Speciale, S. G., and Zuccarello, M. (2002). C-tau biomarker of neuronal damage in severe brain injured patients: association with elevated intracranial pressure and clinical outcome. *Brain Research*, 947(1):131–139.

Zetterberg, H. and Blennow, K. (2016). Fluid biomarkers for mild traumatic brain injury and related conditions. *Nature Reviews Neurology*, 12(10):563–574.

Zhang, H., Avants, B. B., Yushkevich, P. A., Woo, J. H., Wang, S., McCluskey, L. F., Elman, L. B., Melhem, E. R., and Gee, J. C. (2007). High-dimensional spatial normalization of diffusion tensor images improves the detection of white matter differences: An example study using amyotrophic lateral sclerosis. *IEEE Transactions on Medical Imaging*, 26(11):1585–1597.

Zhang, Y., Brady, M., and Smith, S. (2001). Segmentation of brain mr images through a hidden markov random field model and the expectation-maximization algorithm. *IEEE Transactions on Medical Imaging*, 20(1):45–57.

Zhou, Y., Kierans, A., Kenul, D., Ge, Y., Rath, J., Reaume, J., Grossman, R. I., and Lui, Y. W. (2013). Mild Traumatic Brain Injury: Longitudinal Regional Brain Volume Changes. *Radiology*, 267(3):880–890.